

Fragility Analysis of Coastal Bridges Susceptible to Hurricanes Incorporating
Uncertainties in Extreme Wave Parameters by Means of Wave Spectra and Enhancement
of Vulnerability Assessment Methodologies

by

ARASH SAEIDPOUR

(Under the Direction of Mi G. Chorzepa)

ABSTRACT

Numerous bridges along the Gulf Coast of the United States sustained significant damage in the recent hurricanes. The overall cost to repair and rebuild damaged bridges by hurricane Katrina alone was estimated over \$1 billion. Besides physical damage, any loss of functionality in transportation networks will disrupt the post-disaster recovery operations in the near term and will lead to slow economic and social development of affected regions in the long run. Reliability of the transportation infrastructure during hurricane events is mainly dependent on the bridges as they are most vulnerable nodes of the network. A comprehensive hurricane risk analysis of bridges enables the owners to assign their resources to the most critical bridges in the inventory through a risk-informed decision making process and minimize the potential loss.

In the present dissertation, a probabilistic framework for fragility analysis and risk assessment of coastal bridges vulnerable to hurricanes is proposed. Various sources of uncertainty associated with hurricane hazard and bridge response are identified and incorporated in the fragility analysis. Two different methods for conducting fragility

analysis of bridges are proposed. In the first method, a detailed procedure for deriving parameterized fragility functions, by means of surrogate models, is introduced for bridges subjected to hurricane forces. Several surrogate models are compared in terms of prediction accuracy, and the Random Forest method is shown to yield the most accurate results. A parametric finite element model for nonlinear dynamic analysis of bridges is developed in OpenSees and is used to obtain the response of bridge samples under hypothetical hurricane scenarios. The second method is a computationally efficient single hazard Intensity Measure (IM)-based risk assessment approach developed for simply supported bridges. The novelty of the proposed method includes the consideration of uncertainties in extreme wave height and wave period, by means of a wave spectral density distribution, in the calculation of wave forces. The proposed hurricane risk analysis method was successfully applied to approximately 500 coastal bridges located in the state of Georgia, U.S.A.

INDEX WORDS: Fragility, Risk, Reliability, Catastrophe, Hurricane, Machine Learning, Metamodel, Random Forest, Wave Spectra

Fragility Analysis of Coastal Bridges Susceptible to Hurricanes Incorporating
Uncertainties in Extreme Wave Parameters by Means of Wave Spectra and Enhancement
of Vulnerability Assessment Methodologies

by

ARASH SAEIDPOUR

B.S., Zanjan University, Iran, 2009

M.S., Amirkabir University of Technology, Iran, 2011

A Dissertation Submitted to the Graduate Faculty of The University of Georgia in Partial
Fulfillment of the Requirements for the Degree

DOCTOR OF PHILOSOPHY

ATHENS, GEORGIA

2017

© 2017

Arash Saeidpour

All Rights Reserved

Fragility Analysis of Coastal Bridges Susceptible to Hurricanes Incorporating
Uncertainties in Extreme Wave Parameters by Means of Wave Spectra and Enhancement
of Vulnerability Assessment Methodologies

by

ARASH SAEIDPOUR

Major Professor: Mi. G. Chorzepa
Committee: Stephan A. Durham
Jason K. Christian

Electronic Version Approved:

Suzanne Barbour
Dean of the Graduate School
The University of Georgia
August 2017

To my father, whom, if I could be half the man he was, that would mean I lived the perfect life.
To my mother, my rock, my best friend and the one who always has been there for me.
To my wife, the best part of everyday.

ACKNOWLEDGEMENTS

Pursing a Ph.D. is a long journey full of twists and turns. Throughout the course of this journey, we are touched by a number of individuals. I would like to express my appreciation toward those who assisted me throughout the course of this arduous journey and made it less complicated, if not easier.

I cannot express my gratitude enough to my advisor, Dr. Mi Geum Chorzepa, for her guidance, encouragement, friendship, and continuous support throughout my Ph.D. It was a privilege to work under the supervision of Dr. Chorzepa and her inspiration and influence will guide me for many years. I would like to extend gratitude to my dissertation committee member, Drs. Stephan Durham and Jason Christian for their insight, critical assessment and valuable advice.

I have been blessed with the most wonderful people in Athens. Thank you Jeff, Matt and Bettina! I'm also grateful for having such a great officemate, Amin.

Most importantly, I would like to thank my family for their unconditional love and support throughout the years, without which, I would likely not be here today. My parents, Aman and Parvin, made countless sacrifices for my success, and I simply owe them everything. I also would like to thank my wife, Sanaz, who patiently stood by me during the toughest part of this journey.

Finally, I would like to express my acknowledgement to the Georgia Department of Transportation for having funded this work.

TABLE OF CONTENTS

	Page
LIST OF TABLES	ix
LIST OF FIGURES	x
CHAPTER	
1 INTRODUCTION	1
1.1. BACKGROUND	1
1.2. LITERATURE REVIEW	2
1.3. PROBLEM STATEMENT	6
1.4. SCOPE AND OBJECTIVES	7
1.5. DISSERTATION OUTLINE.....	9
2 ANALYTICAL 3D BRIDGE MODEL.....	11
2.1. INTRODUCTION	11
2.2. MODELING OF BRIDGE COMPONENTS	12
2.3. APPLIED LOADS.....	23
2.4. SUMMARY.....	25
3 PARAMETERIZED FRAGILITY ASSESSMENT OF BRIDGES UNDER HURRICANE EVENTS USING METAMODELS AND MULTIPLE ENVIRONMENTAL PARAMETERS	26
ABSTRACT.....	26
3.1. INRODUCTION.....	27

3.2. STATE OF RESEARCH	28
3.3. RESEARCH SCOPE AND SIGNIFICANCE.....	30
3.4. PROPOSED HURRICANE VULNERABILITY ASSESSMENT METHODOLOGY	32
3.5. STAGE 1: DESIGN OF EXPERIMENT (DOE).....	33
3.6. STAGE 2: IDENTIFICATION OF THE BEST PERFORMING METAMODEL	45
3.7. STAGE 3: CONSTRUCTION OF A FRAGILITY SURFACE	50
3.8. IMPLEMENTATION OF THE PROPOSED PARAMETERIZED FRAGILITY ASSESSMENT APPROACH	52
DISCUSSION.....	58
CONCLUSIONS	59
4 Fragility Analysis of Coastal Bridges Subjected to Hurricane Forces Using Wind Speed as a Single Hazard Intensity Measure and Risk Assessment	61
ABSTRACT.....	61
4.1. INTRODUCTION	62
4.2. FRAGILITY ANALYSIS METHODOLOGY.....	65
4.3. RISK ASSESSMENT	88
4.4. IMPLEMENTATION OF THE PROPOSED RISK ASSESSMENT METHODOLOGY: COASTAL BRIDGES IN GEORGIA.....	70
4.5. CONCLUSION.....	95
5 SUMMARY AND CONCLUSIONS	97

6 FUTURE RESEARCH.....	100
REFERENCES	102
APPENDICES	
A IMPLEMENTATION OUTCOMES.....	107

LIST OF TABLES

	Page
Table 2.1. Properties of experimental testing of column section under cyclic loading.	20
Table 3.1. Bridge parameters and their probabilistic distribution.	41
Table 3.2: Bridge dimensions and other properties used to generate the fragility.	56
Table 3.3: Performance measures for seven metamodels.	57
Table 3.4: Confusion matrix from the Random Forest model.	58
Table 4.1: Probabilistic distributions of wave height, wave period and surge height	74
Table 4.2: Summary of implemented wave spectra and their parameters	82
Table 4.3: Probabilistic distributions of capacity variables and their parameters used	91

LIST OF FIGURES

	Page
Fig. 2.1: Schematic layout of the 3D OpenSees bridge model	12
Fig. 2.2: Schematic representation of (a) Elastomeric bearing	14
Fig. 2.3: Fixed (left) and expansion (right) bearings material model cyclic reactions	15
Fig. 2.4: Bearing model nodes and elements configuration.....	17
Fig. 2.5: Schematic representation of a concrete section discretized to fibers	19
Fig. 2.6: Comparison of test results vs. OpenSees model of hysteretic behaviour.....	20
Fig. 2.7: Material models and their parameters	22
Fig. 2.8: Passive response of a single pile under cyclic loading.....	23
Fig. 2.9: Response of abutment under cyclic loading in longitudinal direction	23
Fig. 2.10: Wave force components in vertical directions	24
Fig. 2.11: An example of a hurricane wave force time history in vertical direction	25
Fig. 3.1: Flowchart showing the parameterized fragility analysis procedure	34
Fig. 3.2: Wind speed (U_{10min}) vs. deck force components: Max. vertical force	37
Fig. 3.3: Storm water elevation (d_s) vs. deck force components.....	38
Fig. 3.4: Variables that affect the force components	39
Fig. 3.5: Schematic layout of the 3D OpenSees bridge model	42
Fig. 3.6: Wave force demands vs. U_{10min} and/or d_s	56
Fig. 3.7: Fragility surfaces for the studied bridge with (a) dowel connection.....	59
Fig. 3.7: Fragility surfaces for the studied bridge with (a) dowel connection.....	59

Fig. 4.1: Flowchart of the proposed risk assessment framework.....	66
Fig. 4.2: (a) Surface (b) contour of the joint probability density of wave height	75
Fig. 4.3: $F(H_{max})$ for different values of N	75
Fig. 4.4: Variation of significant wave height H_S during passage of hurricane	77
Fig. 4.5: Hurricane Ike (2008) track and intensity, while passing by the NDBC	84
Fig. 4.6: Median and quartiles of predicted storm surge elevation from SLOSH	90
Fig. 4.7: Spans, lower bound and upper bound fragility curves	93
Fig. 4.8: maximum hurricane induced wind speeds on land along GA/SC.....	95
Fig. 4.9: maximum hurricane induced wind speeds on land along GA/SC.....	95
Fig. 4.10: Mean annual rate of failure (λ_{Bridge}) of Georgia coastal bridges.....	96
Fig. 4.11: Mean annual rate of failure (λ_{Bridge}) of Georgia coastal bridges.....	96

CHAPTER 1

INTRODUCTION

1.1 BACKGROUND

Fifty eight sunken spans, 66 misaligned spans, and thousands of cars having to make a 210 km detour out of their way daily were the results of what hurricane Ivan (2004) wrath left behind, when passing over 4.1 km long Interstate 10 bridge, spanning Escambia Bay, in September 2004 (Douglass et al. 2004).

The Escambia Bay bridge was not the only bridge that has been severely damaged by a hurricane. In fact, hurricanes and other severe storms have repeatedly proven themselves to be one of the major threats to coastal transportation infrastructure throughout the world, particularly to bridges. Hurricanes Katrina and Rita in 2005, as two of the most intense Atlantic hurricanes, inflicted devastating damage to highway bridges in Florida, Alabama, Mississippi, Louisiana and Texas (Cauffman 2006). Some of the major bridges that suffered significant damage from these hurricanes include bridges over Lake Pontchartrain, I-10 twin span bridges, US-11 bridge, Norfolk Southern Railroad bridge, Lake Pontchartrain Toll Causeway, bridges over St. Louis Bay, US-90 bridge, CSX Railroad bridge, bridges over Biloxi Bay and Back Bay, I-110 bridge including ramps, Popp's Ferry bridge, and bridges over Mobile Bay (Cauffman 2006). Hurricane Ike in 2008 caused notable damage to bridge structures in Houston/Galveston regions of Texas (Stearns and Padgett 2011). There are approximately 36,000 bridges within 30 km of the US coasts, out of which more than 1,000 bridges remain susceptible to similar damage.

The overall cost to restore or rebuild damaged bridges after Hurricane Katrina alone, was estimated to exceed \$1 billion (Padgett et al. 2008). Hurricane death toll rates are usually much lower than those of earthquake's, because vulnerable regions are evacuated well ahead of hurricane landfall. However, past hurricane events have clearly demonstrated that the economic and social impacts to the communities recovering from a disaster are excruciating and unsustainable. Any loss of functionality in transportation networks will disrupt the post-disaster response and recovery operations in the near term and will lead to slow economic and social development of affected regions in the long run.

Near 50% (153 millions) of the US population currently live within 80 km of coastline and over the half of the US economic productivity is located within coastal regions. There are nearly 60,000 miles of roads in these regions which are susceptible to tropical storms and hurricane induced surges and waves (Douglass and Krolak 2008). Coastal communities along the Eastern U.S. and Gulf coasts have learned through experience how vulnerable their transportation infrastructure is to hurricane impact, but such experience may not be the most efficient way to learn these important lessons.

1.2. LITERATURE REVIEW

In the wake of above mentioned facts, there has been a surge in the number of studies investigating the vulnerability of coastal bridges to hurricane hazard in the last decade. Several studies focused on the derivation of wave and surge forces on bridge structure by extending the available methods from the offshore industry. The effect of wave and surge forces on offshore structures has been extensively studied in the literature. Kaplan (Kaplan 1992; Kaplan et al. 1995) proposed theoretical equations for predicting wave forces on offshore platform structures by extending Morrison's equation (Morison et al. 1953) which

was originally developed to describe wave forces on piles. While these equations prove fruitful, they are not directly applicable to coastal bridges since the bridges are often built over relatively shallower water with much shorter wave periods and lengths than that of offshore structures. Moreover, the structure-to-wavelength ratio is not analogous.

Marin and Sheppard (Marin and Sheppard 2009; Sheppard and Marin 2009) developed a set of equations to quantify wave forces and moments on bridge superstructure by modifying Kaplan's equations. They modified the change of added mass term and incorporated the effect of trapped air between water surface and bottom surface of the deck section. Within these equations drag, inertia coefficients, and slamming force parameters were empirically derived.

Following the hurricane Ivan (2004) and Rita (2005), the Federal Highway Administration (FHWA) and ten U.S. states conducted a research study whose results were published in the AASHTO "Guide specification for bridges vulnerable to coastal storms" in 2008, hereafter referred to as the 'AASHTO guide' (Kulicki and Mertz 2008). AASHTO guide recommends using Marin and Sheppard equations for wave force calculations. A series of tests were later conducted to examine the influence of wave height, wave period, and water elevation on exerted forces on a 1:5 scale reinforced concrete (RC) bridge superstructure with a "variable transverse stiffness support system" (Bradner et al. 2010). It was concluded that the quasi-static vertical and horizontal forces determined by the equations in the AASHTO guide reasonably agree with the experimental results when water elevation is lower than the superstructure's low chord. Yet, the equations over-predict the total vertical forces once the superstructure is partially submerged by a storm surge based on this experimental study.

Douglas et al. (Douglass et al. 2006) proposed another set of equations for predicting lateral and vertical wave forces on bridge superstructures by modifying McConnell's (McConnell et al. 2004) method which was originally developed for finding wave forces on jetties. They suggested that the maximum vertical and horizontal wave forces could be expressed as a linearly increasing function of apparent hydrostatic forces. In another study, Cuomo et al (Cuomo et al. 2009) conducted laboratory tests on a *1:10* scale bridge model to quantify wave loads on coastal bridges. They investigated the effect of entrapped air and openings on the magnitude of the quasi-static and impulsive forces in their tests. Serinaldi and Cuomo (Serinaldi and Cuomo 2011) applied statistical models to the measured experimental results and made practical recommendations for quantifying impulse forces from wave impact maxima and rise times.

Recent studies on the wave force quantification also include numerical methods to investigate wave-structure interactions. Huang and Xiao (Huang and Xiao 2009) applied the finite difference method to solve a wave-deck interaction model based on Reynolds averaged Navier–Stokes equations and validated their model with experimental results from a test on a horizontal platform. Implementing their model, they illustrated that the I-10 bridge deck failure over Escambia bay was attributed to the vertical uplifting forces being greater than its overall deck weight. In addition compared their model with Douglas et al. (Douglass et al. 2006) and Bea et al. (Bea et al. 2001) parametric equations and concluded that both Douglas and Bea equations overestimate the horizontal and vertical wave forces. Jin and Meng (Jin and Meng 2011) developed two numerical models to characterize the wave-deck interaction: (1) a flow-3D model and (2) a 2D potential flow model. 2D model was verified with 3D models. Once validated, parametric studies were

performed using the 2D model. Simple equations were then derived for quantifying wave forces in horizontal and vertical directions. They suggested that the AASHTO equations and McConnell model yield conservative results, compared to their model. Bozorgnia and Lee (Bozorgnia and Lee 2013) implemented the finite volume numerical method on the Navier Stokes equation to simulate wave forces on a 1:5 scale model of the I-10 bridge. They concluded that their results are compatible with experimental data from Oregon state's laboratory tests (Bradner et al. 2010). They suggested that, neither compressibility of the air nor assuming water as a viscous fluid, has a major effect on the wave forces.

A number of studies focused on hurricane wave and surge prediction by means of hurricane hindcasting. Chen et al. (Chen et al. 2007) coupled ADCIRC surge model and SWAN wind wave model to simulated landfall of hurricane Georges (1989) and concluded that surge hydrographs obtained from the model were in good agreement with measured data. ADCIRD+SWAN has been used in a number of other studies for hurricane surge and wave estimation (Dietrich et al. 2011; Sebastian et al. 2014) . National Weather Center (NWS) developed the Sea, Lake and Overland Surge from Hurricanes (SLOSH) model for surge height prediction. SLOSH provides various products including the Maximum of the Maximum Envelope of High Water (MOM) data, which determines the worst case scenario surge height for a particular hurricane category at each location.

There are only a few studies on probabilistic analysis of bridges exposed to hurricane hazard. Ataei and Padgett proposed a fragility analysis method in which fragility of each bridge was separately assessed (Ataei and Padgett 2012). The two hurricane Intensity Measures (IM) selected in their study are: the maximum wave height, H_{max} , and distance between storm water elevation and deck low chord elevation, Z_c . Kameshwar and

Padgett (Kameshwar and Padgett 2014) proposed a surrogate modelling approach for multi-hazard fragility analysis and risk assessment of bridges vulnerable to seismic and hurricane hazards. Mondoro et al. (Mondoro et al. 2016) proposed a risk management strategy in which both deteriorating conditions of bridges under repeated traffic loads and repair/retrofit actions performed to mitigate hurricane hazard are considered through a multi-objective optimization algorithm.

1.3. PROBLEM STATEMENT

Any risk mitigation strategy to reduce the hurricane impact on coastal bridges in a region requires a comprehensive reliability analysis and risk assessment study. This helps decision makers to identify their most critical bridges and assign their resources to their most critical assets. Furthermore, a risk assessment can contribute to the establishment of Disaster Recovery and Redevelopment Plans.

It is extremely important to understand how hurricanes will likely impact transportation infrastructure networks to include quantifying the magnitude and extent of expected damage across the transportation system, predicting structural resilience for specific at-risk or mission critical bridges, estimating loss of system capacity through the network grid, and planning to mitigate infrastructure or operational vulnerabilities.

Despite recent advances in the field, a comprehensive framework for reliability analysis and risk assessment and risk-based scoring of bridges is not available in the literature.

1.4. SCOPE AND OBJECTIVES

This study introduces a novel risk assessment framework for coastal bridges subjected to hurricane hazard. The proposed framework is intended to evaluate the following integral:

$$\lambda_{Bridge} = \int_{IM=0}^{\infty} -P_f(IM) \frac{dG(IM)}{dIM} dIM \quad (1.1)$$

In Eq. (1.1), λ_{Bridge} is the mean annual rate of bridge failure caused by hurricane hazard; IM is a hurricane hazard intensity measure; $P_f(IM)$ is the fragility function; and $G(IM)$ is the hurricane hazard curve.

Eq. (1.1) is in fact an extension of Pacific Earthquake Engineering Research Center (PEER) Performance Based Earthquake Engineering (PBEE) framework (Porter 2003) for hurricane hazard, which quantifies the risk (λ_{Bridge}) by incorporating the uncertainties of variables that define the hurricane hazard, structural demand imposed on a bridge by the hurricane, and capacity of the bridge against hurricane forces.

Evaluation of Eq. (1.1) requires defining quantitative measures for damage, demand, capacity, and hazard intensity. The first step in this study involves identification and characterization of the damage state to design the risk analysis framework. Surveying of available literature revealed that most severely damaged bridges during past hurricanes were simply supported with insufficient vertical connections between superstructure and substructure whose spans were uplifted or shifted by hurricane waves (Okeil and Cai 2008; Padgett et al. 2008; Robertson et al. 2007). Therefore, a single damage state is defined herein and is quantified as a binary variable which takes 1 when bridge is uplifted/shifted and 0 otherwise. The fragility function, $P_f(IM)$ in Eq (1.1), is determined from the

evaluation of the damage state by comparing the demand and capacity of bridge spans for incremental values of IM.

In this dissertation, the fragility function is defined by Eq. (1.2), in which D and C are the demand and capacity of bridge spans, respectively.

$$P_f(IM) = P[D - C > 0 | IM] \quad (1.2)$$

Two different approaches are proposed for fragility analysis of bridges vulnerable to hurricane hazard. In the first method, namely ‘parameterized fragility analysis’, implementation of metamodels for hurricane fragility analysis of bridges is proposed. A computer experiment is arranged based on the Design of Experiment (DoE) principles to generate bridge models and hypothetical hurricane scenarios.

An inventory of coastal bridges in the state of Georgia (U.S.A) is created by a GIS analysis of surge prone regions. As-built and construction plans of identified bridges are investigated to obtain statistical distributions of bridge parameters. A parametric Finite Element model is developed in OpenSees for nonlinear dynamic analysis of bridges. An OpenSees model is developed based on the work of Nielson and Ataei and was specifically configured to capture the bridge deck unseating damage state using contact elements. Various binary metamodels in terms of classification accuracy was compared, and the Random Forest method is identified to be the most accurate.

Two new intensity measures (IM), storm water elevation and wind speed, were proposed for fragility analysis, and fragility surfaces of all identified bridges in the inventory are obtained. It is concluded that the proposed method generates conservative approximation of bridge fragilities since it uses conservative values for wave parameters

to obtain wave forces, in accordance with the AASHTO Guide Level I analysis method, and thus the need for improvement and the second method.

The second proposed method is a single IM fragility analysis procedure with significantly lower computational cost and accuracy. The investigation of Georgia's coastal bridges revealed that a majority of bridges in the inventory have simply supported spans with dowel or anchor bolt tie-downs between the superstructure and substructure, which makes them the most vulnerable class of bridges against hurricane forces as shown in the past events. The proposed approach is developed suitable for fragility analysis of this class of bridges, where there is limited or no vertical super/substructure connections and deck unseating/shifting is the most probable mode of failure. A novel procedure is introduced in this method to incorporate the uncertainty of extreme wave heights and wave period in calculation of forces by deriving their probabilistic distributions from wave spectral density, as suggested by AASHTO Level III method.

1.5. DISSERTATION OUTLINE

This dissertation is organized in 7 chapters. A brief review of each chapter is provided here:

Chapter 2 presents parametric finite element modeling of bridges in OpenSees. Details of materials and element types for various bridge components is discussed. Implementation of contact elements to capture the unseating/shifting failure of bridge deck is described.

Chapter 3 describes the application of metamodels for fragility analysis of bridges. 7 binary classification methods are introduced and applied to predict the response of bridges subjected to hurricane wave forces. Accuracy of the methods is compared in terms of

misclassification measures to find the most accurate method. Implementation of the proposed method is illustrated.

Chapter 4 proposes an efficient risk assessment and fragility analysis method. Probabilistic description of extreme wave height and wave period is discussed. The hurricane hazard curve is derived and convolved with fragility functions to obtain the risk. The proposed method is implemented for risk assessment of coastal bridges in the state of Georgia, U.S.A.

Chapter 5 summarizes the findings of this dissertation.

Chapter 6 provides recommendations for future research.

Appendix A Provides the implementation outcomes of the proposed method for risk assessment of Georgia coastal bridges.

CHAPTER 2

ANALYTICAL THREE-DIMENSIONAL MODELING OF BRIDGES

2.1. INTRODUCTION

Fragility is a conditional statement which determines the probability of the demand placed on the structure exceeding the structural capacity conditioned on a hazard intensity measure. To determine the demand placed on a bridge subjected to hurricane hazard, analytical simulations must be performed.

Simulating and characterizing the deck unseating/shifting failure mode of coastal bridges subjected to hurricane wave forces through a numerical model is complicated due to the rigid body motion of the bridge deck when it is dislodged from bearings.

In this chapter, an analytical modeling of bridge structures is discussed. A parametric finite element model is developed in OpenSees (Mazzoni et al. 2006) on the basis of previous studies by Nielson and Ataei (Ataei 2013; Nielson 2005). OpenSees (the Open System for Earthquake Engineering) is an open-source finite element modeling software framework with inclusive material and element libraries.

Fragility analysis requires generating and simulating numerous samples from the possible range of random variables associated with the demand, capacity and hazard. The parametric OpenSees model developed in this study is able to generate and simulate a large number of bridge models with varying geometry and material properties and under different hurricane scenarios once the distribution function of the random variables is provided.

2.2. MODELING OF BRIDGE COMPONENTS

Figure 2.1 illustrates a schematic representation of an OpenSees model for a 3-span pile-bent bridge. Material models, element types, applied loads and capacity of bearings are provided in this section.

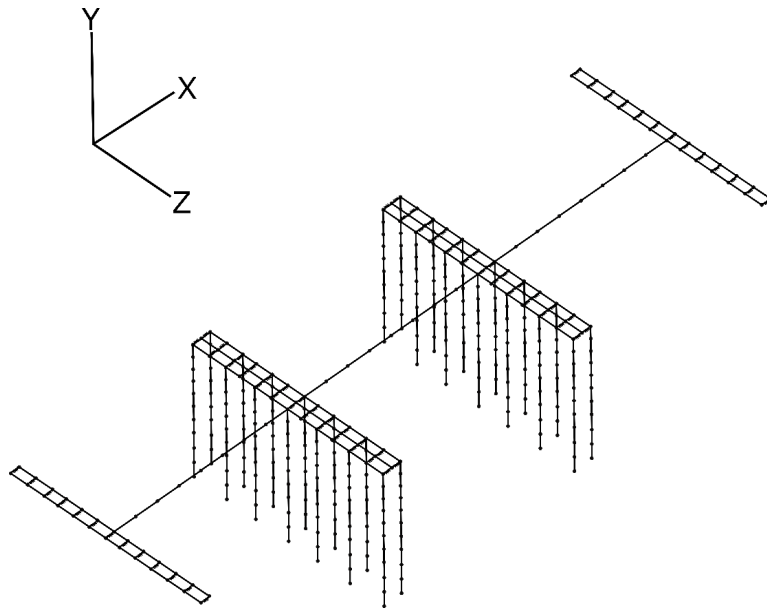


Fig. 2.1. Schematic layout of the 3D OpenSees bridge model

2.2.1. BRIDGE DECK

The bridge superstructure is modeled using ‘*elastic beam-column*’ elements. The literature has indicated that a nonlinear deck section analysis is not necessary for hurricane loading because deck unseating is the most likely failure mode (Padgett et al. 2008; Stearns and Padgett 2011). Therefore, an elastic section is used to represent the rigid body motion of the superstructure. The deck section properties such as mass per unit length, moments of inertia, and area are assigned to the elastic deck.

2.2.2. ELASTOMERIC BEARING

Bearing connections are provided to control the mechanism by which forces are transmitted from superstructure to substructure. After reviewing as-built plans of existing Georgia coastal bridges it was determined that elastomeric bearings are the most common type of bearings used. This type of bearings consists of an elastomeric bearing pad, anchored to the substructure by means of anchor bolts or dowels (see Fig. 2.2 (a)).

The mechanism by which forces are transmitted from superstructure to substructure in horizontal direction is similar in these two bearing set-ups, however, dowel type bearings are not designed to provide any vertical resistance, unlike anchor bolts. Fig. 2.2. Illustrates typical dowel and anchor bolt bearing connection types details and schematic representation of their material models. Modeling of the bearing behavior in shear and tension is provided in the following section.

2.2.2.1 SHEAR

Shear response of elastomeric pads and anchor bolts/dowels are first individually modeled and their composite behavior is then obtained by parallelizing their individual material models.

Steel01 material models is used for elastomeric pads (Fig. 2.2. (d)). The initial stiffness of the elastomeric pads (K_i) is determined by the following equation (Choi 2002):

$$K_{shear} = \frac{GA}{h} \quad (2.1)$$

In which G, A and h are initial stiffness, shear modulus, are and thickness of the elastomeric pad. Different value for G can be found in the literature (Itoh and Gu 2009; Nielson 2005). A and h are extracted from bridge drawings.

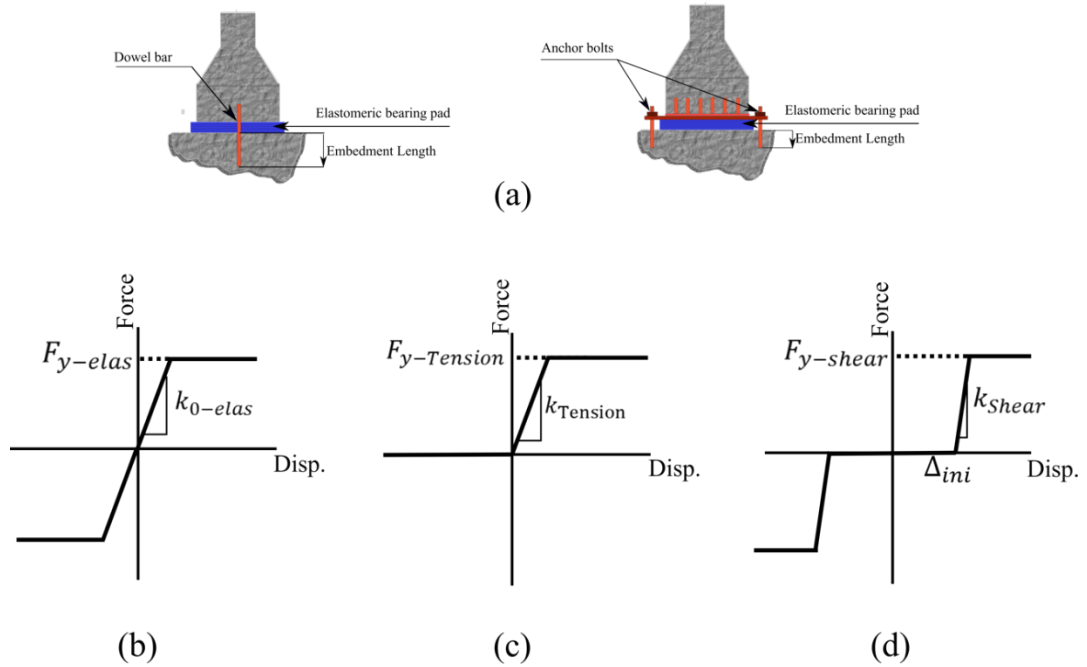


Fig. 2.2. Schematic representation of (a) Elastomeric bearing connections with dowel and anchor bolts (b) Anchor bolts/dowel material model in shear (*Hysteretic*) (c) Anchor bolts/dowel material model in tension (d) Elastomeric bearing material model (*Steel01*)

The friction force threshold (sliding threshold) of girder-pad contact surface is deemed as the yield point of the elastomeric pad material model ($F_{y-shear}$ in Fig. 2.2. (d)). The coefficient of friction between a girder surface and bearing pad is given by the equation (2.2):

$$\mu_{Girder-Elastomer} = 0.05 + \frac{0.4}{\sigma_{normal}} \quad (2.2)$$

In which $\mu_{Girder-Elastomer}$ is the coefficient of friction and σ_{normal} is the normal stress in MPa. The yield force, $F_{y-shear}$, is given by equation (2.3):

$$F_Y = \mu_{Girder-Elastomer} N \quad (2.3)$$

In which N is the normal force.

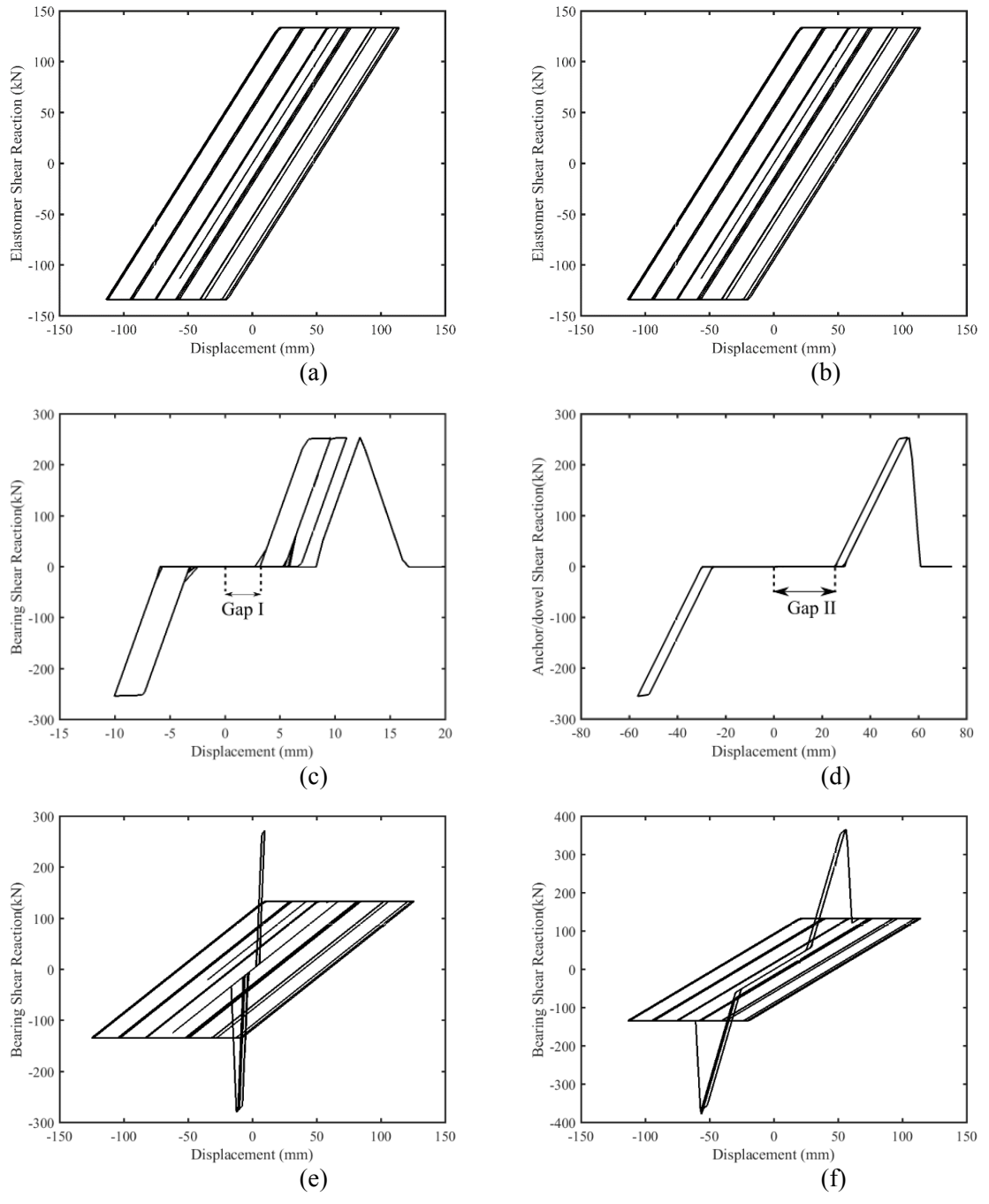


Fig. 2.3. Fixed (left) and expansion (right) bearings material model cyclic reactions (a),(b) Elastomeric bearing (c),(d) Anchor bolts (e), (f) composite reaction

To model the gap between the bearing hole edge and anchor bolts/dowel, an initial gap (Δ_{ini}) was defined in the dowel/anchor material model backbone. For fixed bearings, considered gap size in both directions is 3.2mm. For expansion bearing this gap is considered to be 25.4mm in longitudinal direction and 3.2mm in transverse direction.

Shear response of anchor bolts/dowels is modeled by *Hysteretic* material model (Fig. 2.2. (b)). Ultimate shear strength of the dowels/anchors (F_{y-elas}) are determined in accordance to the ACI 318-14 (ACI 2014).

Bearing are modeled as '*Zerolength*' elements. The parallelized material model for the composite reaction of bearings in shear is assigned to the '*Zerolength*'. Shear force vs displacement envelope of the fixed and expansion bearings under cyclic loading is presented in Fig. 2.3.

2.2.2.2 TENSION

While the dowels provide no vertical resistance against uplifting forces, anchor bolts on the other hand tie the bridge deck to the substructure. Reaction of anchor bolts to tension forces is modeled by a *Hysteretic* material model.

Elastomeric bearing in this study are specifically modeled to capture the unseating/shifting of a bridge superstructure. Once uplifting wave forces overcome the vertical capacity of the deck, and dislodge the deck from the superstructure, deck undergoes a rigid body motion (Ataei 2013). This causes the stiffness matrix to become singular and a unique solution for the displacement can't be found. To overcome the issue, *zeroLengthContact3D* elements were implemented to build an interface between the deck and substructure nodes. B1 and B2 in Fig. 2.4. show the configuration of '*Zerolength*' and *zeroLengthContact3D* in bearings. *ZeroLengthContact3D* also allow

for modeling the progressive collapse of bearings by preventing the penetration of deck nodes into substructure elements.

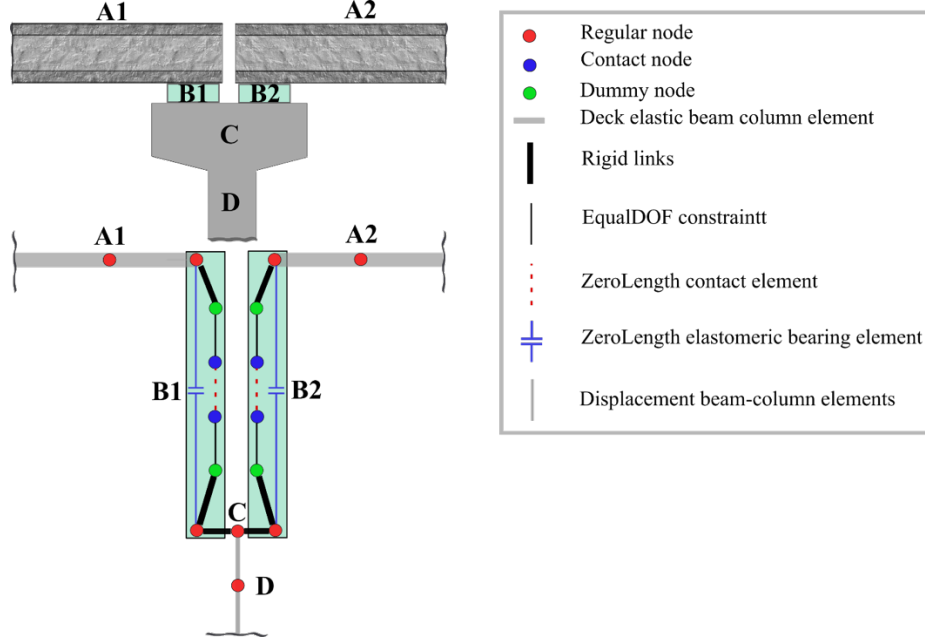


Fig. 2.4. Bearing model nodes and elements configuration

The ultimate strength of bolts ($F_{y-Tension}$ in Fig. 2.2. (c)) is deemed as the minimum of anchor yield strength, anchor pull out strength and concrete breakout force in accordance to the *ACI 318-14*. Stiffness of the bolt group $k_{Tension}$, is defined by Eq. (2.4):

$$k_{Tension} = n_{AB-D} \left(\frac{E_s A_{se,N}}{L_{emb}} \right) \quad (2.4)$$

where E_s is the elastic modulus of steel, n_{AB-D} is the number of anchor bolts per bearing, $A_{se,N}$ is the effective area of a single anchor bolt, and L_{emb} is the anchor embedment length into the substructure (i.e., concrete). Shear stiffness of anchor bolts group (k_{0-elas} in Fig. 2.2. b) is determined by Eq. (2.5),

$$k_{0-elas} = n_{AB-D} \left(\frac{37}{32} \right) \left(\frac{G_s A_{se,N}}{L_{emb}} \right) \quad (2.5)$$

Where G_s is the shear modulus of steel.

2.2.3 CONCRETE SECTIONS: PILES, COLUMNS AND CAP BEAMS

Concrete members (piles, columns, cap beams) are modeled using the ‘*Displacement-based beam-column*’ element. Each element is discretized into a fiber section for a nonlinear section analysis. Due to similar representation, a fiber section of a pile represents the discretization of a pile cross section into fibers, including reinforcing steel layers as illustrated in Fig. 2.5. The fiber section analysis allows for monitoring of the stress-strain response at any of the fiber locations. Each concrete section consists of three zones: Cover, Core and reinforcing steel. “Unconfined concrete” and “confined concrete” material models, were assigned to cover and core sections respectively. Schematic representation of a concrete section is shown in Fig. 2.5. *Concrete02* (Mazzoni et al. 2006) material model from OpenSees library was used to model the concrete fibers. Past studies have shown that concrete strength and ductility increases when confined by transverse reinforcement (Mander et al. 1988). To reflect this effect in the model, compressive strength and strain of the unconfined concrete was defined first, then a modification factor was used to obtain the compressive strength and strength of the confined concrete. This modification factor is a function of “The ratio of volume of steel hoops to volume of concrete core (ρ_s)” and “The ratio of the yield strength of the steel hoops to the unconfined concrete compressive cylinder strength (f_{yh}/f'_c)”.

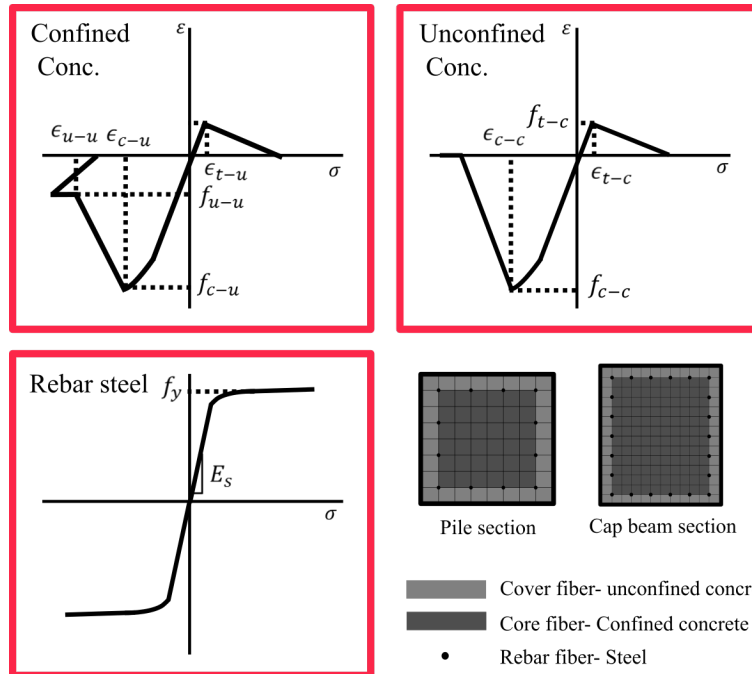


Fig. 2.5. Schematic representation of a concrete section discretized to fibers and its material model[see (Mazzoni et al. 2006) for parameters]

2.2.4 REINFORCING STEEL MODEL

The reinforcement is assumed fully bonded to the concrete substrate, and the steel fibers are represented by the *Steel02* (Spacone et al. 1996) material model from OpenSees library, as shown in Fig. 2.5. .

To validate the concrete sections, experimental test data from the PEER Structural Performance Database was extracted (Berry et al. 2004). Test properties are shown in Table.2.1. As shown in Fig. 2.6, despite some discrepancies in unloading/reloading stiffnesses, analytical forces and displacements at each cycle are in good agreement with test results.

Table 2.1. Properties of experimental testing of column section under cyclic loading

Type	Circular column with spiral transverse reinforcement
Concrete Strength	36.5MPa
Transverse steel yield stress	691.5MPa
Longitudinal steel yield stress	458.5MPa
Column diameter	406mm
Length	1854.2mm
Test configuration	Cantilever
Axial load	0
Diameter of longitudinal reinforcement	12.7mm
Number of longitudinal bars	12
Reinforcement ratio	0.0117
Diameter of spiral reinforcement	4.5mm
Hoop spacing	31.8mm
Distance between outer surface of column and center of spiral reinforcement	15mm
Volumetric transverse reinforcement ratio	0.53

*Fig 2.3. include the monotonic stress-strain relationship used for confined and unconfined concrete elements.

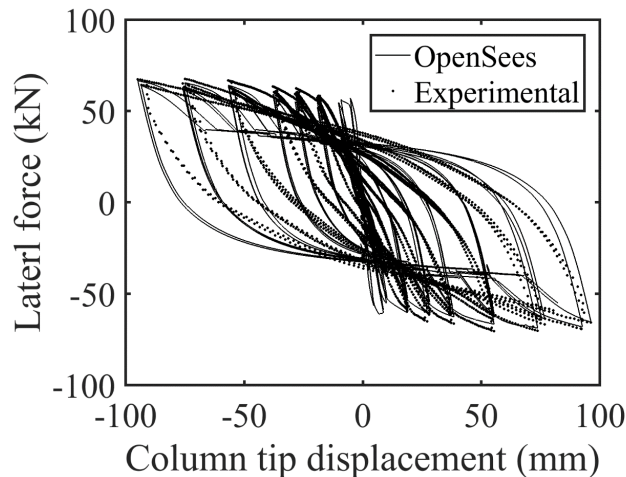


Fig. 2.6. Comparison of test results vs. OpenSees model of hysteretic behaviour of a column under cyclic loading

2.2.5 ABUTMENT

Pile-bent types shown in Fig .2.9(a) are common in the state of Georgia coastal area and are considered in this study. There are two major components that contribute to horizontal resistance in pile-bent abutments. These are the capacity of piles and backfill soil pressure as shown in Fig. 2.9(b) and (c). While piles provide shear resistance in any

direction, passive backfill soil pressure only engages when the abutment applies pressure against the soil.

Both the response of the piles and embankment from passive soil pressure is represented by a 'Hysteretic' material model from the OpenSees library, as shown in Figs. 11 (b) and 11(c). These two force-displacement relationships are parallelized to obtain the abutment response in the longitudinal and transverse directions. The initial soil stiffness applied on the abutment is assumed 14.4~28.7 kN/mm/m (per each meter of abutment width) based on the recommendation made by Caltran (Caltrans 2008). The ultimate soil pressure is assumed 239 kPa based on available full-scale abutment tests conducted by Caltran (Maroney 1995). The ultimate abutment passive resistance is determined by Eq. (2.6) :

$$P_3 = h \times w \times 239 \text{ kPa} \times \left(\frac{h}{1.7 \text{ m}} \right) \quad (2.6)$$

Where w and h are width and height of abutment respectively. This study employs a quad-linear model for abutment passive resistance. Nielson (Nielson 2005) proposed an equation based on this finding to calculate the ultimate deformation of the abutment. This equation, with some modification on initial stiffness range, is used in this study:

$$\Delta_{3Abu} = \left(0.06 + \left(\frac{K_1 - 14.35}{28.7 - 14.35} \right) (0.04) \right) \times h \quad (2.7)$$

The deformation at first and second yield (Δ_{1Abu} and Δ_{Abu2}) is presumed to be 5% and 25% of Δ_{3Abu} respectively. The force at the first yield is obtained by multiplying $K_{Abument}$ by the Δ_{1Abu} :

$$F_{1Abu} = K_{Abument} \times \Delta_{1Abu} \quad (2.8)$$

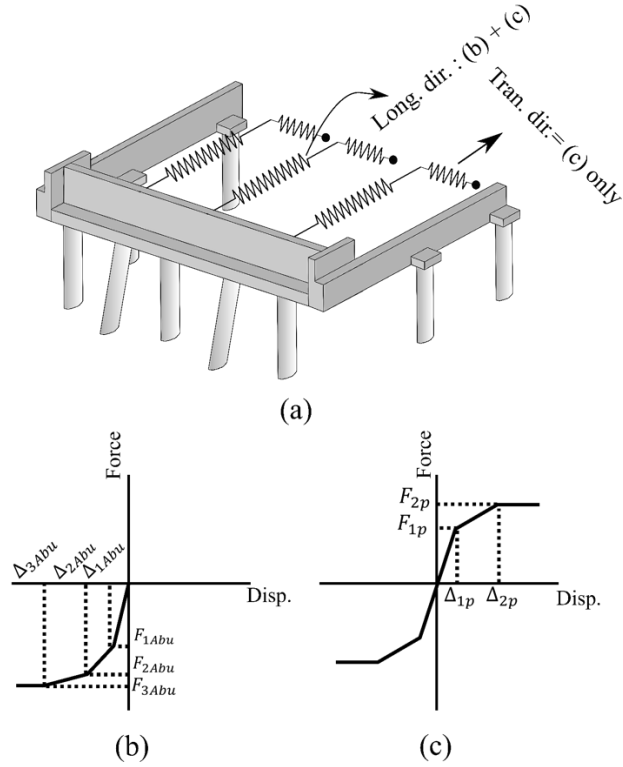


Fig. 2.7. Material models and their parameters (a) Bearing (b) Abutment (c) Bents

And the force at the second yield, F_{2Abu} , is given by:

$$F_{2Abu} = F_{1Abu} + 0.55(F_{3Abu} - F_{1Abu}) \quad (2.9)$$

This study applies a tri-linear material model for piles at abutments. The initial stiffness, ultimate capacity and ultimate tip displacement of the piles is assumed to be 7kN/mm/, 119kN and 25.4mm respectively. Defined material model for the piles includes two levels of stiffness degradation before reaching to perfect plastic stage. First yielding (Δ_{1p} , F_{1p}) records the yielding of the soil surface and second (Δ_{2p} , F_{2p}) corresponds to piles becoming plastic. The first yielding point is presumed to occur once pile tip displacement reaches 7.62mm (30% ultimate pile tip displacement) and associated force is assumed to be 70% ultimate pile capacity.

Individual and composite response of piles and abutment is shown in Figs. 2.8 and 2.9. respectively.

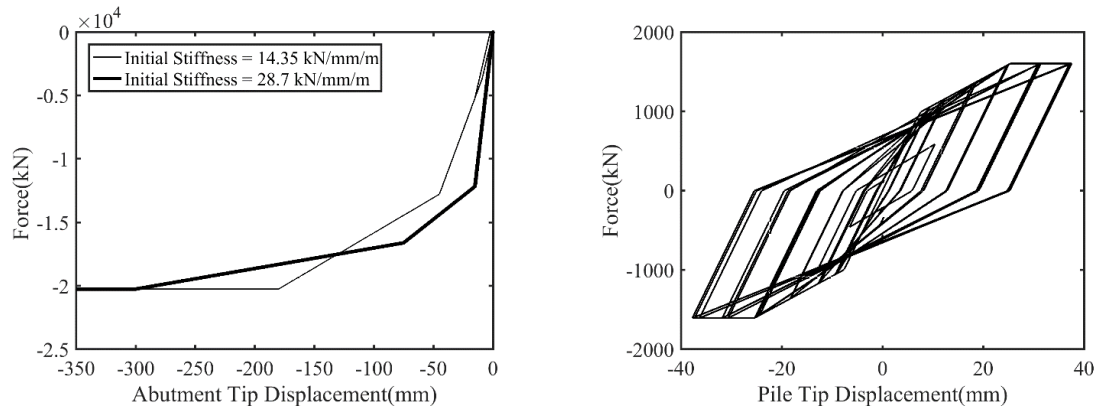


Fig. 2.8. (a) Passive response of a single pile under cyclic loading (b) Passive response of abutment under longitudinal loading

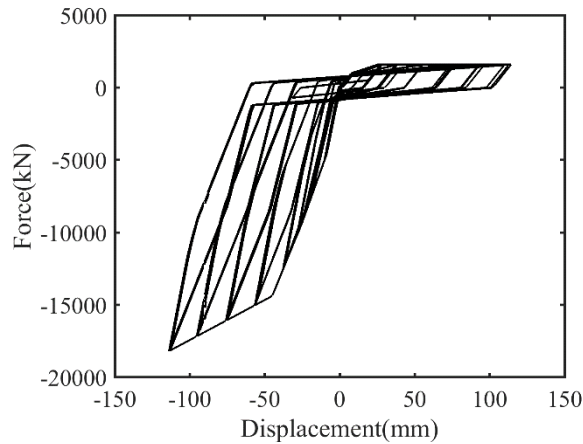


Fig. 2.9. Response of abutment under cyclic loading in longitudinal direction

2.3. APPLIED LOADS

2.3.1 GRAVITY LOAD

A static gravity-load analysis is conducted, followed by a dynamic time history analysis during which vertical and horizontal forces are applied as line loads on the deck

elements. Overturning moments, which are generally produced by the eccentricity of the vertical forces, are calculated at each time step and applied to the deck section.

2.3.2 HURRICANE-INDUCED SURGE AND WAVE LOADS.

In modeling the failure behavior, a time-history analysis is necessary so as to characterize the inelastic behavior of different bridge components that are damaged or fail by hurricane induced wave loading. Therefore, a time history of the wave force must be defined.

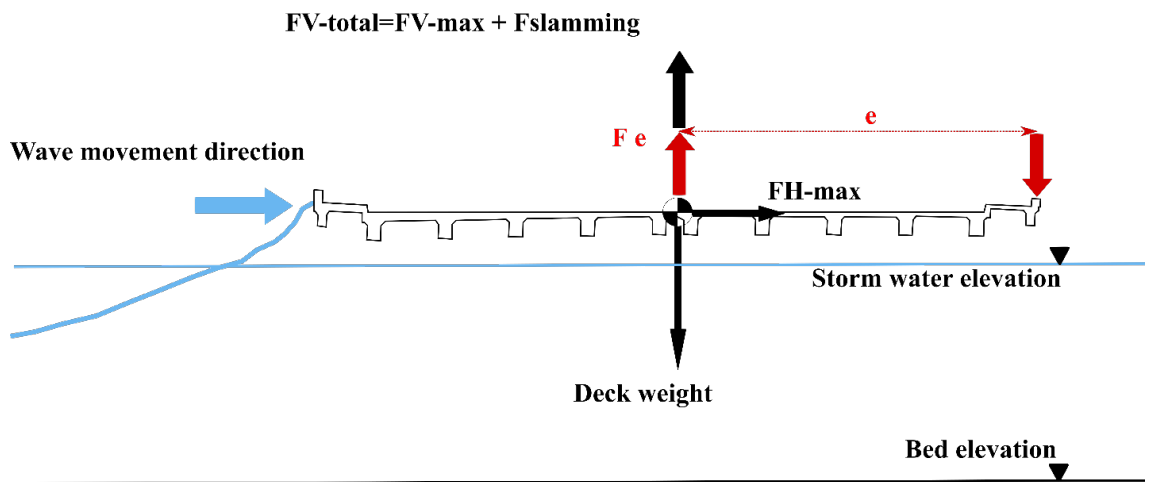


Fig. 2.10. Wave force components in vertical directions

The maximum vertical and horizontal wave forces acting on a bridge superstructure are determined by the AASHTO guide in this study (Kulicki and Mertz 2008). This study uses a sinusoidal time history of the horizontal wave forces as shown in Fig. 2. 11. The wave period and maximum horizontal force for the sinusoidal time history is determined by the AASHTO guide. In the case of the vertical force-time history, a quasi-static time

history is applied based on the maximum vertical force computed using the AASHTO code. In applying an impulse load history, the number of pulses are equivalent to the number of air chambers (or number of voids between bridge girders). Overturning moments are applied to the bridge deck section for varying eccentricities, which is illustrated in Fig. 2.10.

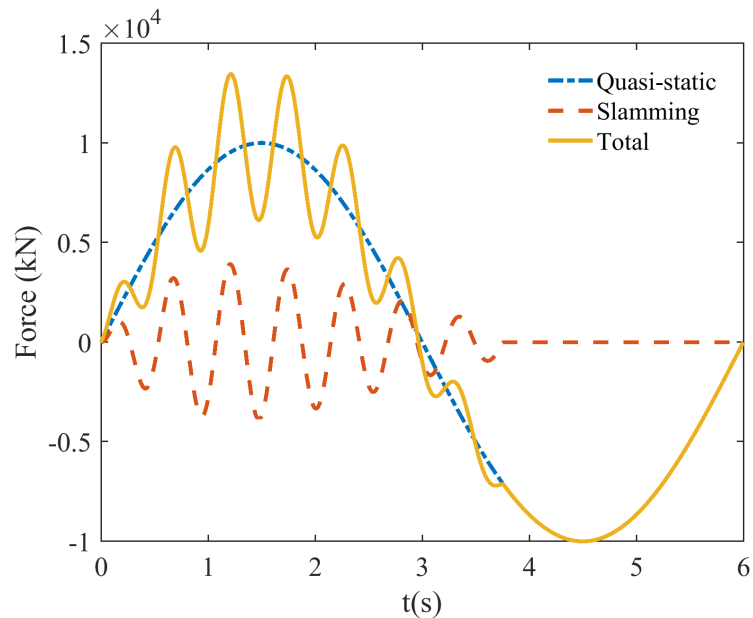


Fig. 2.11. An example of a hurricane wave force time history in vertical direction

2.4. SUMMARY

Details of parametric finite element model used in this study in order to determine response of bridges subjected to hurricane wave forces were provided in this section. Material models and element types of different bridge components were discussed. Implementing '*ZeroLengthContact3D*' for modeling the rigid body motion of bridge superstructure caused by hurricane forces was described.

CHAPTER 3
PARAMETERIZED FRAGILITY ASSESSMENT OF BRIDGES UNDER
HURRICANE EVENTS USING METAMODELS AND MULTIPLE
ENVIRONMENTAL PARAMETERS¹

ABSTRACT

A vulnerability assessment of coastal bridges under hurricane events will be beneficial to policy makers prioritizing their critical assets for inspection, maintenance, and retrofit plans. The proposed parameterized fragility assessment effectively builds a relationship between the hurricane hazard intensity/bridge parameters and bridge response by implementing a meta-modeling approach, and produces a fragility surface which describes the probability of failure in terms of two hazard intensity measures: wind speed and water elevation. These multiple environmental parameters are practical indicators of hazard intensity and a key element of the proposed approach. The independent variables comprise of bridge material/geometric parameters as well as hazard intensity parameters, and the output parameters represent a binary classification of bridge failure or no-failure states. The proposed approach is used in a vulnerability assessment of Georgia's coastal bridges using three-dimensional finite element models. One thousand and five hundred statistical samples are generated using a range of parameters determined from common bridge types to study seven meta-models. The results indicate that the Random Forest model is the most

¹ A. Saeidpour, M. G. Chorzepa, J. K. Christian and S.A. Durham Submitted to *Journal of Infrastructures Systems*, 6/19/2016.

suitable in predicting hurricane-induced failure, and that fragility surfaces are successfully created for two hazard intensity parameters.

3.1 INTRODUCTION

Hurricanes and other severe storms have proven themselves to be one of the major threats to transportation assets throughout the world, particularly to bridges located along the coastlines. There are nearly 60,000 miles of roads located along the coastal regions of the United States susceptible to tropical storms and hurricane induced surges and waves (Douglass et al. 2006). Bridges as key components of transportation networks have shown to be one of the most vulnerable assets to these natural hazards. A large number of bridges along the Gulf coast of U.S. suffered severe damage during recent hurricanes such as Ike, Ivan, Katrina, and Rita. These events have raised a national awareness of infrastructure resilience and reliability of transportation networks vulnerable to severe weather events. For instance, the interstate (I-10) bridge over Escambia Bay in Florida suffered significant damage from Hurricane Ivan in September 2004, resulting in a loss of 63 spans and dislocation of 52 others (Sheppard and Marin 2009). The bridge was closed to traffic for nearly two months. Hurricanes Katrina and Rita in 2005, as two of the most intense Atlantic hurricanes, inflicted devastating damage to highway bridges in Florida, Alabama, Mississippi, Louisiana, and Texas. Some of the major bridges that suffered significant damage from these hurricanes include bridges over Lake Pontchartrain, I-10 twin span bridges, US-11 bridge, Norfolk Southern Railroad bridge, Lake Pontchartrain Toll Causeway, bridges over St. Louis Bay, US-90 bridge, CSX Railroad bridge, bridges over Biloxi Bay and Back Bay, I-110 bridge including ramps, Popp's Ferry bridge, and bridges over Mobile Bay (Gutierrez et al. 2006).

Past events have clearly demonstrated that the economic and social impacts to the community are excruciating (Padgett et al. 2008). Any loss of functionality in transportation networks will hinder the post-event emergency services and recovery efforts in the near term and will slow down economic and social development of affected regions in the long run. It has been estimated that there are 36,000 bridges within 15 nautical miles of the US coasts, out of which more than 1,000 bridges remain susceptible to similar damage (Douglass and Krolak 2008). This study presents an effective vulnerability assessment approach for coastal bridges under hurricane events using multiple hazard intensity and bridge parameters. Finally, the proposed approach is implemented to assess a vulnerability of Georgia's coastal bridges.

3.2 STATE OF RESEARCH

The current state of research on the vulnerability assessment of bridges is included in this section, leading to a literature review of fragility analysis models.

3.2.1 LITERATURE REVIEW

Fragility models provide a measure of structural reliability used to assess the vulnerability of different types of structures, including bridges, subjected to various hazards such as hurricanes and earthquakes. Reliability analysis methods generally provide necessary information for risk-based decision making considering all aleatory and epistemic uncertainties associated with structural response and hazard nature. The fragility analysis as a means of structural reliability assessment describes the probability of demand exceeding the capacity conditioned on a hazard intensity measure and other environmental parameters.

Fragility analysis of bridges subjected to various hazards has been extensively studied in recent years. Oftentimes, fragility estimates were used for seismic hazard (Guikema and Gardoni 2009; Karamlou and Bocchini 2015; Li et al. 2014). Nielson and DesRoches (2007) proposed a component-level approach for seismic fragility analysis of highway bridges in the central/southeastern regions of the United States. In their approach, the contribution of main bridge components such as columns and bearings to overall system fragility under earthquake events was investigated. Tavares et al. (2013) applied a similar method to generate fragility curves of highway bridges in Quebec for seismic events. Padgett and DesRoches (2008) expanded this method to generate fragility curves for seismically retrofitted bridges.

All aforementioned fragility analyses share a common feature. That is, the fragility is conditioned solely on hazard intensity measures. This type of fragility analysis can estimate how a certain class of bridges generally responds to different hazard intensity levels by presenting the probability of damage. However in this approach, the probability of structural damage is not traditionally conditioned on bridge parameters.

Contrary to this traditional fragility analysis method, parameterized fragility analysis model estimates the probability of structural damage P conditioned on two vectors: an intensity measure vector (\mathbf{IM}) and a bridge parameter vector (\mathbf{X}) as shown in Eq. (3.1):

$$P[\textit{Demand} > \textit{Capacity}|\mathbf{IM}, \mathbf{X}] \quad (3.1)$$

The key to this parameterized fragility analysis lies in ‘meta-models’. Meta-models, which are also referred to as surrogate models, are statistical methods which can predict the outcome of another model without making future inquiries to the original model. In this study, meta-models predict failure of a specific bridge under various hurricane events.

Once a surrogate is trained using a sample dataset, it is able to predict the performance of any bridge provided that the bridge parameters are within the range of the sample dataset.

Simpson et al. (2001) studied different meta-modeling techniques and their applications for various engineering problems. The application of meta-models in reliability analysis of structures has recently gained significant attention in earthquake engineering. Towashiraporn (2004) implemented meta-modeling techniques for a seismic fragility analysis of unreinforced masonry buildings. Ghosh (2013) performed a reliability assessment of aging highway bridges for seismic hazards using meta-models.

Application of fragility analysis is not limited to seismic hazard (Gernay et al. 2016). Ataei and Padgett (2012) conducted a fragility analysis of coastal bridges for hurricane-induced surge and wave forces. In their study, the distance from storm water level to the bottom of girder (Z_c) and maximum wave height (H_{max}) were used as hazard intensity measures. In a subsequent study, Kameshwar and Padgett (2014) presented a risk assessment method for highway bridges under multiple natural hazard events using meta-models.

3.3. RESEARCH SCOPE AND SIGNIFICANCE

The main goal of this paper is to study the problem of unseating of coastal bridges during hurricane events by leveraging three-dimensional finite element models. Therefore, this paper focuses on developing a novel approach for assessing such vulnerability of coastal bridges subjected to hurricane-induced wave forces by means of metamodels. Metamodels, or surrogate models, are models that approximate a more sophisticated model and intend to reduce the computational cost and increase the efficiency of computationally expensive analyses (Simpson et al. 2001). In this study, metamodels are developed to estimate the

response of finite element models of coastal bridges. It has been recognized that the evaluation of sustainability, resilience, and risk is beyond the scope of this study (Bocchini et al. 2013). The outcomes of this study which are given in terms of fragility surfaces may be used for such evaluation.

Most of the severely damaged bridges during recent hurricanes were simply supported concrete bridges which either lacked vertical and horizontal restraints or had poor connections between the substructure and superstructure (Gutierrez et al. 2006). Furthermore, it is well documented in the literature that bridge failures during hurricane events are primarily attributed to deck-unseating due to vertical wave forces imposed by a storm surge and associated wave actions (Douglass et al. 2006; Okeil and Cai 2008; Padgett et al. 2008; Stearns and Padgett 2011). Therefore, this study considers a failure mode in which the dislocation of a bridge superstructure occurs by hurricane wave forces, and thus does not include other less severe damage types observed during past hurricanes such as damage due to impacting/floating debris, scour, and electrical and mechanical equipment.

This study proposes a systematic procedure for parameterized fragility assessment of bridges against hurricane events using two hazard intensity measures. It is hypothesized that the proposed approach can be applied for reliability assessment of bridges in any hurricane prone region, although the vulnerability of a particular bridge class (simply supported reinforced concrete deck girders on pile bents) is assessed for illustration. Furthermore, the assessment technique may be applicable for other structural and hazard types. The reliability of bridges is ultimately presented as a fragility surface which is a byproduct of a parameterized fragility function described in terms of bridge and hazard intensity parameters. Because of the binary nature of the bridge deck unseating, seven

classification techniques are used to predict the bridge response: Naïve Bayes, Linear Discriminant Analysis, Quadratic Discriminant Analysis, Logistic Regression, Support Vector Machines with two different kernels and Random Forest. These algorithms are compared in terms of the prediction accuracy. The method which provides the least classification error will be selected for fragility estimates.

A fragility surface is defined by two hazard parameters, (1) the peak 10-minute wind speed averaged at the standard height of 10m (U_{10min}) and (2) storm water elevation at bridge location (d_s), and relates the intensity of a hazard event to the probability of bridge failure. In order to assess the vulnerability over a practical range of the two intensity measures, the wave and surge parameters need to be derived for each **IM** combination. A mesh grid on the X - Y horizontal plane represents the hazard intensity plane, and each node of this grid corresponds to a particular combination of hazard intensity parameters (or a hazard event). Fragility is assessed at each of these nodes.

3.4. PROPOSED HURRICANE VULNERABILITY ASSESSMENT METHODOLOGY

The proposed vulnerability assessment method uses meta-models to obtain a parameterized fragility estimate of coastal bridges for hurricane events. In the recent past, considerable attention has been paid to application of meta-models in fragility analysis of structures (Ghosh 2013; Kameshwar and Padgett 2014). A meta-model, or a surrogate model, in this study refers to a statistical model which predicts the performance of any selected bridge without having to create an analysis model. It is proposed that binary classification models (or meta-models) can predict the performance of coastal bridges. In a binary classification, the unity represents a failure state, and the zero value represents a no-failure state. The proposed parameterized fragility analysis procedure is mainly divided into three stages: (1)

Design of experiment; (2) Selection of a meta-model which best describes the observed dataset; and (3) Fragility analysis. A flowchart showing the assessment process is presented in Fig. 3.1. The input variables comprise of bridge material/geometric parameters as well as hazard intensity parameters, and the output variables represent a binary classification of bridge failure or no-failure states (i.e., 1 or 0).

3.5. STAGE 1: DESIGN OF EXPERIMENT (DOE)

3.5.1. Identification and statistical analysis of independent variables

In this first step, various structural, material properties, and hazard intensity parameters which affect the bridge performance are determined. Meta-models estimate the bridge response (dependent variable) as a function of these parameters (independent variables). Fourteen independent variables are defined in this study. The dependent variable is binary and thus is '1' if a bridge fails and '0' otherwise. To consider any uncertainty associated with each of the identified independent variables, a statistical distribution representing a wide range of likely values is defined for each variable. This step requires an accurate assessment of structural drawings and other resources to obtain a statistical distribution of each variable.

3.5.2. SELECTION OF HAZARD INTENSITY MEASURES (IMS)

The level of uncertainty in a fragility model is highly dependent on hazard intensity measures or *IMs* (Padgett et al. 2008) selected for analysis. A suitable *IM* is directly correlated with the level of demand exerted on the bridge while it is a measure of hazard intensity. This study uses two *IMs*, U_{10min} and d_s , to generate a fragility model. U_{10min} is selected because sustained wind speed is a measure used for hurricane categories in

Design of Experiment

- Identification and statistical analysis of independent variables
- Selection of hazard Intensity Measures (IMs).
- Generate bridge samples using the LHS method and couple them with hazard scenarios.
- Run bridge analysis and obtain results.

Formulation of Metamodels

- Generate N random bridge samples each matched with a random hurricane scenario and estimate their responses using selected metamodel.
- Input a vector of independent parameters values (IMs and bridge parameters) of each model paired with the binary (failed or not-failed state) response into metamodels.
- Estimate prediction performance of metamodels using the k -fold cross validation technique.
- Compare different metamodels using the measures of “Goodness of fit” and select the most suitable model for fragility analysis.

Fragility Estimation

- Generate n realizations of predictors for a desired bridge under a specific loading scenario: \mathbf{X}_i
- Introduce each \mathbf{X}_i into the trained logistic regression function to obtain $P_f | d_s, U_{10min}, \mathbf{X}_i$
- Integrate over the domain of failure to calculate the probability of failure $P_f | d_s, U_{10min}, \mathbf{X}_c$
- Repeat the last step for each node of the loading scenario grid (IM #1 and IM #2).

Fig. 3.1. Flowchart showing the parameterized fragility analysis procedure by utilizing metamodels.

Saffir-Simpson scale (Simpson and Saffir 1974), thus an acceptable measure of hurricane intensity. While the wind speed is directly related to wind wave heights and forces, it cannot represent the magnitude of wave forces applied to the bridge deck by itself as bridges with greater freeboard height are less prone to wave forces. Thus, it is necessary to select d_s as the second IM in this study.

3.5.3. DETERMINATION OF WAVE INDUCED FORCES

Equations (3.2) through (3.4), shown below, are provided in the “AASHTO Guide Specifications for Bridges Vulnerable to Coastal Storms” (2008), referred to as the “AASHTO guide” hereafter, and are the result of extensive studies conducted by Sheppard (2008). Wave forces include the contribution of both hydrostatic and hydrodynamic forces.

The vertical wave force comprises of a low-frequency quasi-static mechanism and a short-duration, high-frequency slamming force. The vertical quasi-static wave force, F_{V-Max} , includes the effect of buoyancy force, drag force and inertia forces. To calculate wave forces, wave parameters (period, height, and length) are derived for each *IM* combination and are used to determine the maximum vertical/horizontal forces and overturning moments. Wave parameters for a given location are a function of (a) wind speed, (b) water depth, (c) fetch length, and (d) wind duration. The maximum vertical quasi-static wave force per unit length of the deck, F_{V-Max} , is obtained by Eq. (3.2), where γ_w is the unit weight of water, \bar{W} is the deck width factor, b is a function of wave crest height and distance between water level and deck low chord, H_{max} is the maximum wave height, d_s is the storm water elevation at the bridge location, T_p is the wave period, $y = H_{max}/\lambda$, and λ is the wavelength. Parameters b_0 - b_6 and *TAF* (Trapped Air Factor) are related to the effect of trapped air between water surface and voids beneath bridge girders.

$$F_{V-Max} = \gamma_w \bar{W} \beta \left(-1.3 \frac{H_{max}}{d_s} + 1.8 \right) (1.35 + 0.35 \tanh(1.2 T_p - 8.5)) \left(b_0 + b_1 x + \frac{b_2}{y} + b_3 x^2 + \frac{b_4}{y^2} + \frac{b_5 x}{y} + b_6 x^3 \right) (TAF) \quad (3.2)$$

The maximum horizontal force per unit length of the deck, F_{H-Max} , is determined by Eq. (3.3), where ω is defined by Eq. (3.3-a), in which η_{max} is the wave crest height above storm water, d_b is the deck height, r is the rail height, and W is the deck width. The vertical slamming force, F_s , per unit length of the deck is determined by Eq. (3.4), where A , B are two factors which are determined as a functions of Z_c/η_{max} .

$$F_{H-Max} = F_{H-Max}^* \exp \left(-3.18 + 3.76 \exp \left(\frac{-\omega}{\lambda} \right) - 0.95 \left(\ln \left(\frac{\eta_{max} - Z_c}{d_b + r} \right) \right)^2 \right) \quad (3.3)$$

$$\omega = \min \left(\lambda - 1/2 (Z_c + 1/2 H_{max}) \left(\frac{\lambda}{H_{max}} \right), W \right) \quad (3.3-a)$$

$$F_s = A \gamma_w H_{max}^2 \left(\frac{H_{max}}{\lambda} \right)^B \quad (3.4)$$

These vertical and horizontal forces represent possible peak values, and the AASHTO guide does not explicitly describe how these forces should be applied to the bridge structures or components. No detailed discussion of a wave load-time history that may be exerted on a bridge is available in the AASHTO guide. Therefore, this study adopts the method suggested by Ataei (2013) to generate a time history function for waves forces. Quasi-static components of wave forces in both vertical and horizontal directions are considered to be in phase with wave and vertical slamming forces. Figs. 3.2 and 3.3 depict a variation of maximum values of vertical, slamming and horizontal components of wave force (F_{V-Max} , F_s or F_{H-Max}) versus variations of U_{10min} and d_s , respectively, for a sample bridge computed in accordance of the AASHTO guide. Z_c in Fig. 3.2 denotes the distance between the storm water level and bottom of a bridge deck. A negative value indicates that the water elevation is above the height of bridge low chord. In both cases ($Z_c > 0$ and $Z_c < 0$), Fig. 3.2 shows that the vertical force components (F_{V-Max} , F_s) generally increase as the wind speed increases, although a slight decrease is observed between Categories 4 and 5 (indicated as ‘CAT’ 4 and 5 in the figure). The horizontal force component does not necessarily increase with increasing wind speed. Fig. 3.3 depicts a variation of wave forces as the storm water elevation changes. A significant correlation is observed between the quasi-static component (F_{V-Max}) and storm water elevation (d_s).

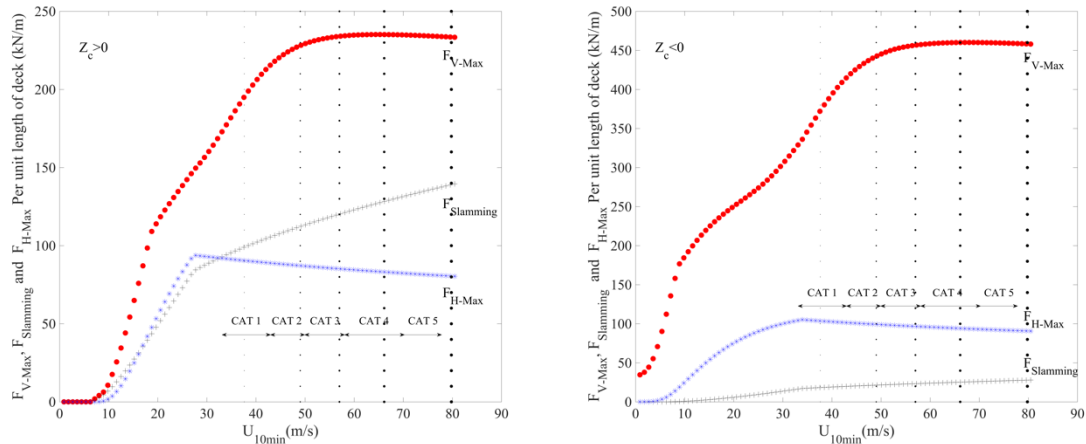


Fig. 3.2. Wind speed (U_{10min}) vs. deck force components: Max. vertical force (F_{V-Max}), Max. Slamming force ($F_{Slamming}$), and Max. horizontal force (F_{H-Max}).

There are other interesting trends observed from these two figures. To better investigate the effect of the variables on the vertical wave force, F_{V-Max} , shown in Eq. (3.2), Fig. 3.4 presents the variables as a function of U_{10min} and d_s . As stated above, the vertical force (F_{V-Max}) increases until the threshold wind speed for *CAT 4* hurricane is reached and remains constant. However, it slightly decreases through categories 4 and 5. While the magnitude of F_{V-Max} is dependent on various terms, the trend is mainly attributed to the terms including the effect of wave period (T_p) as shown in Fig. 3.4(d).

While the vertical force (F_{V-Max}) is generally greater when a bridge is submerged ($Z_c < 0$), provided the wind speed remains constant, the slamming force component is much smaller and thus is considered insignificant. This can be explained by the fact that the quasi-static component is mainly governed by hydrostatic forces and thus is greater when a bridge is submerged. On the other hand, slamming forces decrease because there is no air trapped between water surface and bridge deck once the bridge is submerged. As shown in Fig. 3.4(a), the term representing the effect of wavelength (\bar{W}) increases with

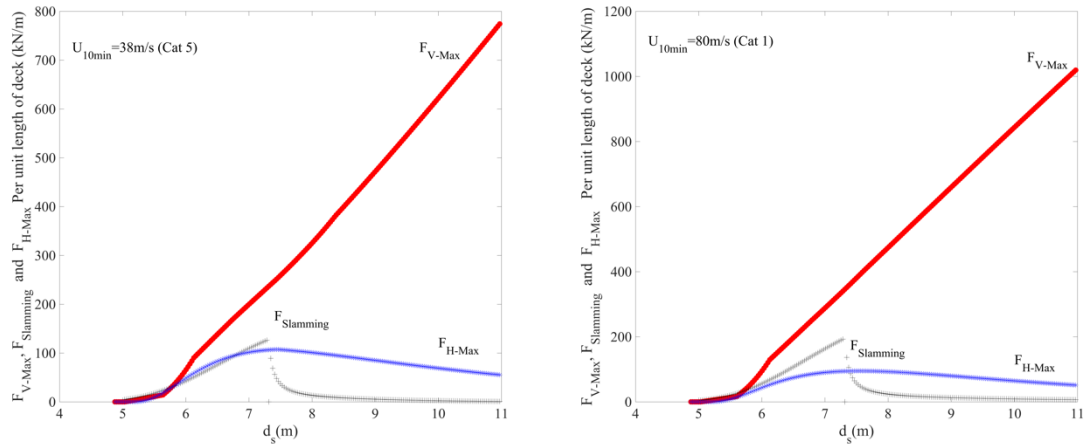


Fig. 3.3 Storm water elevation (d_s) vs. deck force components: Max. vertical force (F_{V-Max}), Max. Slamming force ($F_{Slamming}$), and Max. horizontal force (F_{H-Max}).

growing wind speed. This is due to the fact that waves generated by stronger winds have greater wavelengths. This consequently results in a wider bridge area affected by waves. Fig. 3.4(b) shows a variation of the term β which represents the effect of hydrostatic forces. As expected, β , increases with increasing wind speed because a greater portion of bridge deck submerges as the wave height increases. As presented in Fig. 3.3, the slamming force component in both cases is increased to the point where a snap-through occurs, and slamming forces is reduced beyond this point. This is the point where the bridge is submerged, and trapped air pockets are fully vented. As shown in Fig. 3.4(a), \bar{W} increases as the water elevation rises for a constant wind speed. Fig. 3.4(b) illustrates the importance of considering sufficient freeboard height as β increases due to rising water elevation.

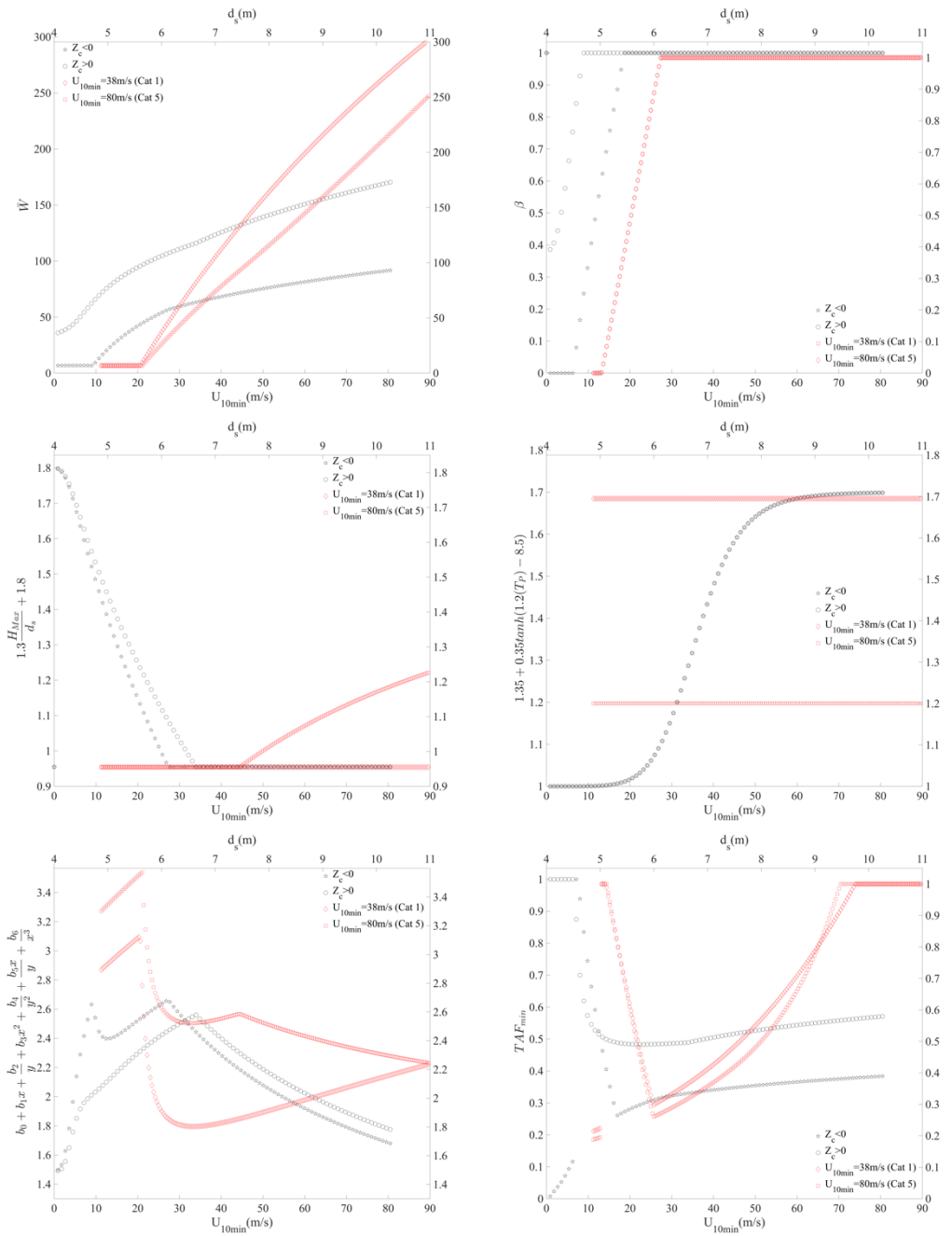


Fig. 3.4. Variables that affect the force components as U_{10min} or d_s varies.

3.5.4. GENERATE BRIDGE SAMPLES USING LHS METHOD AND COUPLE THEM WITH HAZARDS SCENARIOS

In order to generate a training and testing dataset for metamodels and predict the response of bridges for a reasonable range of predictors containing bridge and hazard parameters, statistical samples of bridges and hurricane intensity parameters must be generated from statistical distribution of random variables. Each bridge samples is paired with a hurricane scenario to perform FE simulations. Random variables used in the simulations are given in Table 3.1. Each hurricane scenario is a pair of U_{10min} and d_s . Since fragility surfaces are conditioned on U_{10min} and d_s , no prior knowledge about their uncertainty is needed, and a uniform distribution is assumed for both. The Latin Hypercube Sampling (LHS) method is used to divide each predictor's probability distribution function into ' n ' intervals, where the width of each interval is determined to give an equal probability of occurrence (Ayyub and Lai 1989). Subsequently, a predictor value is arbitrarily selected from each interval and is paired with the other randomly selected predictor values to generate ' n ' bridge samples and ' n ' hurricane scenarios. In this study, a total of 1500 bridge samples and 1500 hurricane scenarios are created to run 1500 FEA simulations.

3.5.5. BRIDGE ANALYSIS AND ANALYSIS RESULTS

This study uses the Level-I analysis procedure from the *AASHTO Guide* to obtain wave parameters such as wave period, maximum height, and length. These values will then be used to obtain maximum vertical, horizontal, and slamming forces. Vertical unseating of deck due to wave and surge forces is considered as the sole damage state in this study.

There are two key components that improve the resistance of bridge superstructures against wave forces: (1) self-weight of bridge deck and (2) connection strength between

Table 3.1. Bridge parameters and their probabilistic distribution.

Variables	Distribution	Parameters		Unit
Deck width	-	12, 24		m
Number of spans	Uniform(a,b)	a=3	b=7	-
Spans length	Uniform(a,b)	a=9.14	b=21.33	m
Bridge height	Uniform(a,b)	a=2.6	b=6	m
Shear modulus of elastomeric bearing pad	Uniform(a,b)	a=0.66	b=2.07	MPa
Concrete strength	Normal(μ,σ)	$\mu =33.8$	$\sigma=4.3$	MPa
Steel strength	Lognormal	$\mu =6.13$	$\sigma=0.08$	MPa
Entrapped air	Uniform(a,b)	a=0	b=100	-
Pile diameter	-	0.30,0.35,0.40,0.46,0.51		m
Deck weight factor	Uniform(a,b)	a=0.95	b=1.05	-
Dowel or anchor	Deterministic			-
Dowel/anchor size	-	0.025,0.032,0.038		m
Dowel/anchor embedment length	Uniform(a,b)	a=0.23	b=0.41	m
Slab height	Uniform(a,b)	a=0.15	b=0.25	m

superstructure and substructure. Once wave and surge induced forces overcome the capacity of these two components, bridge deck becomes vulnerable to deck unseating due to vertical and/or horizontal shifting. In this study, a wave load-time history is applied to bridge models by means of a line load. The overturning moment in each step is determined by the product of the total vertical force and its distance from the central axis of a bridge deck section. The process described in this section is repeated for each set of *IMs* to derive force-time histories and review the bridge response from each loading history.

3.5.6. DEVELOPMENT OF BRIDGE MODELS

A three dimensional (3D) finite element model shown in Fig. 3.5 (a) is developed using the ANSYS program (v16.2) to study potential failure modes and validate the performance of simplified 3D frame models developed in OpenSees. The 3D model consists of solid elements and full bearing connection details including anchor bolts. While the discussion of the 3D ANSYS model is omitted due to length limitation, it is concluded from the 3D ANSYS model that a parameterized OpenSees model effectively simplifies

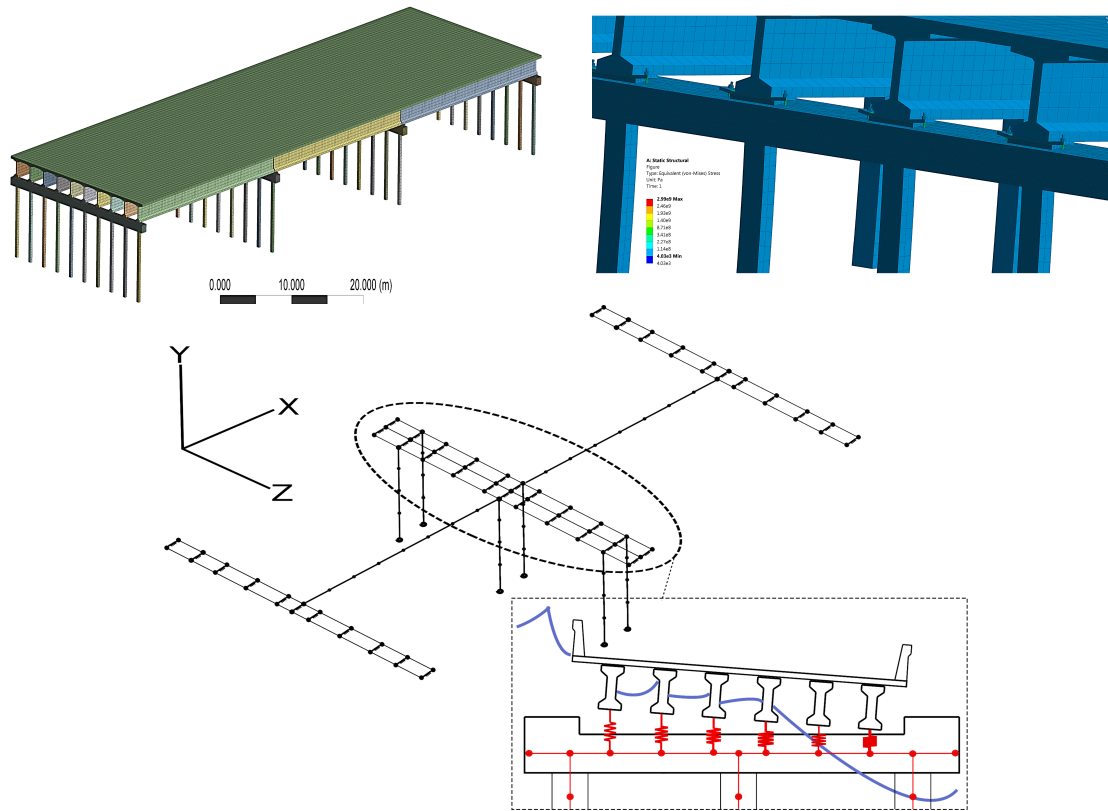


Fig. 3.5. 3D bridge models: (a) ANSYS 3D solid model; (b) ANSYS 3D solid model showing anchor bolt failure; and (c) OpenSees bridge model.

geometry building while capturing the nonlinear response of anchor bolt failure in the bearing connections as shown in Fig. 3.5 (b). Therefore, the prevailing failure mechanism (i.e., bridge deck uplifting/unseating) identified in the literature (Okeil and Cai 2008; Padgett et al. 2008; Stearns and Padgett 2011) is well represented by a 3D simplified OpenSees model (see Fig. 3.5c) described below.

Bridge models are constructed in the OpenSees (the Open System for Earthquake Engineering Simulation) software (Mazzoni et al. 2006). A parameterized finite element model is developed in OpenSees. The parameterized models in OpenSees allows the generation of bridge models with multiple variables without having to manually change the input variables for each bridge model. This is particularly important for a multi-variable

reliability analysis where a significant number of models must be generated and analyzed. The model building procedures in OpenSees and associated material models is well summarized by Nielson (2005) who studied the seismic response of bridges in the central and southeastern United States. Furthermore, Ataei (2013) improved the bridge model for hurricane analysis by capturing the deck unseating behavior using contact elements. This section describes material models and element types selected to construct and analyze bridge models.

Bridge deck is modeled using ‘elastic beam column’ elements available in OpenSees element library. ‘Nonlinear beam-column’ elements had no significant effect on the analysis results. This is reasonable because past events resulted in a rigid-body movement of bridge superstructures upon the failure of connecting components between super- and sub-structures. Deck properties for each span (mass per unit length, I_z , I_y , E , Area) are calculated from available bridge drawings and assigned to the deck elements. Deck weight was applied as a linearly increasing static load to deck elements, followed by a dynamic time history analysis during which vertical and horizontal force time-histories are applied.

Bridge piles are modeled using the ‘displacement-based beam-column’ elements. The cross-section of pile elements is discretized using a fiber-section analysis. Cap beam elements are modeled in a similar manner and are connected to deck-end element by the ‘RigidLink’ elements. The material models used for abutments are developed based on the recommendations from Caltran’s seismic design criteria (2013) and Shamsabadi (2007). Piles and fill passive pressure is represented with two ‘Hysteretic’ material models. Bridge bearings are of two general types (fixed and expansion) similar to the types implemented in central and southeastern bridges in the U.S. (Nielson 2005). Expansion bearings allow

for longitudinal movements for expansion and contraction of bridge spans, whereas fixed bearings prevent movement in the longitudinal direction.

Two material models are combined in parallel to represent the bearing behavior: ‘Steel01’ for elastomeric pad and ‘Hysteretic’ for dowels/anchors. The initial stiffness of the elastomeric pads is determined using the Eq. (3.5) (Choi 2002) in which K_i , G , A and h are the initial stiffness, shear modulus, area, and thickness of the elastomeric pad.

$$K_i = \frac{GA}{h} \quad (3.5)$$

While dowels provide no vertical resistance against vertical wave forces, anchor bolts are able to tie down a bridge deck to its substructure when properly installed. A ‘Hysteretic’ material model is used to represent the response of anchor bolts. Once the deck is completely disengaged from the substructure, its rigid-body movement needs to be characterized. In order to model this rigid-body action, the ‘zeroLengthContact3D’ elements are used between the deck and substructure as an interface (Ataei 2013) element, which also enables modeling of the sequential loss of bearing connections. This primary feature of the OpenSees model is illustrated in Fig. 3.5 (c).

3.5.7 DEMAND VS. CAPACITY EVALUATION

Bridge failure during a hurricane event occurs by deck unseating due to vertical wave forces and/or deck shifting due to horizontal forces. One or two components resist the vertical wave forces. The self-weight of bridge deck is the primary component that provides the vertical resistance to the vertical wave force. The two most common connection types between substructure and superstructure include elastomeric bearing connections with anchor bolts and dowels. Anchor bolts generally provide additional vertical resistance beyond the point when the vertical forces overcome the deck weight,

whereas the dowels do not have the fallback capacity. Both dowels and anchor bolts provide the resistance to horizontal movement against wave induced forces. The capacity of anchor bolts in two directions is calculated as per Chapter 17 of *ACI 318-14*. The tensile strength of anchors is considered to be the smallest value of tensile strength of anchor steel material, concrete breakout strength in tension, and anchor pullout strength (ACI 2014). Shear strength of the dowels is calculated as a function of its cross sectional area and material shear yield stress. Depending on the connection types, the demand-to-capacity ratio of each connection is evaluated to determine the degree of damage.

3.6. STAGE 2: IDENTIFICATION OF THE BEST PERFORMING METAMODEL

This step develops metamodels (or prediction models) using the sample dataset, and the most efficient model which yields the least misclassification loss will be used for predicting bridge response and fragility analysis. In the second stage, the results obtained in the previous stage are introduced to seven metamodels described below. Once all of the bridge models are analyzed with the input parameters (bridge parameters and intensity measures), the input variables paired with the analysis output results in the form of failed/intact (or a binary number of '0's and '1's) are introduced to the seven meta-models described below:

Linear Discriminant Analysis (LDA)

The first metamodel considered herein includes the Linear Discriminant Analysis (LDA). This prediction model assumes that the data points within each class have a Gaussian distribution and projects the data points onto a hyperplane which maximizes the independence of each class while minimizing the distance between the data points and the centroid of the hyperplane. This assures that the data points within each class are populated close to each other. Generally, the LDA finds the projection vector, ω , which

maximizes the following function shown in Eq. (3.6), where $\widetilde{\mu}_1, \widetilde{\mu}_2$ are the mean and σ_1^2, σ_2^2 are the within-class variance of two classes (Failed/Intact), respectively, in the projected space.

$$\text{argmax}_{\omega} \left(\frac{|\widetilde{\mu}_1 - \widetilde{\mu}_2|^2}{\sigma_1^2 + \sigma_2^2} \right) \quad (3.6)$$

In this equation, the numerator evaluates the degree of separation between two classes by measuring the distance of their projected means while the denominator gives a measure of how scattered the data points are in each class around their projected means.

Naïve Bayes

The Naïve Bayes classifier assumes that variables such as hazard intensity and structural parameters independently affect the bridge performance. This method applies the Maximum-A-Posteriori (MAP) decision rule to assign a class to each bridge sample. In other words, the posterior probability of a new bridge sample is computed for two classes (Failed/Not failed) using its vector containing structural and hazard variables (or predictors), and one that yields the greater probability is selected as shown in Eq. (3.7), in which \hat{R} is the predicted bridge class label; c_1 and c_2 are the “Failed” and “Intact” classes, respectively; x_k is the predictor variable, k ; and n is the number of predictor variables.

$$\hat{R} = \text{argmax}_{i \in \{1,2\}} P(c_i) \prod_{k=1}^n P(x_k | c_i) \quad (3.7)$$

Quadratic Discriminant Analysis (QDA)

Quadratic discriminant classifier is considered as a special case of the Bayesian classifier which assumes a multivariate Gaussian distribution for each class. Assuming a loss function consisting of 0 or 1 values and substituting a multivariate Gaussian distribution function in the Bayes decision function yields a quadratic discriminant function, d_i , shown in Eq. (3.8), where \mathbf{X} is the vector of predictor values for a desired bridge whose class is to

be predicted, c_i represents class i ($i=1$ for Failed and $i=2$ represents Intact), and $\boldsymbol{\mu}_i, \boldsymbol{\Sigma}_i$ are mean vector and covariance matrix of predictors of class i . The classification is completed by assigning class $\text{argmax}_i d_i(x)$ to the dataset, \mathbf{X} .

$$d_i(\mathbf{X}) = \ln P(c_i) - \frac{1}{2} \ln |\boldsymbol{\Sigma}_i| - \frac{1}{2} [(\mathbf{X} - \boldsymbol{\mu}_i)^T \boldsymbol{\Sigma}_i^{-1} (\mathbf{X} - \boldsymbol{\mu}_i)] \quad (3.8)$$

Logistic Regression

The Logistic regression method estimates the probability of a dependent variable belonging to a class (Fail/Intact) by using a logistic function. Therefore, it is different from the other methods described above because their responses are categorical. A logistic regression generally evaluates the logarithm of “odds ratio”, which is the probability of a bridge failure divided by the probability of the opposite given its structural and hazard parameters values (or predictors) as a linear function of predictors as shown in Eq. (3.9), where P_f is the probability of bridge failure; α is a constant; \mathbf{b}_{LR} is the vector of regression coefficients; and \mathbf{X} is the vector of predictors. Eq. (3.10) may be used in place of Eq. (3.9) to obtain P_f :

$$\ln \left(\frac{P_f}{1-P_f} \right) = \alpha + \langle \mathbf{b}_{\text{LR}}, \mathbf{X} \rangle \quad (3.9)$$

$$P_f = \frac{e^{\alpha + \beta \mathbf{X}}}{1 + e^{\alpha + \beta \mathbf{X}}} \quad (3.10)$$

Support Vector Machines (SVM)

Support vector machines (SVM) are a class of supervised learning algorithms used for classification and regression. The SVM used in this study finds an optimum hyperplane which best separates the “Failure” domain from the “No-Failure” domain by maximizing the distance (so-called functional margin) between the nearest training data points of each class (support vectors) and the hyperplane. The optimum hyperplane is determined by Eq. (3.11):

$$\omega = \underset{\omega}{\operatorname{argmin}} \frac{1}{2} \|\omega\|^2 + C \sum_{i=1}^n \max(0, 1 - R^i \langle \omega, \mathbf{X}^i \rangle) \quad (3.11)$$

In Eq. (13), ω is the normal vector to the hyperplane, C is a parameter which control the trade-off between maximizing margin for correctly classified data points and minimizing the misclassification error, $R^i = -1, +1$ is the class which i th data point belongs to, and \mathbf{X} is the vector of predictor values for i th data point. The response of a bridge is predicted by Eq. (3.12), where \hat{R} is the predicted response. In this study two types of kernels (Linear and Gaussian radial basis functions) are mainly used to find the minimum misclassification error.

$$\hat{R}(\mathbf{X}) = \operatorname{sign}(\omega, \mathbf{X}) \quad (3.12)$$

Random Forest

Decision tree method is widely used for risk-based decision making in the context of reliability analysis. The Random Forest (RF) method is an extension of the decision tree method. The Random forest methods create m number of random samples (or trees) and construct resamples by replacing samples. This process is generally referred to as ‘bootstrap sampling’. A separate decision tree is developed for each sample. In each individual tree, random subsets of independent variables are used for searching for splits in the decision tree. Once the ‘Random Forest’ model is trained, a class label of unseen data is determined by averaging responses from the trained trees. Thus, the performance of a bridge under a specific hurricane scenario is predicted by comparing the number of trees which determines the bridge failed or intact. This process is illustrated in the implementation section (see Table 3. 3).

3.6.1. ADVANTAGES AND DISADVANTAGES OF THE METAMODELS

Naïve Bayes and LDA are two linear methods which are extremely faster to train and use; however, they both assume that input parameters are independent and thus any correlation among input parameters could degrade their performance. QDA is a generalization of LDA which assumes quadratic decision boundaries between classes; thus, it is more suitable than LDA for a data set with nonlinear boundaries. LR is a linear method which assumes a linear relation between the logit of the dependent variable ('0' or '1' binary outcome) and independent variables. LR holds fewer assumptions about the input data and thus is more flexible compared to other methods and was particularly chosen because it is capable of estimating the probability of binary response. SVM is used to model both linear and nonlinear relations depending on the kernel selected; however, SVM methods are sensitive to scaling of variables. Its data needs to be normalized before being used in SVM. RF is a non-parametric ensemble method which is very fast to train and use and does neither need any pre-processing nor scaling of data.

3.6.2. TRAINING, TESTING, AND VALIDATION OF METAMODELS

The *K-fold* ($k=10$) cross validation method is used; that is, each training dataset is divided into 10 separate folds, and each fold is used as a test/verification dataset while the other 9 folds are used for training. This procedure is repeated for each fold. The seven meta-models are compared in terms of loss, sensitivity, and specificity, and the most suitable model is selected for further analysis. Subsequently, numerous random bridge samples paired with a hurricane scenario are generated, and the metamodels are used to predict the responses. A binary vector which represents the bridge response is determined. This vector along with a matrix of bridge sample variables are used for a logistic regression which estimates the

probability of failure ($P_f|_{d_s, U_{10min}, \mathbf{X}}$) conditioned on the vector pertaining bridge parameters (\mathbf{X}) and intensity measures U_{10min} and d_s) as shown in Eq. (3.10), where $\beta_0, \beta_{U_{10min}}, \beta_{d_s}$ and $\beta_{\mathbf{X}}$ are the regression coefficients. A brief description of seven studied metamodels is given below, and additional information is found in available literature (Hastie et al. 2005).

$$P_f|_{d_s, U_{10min}, \mathbf{X}} = \frac{e^{\beta_0 + \beta_{U_{10min}} U_{10min} + \beta_{d_s} d_s + \beta_{\mathbf{X}} \mathbf{X}}}{1 + e^{\beta_0 + \beta_{U_{10min}} U_{10min} + \beta_{d_s} d_s + \beta_{\mathbf{X}} \mathbf{X}}} \quad (3.13)$$

3.7. Stage 3: Construction of a fragility surface

The ultimate goal of vulnerability assessment is to determine the probability of failure (P_f) of a selected bridge under a wide range of storm water elevations and wind speeds, which are a practical indicator of hurricane intensity. To do so, metamodels trained by the sample dataset are applied to a randomly selected dataset to generate a fragility surface. A fragility surface is constructed for the selected bridge using the most efficient metamodel which predicts the response of bridge samples with the least classification error.

Fragility surfaces provide a quantifiable measure of reliability and give the probability of a structure reaching or exceeding a certain limit state, conditioned on desired intensity measures. Ideally, this evaluation is completed by integrating the limit state function over the domain of failure. However, it is alternatively solved by making an approximation of the limit state hyperplane and/or employing numerical methods. The most popular numerical approach, yet the most accurate, for fragility estimation is the crude Monte Carlo technique. This technique is an exhaustive search method which generates random variables from within possible range of data for each input variable and combines these values to produce all probable outcomes. In case of fragility analysis of bridge

structures, these random variables are structural and hazard related parameters. These combinations will then be analyzed to obtain the bridge response. Ultimately, a probabilistic description of the response will be derived from the outcomes. However, this method is inefficient due to significant computational cost resulting from a time-consuming nonlinear time history analysis. For instance, the number of Monte Carlo simulations required to achieve a 95% confidence level at P_f is 40,000 runs (Mann et al. 1974).

Statistical sampling methods such as the Latin hypercube sampling (LHS) method in fragility analysis were later proposed to minimize such computational effort while maintaining the prediction accuracy. The LHS method divides each input random variable range into n number of intervals with equal probability. Subsequently, random values are selected from within each interval and finally these n values for each random variable are coupled to those of other variables to make n number of samples. These samples are then analyzed/observed to produce n number of responses, and a desired probability distribution is selected. This approach has been extensively utilized in seismic fragility analysis of structures. While this approach efficiently reduces the computational cost relative to the crude Monte Carlo scheme, its validity relies on the type of probability distribution functions selected for bridge response. Various density functions have been proposed in the literature.

In this study, capacity estimates are incorporated in bridge models, and metamodels are used to evaluate the limit state function, i.e. failure (demand > capacity). For a particular bridge under given *IMs*, the probability of failure is obtained by taking an integral over the domain of failure as shown in Eq. (3.14):

$$P_{f|d_s, U_{10min}, \mathbf{x}_C} = \int \dots \int_{\Omega_{X_U}} P_{f|d_s, U_{10min}, \mathbf{x}} f_{p_1} \dots f_{p_n} dp_1 \dots dp_n \quad (3.14)$$

In Eq. (3.14), $P_f|_{d_s, U_{10min}, \mathbf{X}_C}$ is the probability of failure of a bridge including geometrical and structural parameters vector (\mathbf{X}_C) for given storm water elevation (d_s) and wind speed (U_{10min}) scalars. Ω_{X_U} is the feature space of all uncertain predictors over which the integral is taken; $P_f|_{d_s, U_{10min}, \mathbf{X}}$ is the probability of failure for a given point in the feature space; and f_{p_i} represents the probability distribution function of predictor variable i . This integral is determined using Eq. (3.14) at each node on an *IM* grid to find $P_f|_{d_s, U_{10min}, \mathbf{X}_C}$. The only random variable that was treated probabilistically (i.e., random variables) in evaluation of the limit state function in Eq. (3.14) is the “percentage air entrapped”, whereas the other parameters in Table 3.1 are determined from bridge plans and thus are fixed values.

3.8. IMPLEMENTATION OF THE PROPOSED PARAMETERIZED FRAGILITY ASSESSMENT APPROACH

As a proof of the concept, the proposed hurricane vulnerability assessment methodology is applied to bridges along the surge-prone coastal regions of the state of Georgia. A hundred miles of the US Atlantic coastline lies along the eastern border of Georgia. The proposed assessment method is applied to a set of coastal bridges in Georgia to illustrate how the proposed approach is used to assess the vulnerability of existing bridges. This study focuses on evaluating the susceptibility of simply supported reinforced concrete bridges because the majority of the bridges in the studied region are comprised of this class of bridges.

In this study, the Sea, Lake and Overland Surges from Hurricanes (SLOSH) model (Jelesnianski et al. 1992) is used to identify the coastal areas prone to surge inundation under a hurricane category 5 event. All of the bridges located in the identified surge prone

area are considered vulnerable to hurricanes in this study. Pertinent structural and geometrical properties of these bridges are obtained from the National Bridge Inventory (NBI) database and structural drawings available at the Georgia Department of Transportation. These variables along with parameters that define their statistical distribution are presented in Table 3.1. Probabilistic distribution functions present a way to generate bridge samples using randomly generated variables. In this study, the probabilistic distributions of bridge deck width, number of spans, span length, bridge height and diameters, dowel/anchor size and embedment length, girder height and slab height are obtained by a statistical investigation of variables available in the national bridge inventory (NBI) database and available structural drawings. All spans are considered to have equal length in this study. The uncertainty in shear stiffness of elastomeric bearing pads due to aging is characterized by a uniform distribution (Nielson 2005). Ellingwood and Hwang (1985) illustrated that the steel strength for grade 413 rebar follows a right-skewed distribution whose mean strength and coefficient of variation (COV) is 463 MPa and 0.08, respectively. Thus, a lognormal distribution is considered. Similar procedures are used for anchors and dowels. To consider the effect of aging on concrete strength, a normal distribution with a mean of 33.8 MPa and a standard deviation of 4.34 MPa is considered (Choi 2002).

The uncertainty attributed to the loads is characterized by various parameters. In this study, the parameters are deck width, span length which is a proxy for the girder height, slab height, and entrapped air (see Table 3.1), which are used to determine the surge and wave forces. The other parameters are U_{10min} and d_s , which are used to generate fragility surfaces. A uniform distribution is used for these two parameters because no prior

knowledge regarding their uncertainty is needed. On bridges with girders, air may be trapped between water surface and bottom surface of the deck. This entrapped air between girders increases the vertical buoyancy force. Depending on the existence and adequacy of venting between adjacent spans through diaphragms as well as the ratio of design wave crest to the girder height, the amount of entrapped air varies (AASHTO. 2008). To consider this effect, a uniform distribution is considered for percent thresholds. The minimum and maximum thresholds for the percentage of trapped air are given by the AASHTO guide. In most of the coastal bridges in Georgia, the superstructure and substructure are connected by either dowels or anchors. The examination of bridge drawings indicates that the diameter of anchor bolts and dowel bars used in conjunction with bridge bearing plates is: 2.54 cm, 3.18 cm, or 3.81 cm. The anchor/dowel embedment length into a cap beam ranges between 22.86 cm and 40.64 cm.

3.8.1. CASE STUDY - STAGE 1: DESIGN OF EXPERIMENT

A total of 1,500 bridge samples are generated using the LHS method. The samples represent a combination of the bridge parameters and hazard intensity parameters which include varying water elevation (d_s) and wind speed (U_{10min}). A nonlinear time history analysis is performed for each sample, and the results are obtained in terms of ‘Failure’ or ‘No-Failure’ states by monitoring reaction forces at the bearing connection elements.

3.8.2. CASE STUDY - STAGE 2: IDENTIFICATION OF A METAMODEL

Bridge sample parameters and their results are given to seven metamodels for training. The *K-fold* cross-validation technique is used for validation, and the most suitable meta-model is selected.

3.8.3. CASE STUDY - STAGE 3: CONSTRUCTION OF FRAGILITY SURFACES

One of the Georgia's coastal bridges is selected to illustrate how the proposed fragility analysis is completed. Table 3.2 includes the bridge parameters. The probability of failure for each level of *IMs* has been calculated to obtain a fragility surface. To calculate the probability of failure at each *IM* grid node (or a hazard scenario), ten thousand Monte Carlo simulations are performed and in each of the simulations, a logistic regression is used to find the probability, $P_f|_{d_s, U_{10min}, X_C}$ (see Eq. 3.14). In this study, the number of Monte Carlo simulations was selected to achieve a coefficient of variation of 10% for $P_f=1\%$, consistent with Eq. (3.15):

$$COV_{P_f} = \sqrt{(1 - P_f)/(P_f N_{MC})} \quad (3.15)$$

in which COV_{P_f} is the coefficient of variation in estimated P_f , and N_{MC} is the number of Monte Carlo simulations. This process was repeated for each hurricane scenario in order to obtain fragility estimates for each *IM* combination in the *IM* grid.

3.7.4. RESULTS OBTAINED FROM GEORGIA'S COASTAL BRIDGE SAMPLES

The results are used to identify the most suitable metamodel from the seven studied metamodels and predict the performance of coastal bridges. A fragility surface is developed for the selected bridge in order to prescribe the probability of failure for a given set of hazard intensity parameters.

Maximum force demand and capacity at bearing locations

Fig. 3.6 includes the maximum axial loads at bridge bearing connection locations. The maximum and minimum axial capacity of anchor bolts is also depicted in Fig. 3.6. In none of the studied samples, the maximum axial force demand at bearing connection exceeds the maximum capacity of 3.81 cm diameter anchor bolts. That is, bearing connections with

two largest anchors provide sufficient vertical resistance to Category 5 hurricane induced wave forces.

Table 3.2. Bridge dimensions and other properties used to generate the fragility surfaces.

Deck width (m)	Number of spans	Span length (m)	Bridge height (m)	Girder height (m)	Pile diameter (m)	Dowel or Anchor (D or A)	D/A size (m)	D/A embedment length (m)	Slab height (m)
24.0	3	11.1	3.1	0.71	0.4	D	2.54	0.38	0.21

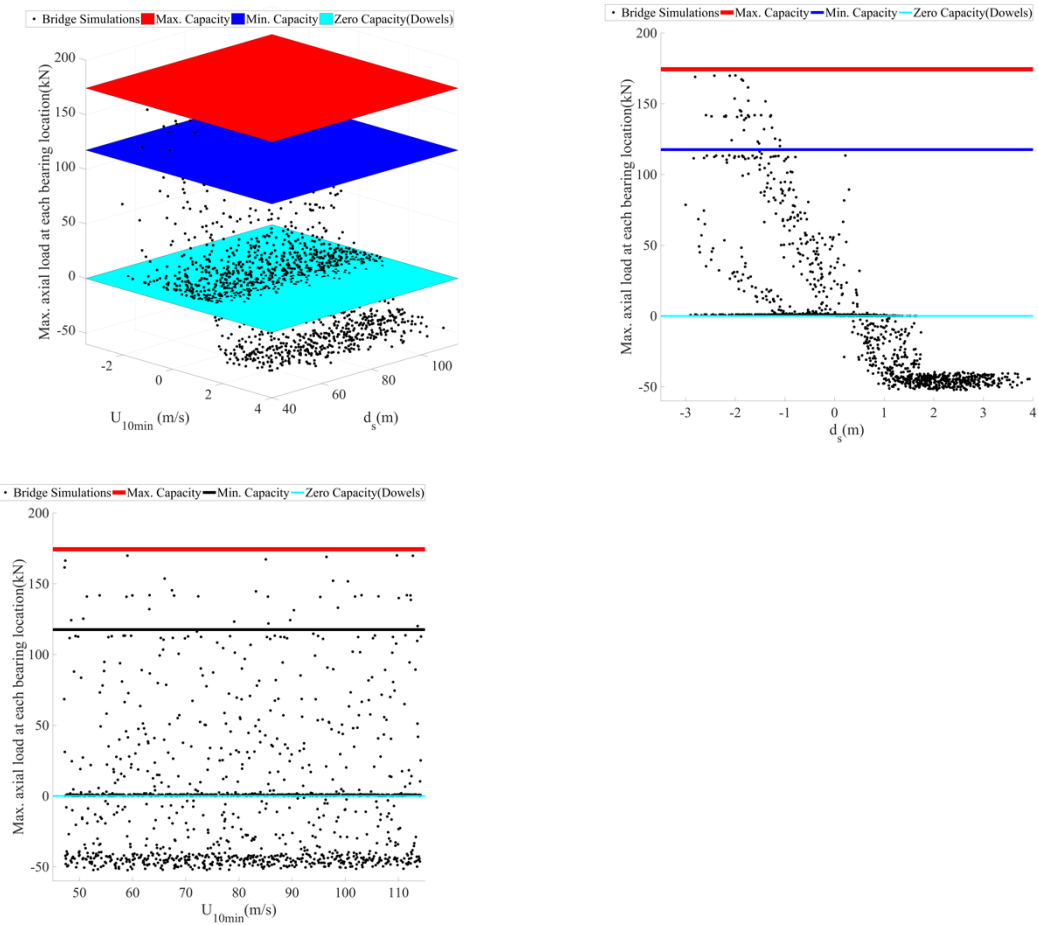


Fig. 3.6. Wave force demands vs. U_{10min} and/or d_s , and the connection capacity: (a) Axial force demand vs. U_{10min} and d_s ; (b) Axial force demand vs. d_s ; (c) Axial load demand vs. U_{10min}

Most suitable meta-model

In Table 3.3, the performance of seven metamodells is compared in terms of classification loss, sensitivity, and specificity (Hastie et al. 2005). The models, other than the SVM with RBF kernels, yielded acceptable results when it comes to the ‘classification loss.’ However, the Random Forest (RF) model outperforms the other models when other metrics are considered. ‘Sensitivity’ considers the probability of bridge failure given the fact that it has actually failed, whereas ‘specificity’ represents the probability of bridges being intact provided that they have indeed remained intact. The confusion matrix for the RF model is presented in the Table 3.4. No failed bridge is misclassified as intact, and only 3 failed bridges are misclassified.

Table 3.3. Performance measures for seven metamodells.

Metamodel	Classification loss	Sensitivity	Specificity
Linear Discriminant Analysis	0.967	0.980	0.937
Naïve Bayes	0.945	0.980	0.942
Quadratic Discriminant Analysis	0.955	0.979	0.941
Logistic Regression	0.960	0.922	0.986
Support Vector Machines – Linear kernel	0.969	0.981	0.940
Support Vector Machines – RBF kernel	0.811	0.982	0.943
Random forest	0.980	0.980	0.943

Fragility surfaces

Fig. 7 includes two fragility surfaces generated for a selected bridge in Georgia. The bridge dimensions and other properties are shown in Table 3.4. Fig. 3.7(a) shows a fragility surface of the bridge which includes dowel connections. Fig. 3.7(b) presents a fragility surface for the same bridge when dowel connections are replaced with the same size anchor bolts. In both cases, the failure surface sharply increases when the storm water elevation reaches a threshold value which is indicated by a solid (red) dot on the d_s axis in Figs.

3.7(a) and (b). This threshold is not affected by the wind speed but affected by bridge super-to-substructure connection types. For the bridge with dowel connections, the threshold value is determined when the storm water elevation, d_s , reaches the low chord of bridge girders, which is indicated as the “ $Z_c=0$ ”. On the other end, for the bridge with anchor bolt connections shown in Fig. 3.7(b), the threshold is increased beyond the “ $Z_c=0$ ” point. It is concluded that the storm water elevation significantly affects the probability of failure, as previously stated by other studies (Ataei and Padgett 2012; Padgett et al. 2008).

There is a range of the storm water elevation (d_s) where the wind speed affects P_f . This range is indicated by the solid (red) line between two dots on the d_s axis in Fig. 3.7. and is referred to as the ‘critical range’ herein. Within this ‘critical range’ of d_s , the probability of failure rapidly changes with increasing wind speed, U_{10min} , towards the center of this range, whereas the wind speed does not significantly affect the probability of failure near the lower and upper bounds of this range. Therefore, in addition to the storm water elevation, the wind speed affects the probability of failure as shown in the fragility surfaces.

Table 3.4. Confusion matrix from the Random Forest model.

Predicted by metamodel	Failed	Not Failed
Results from OpenSees		
Failed	280	0
Not Failed	3	1217

3.9. DISCUSSION

The proposed parameterized fragility assessment method appears to provide an acceptable reliability method for most coastal bridges; however, the probability of failure assessment with such binary classification indicates some possible concerns with comparative

quantification of vulnerability. Since the present assessment method is limited to the simply supported bridge type, future work will be devoted to the development of a fragility assessment method for solving for multiple bridge types. It is possible to conclude from Figs. 3.7(a) and (b) that replacing dowel connections with anchor bolts can enhance bridge performance against hurricane waves. However, increasing the size of anchors or dowels must be considered with caution as it can result in a more catastrophic failure of bridge substructures by transferring wave forces imposed on superstructures to substructures.

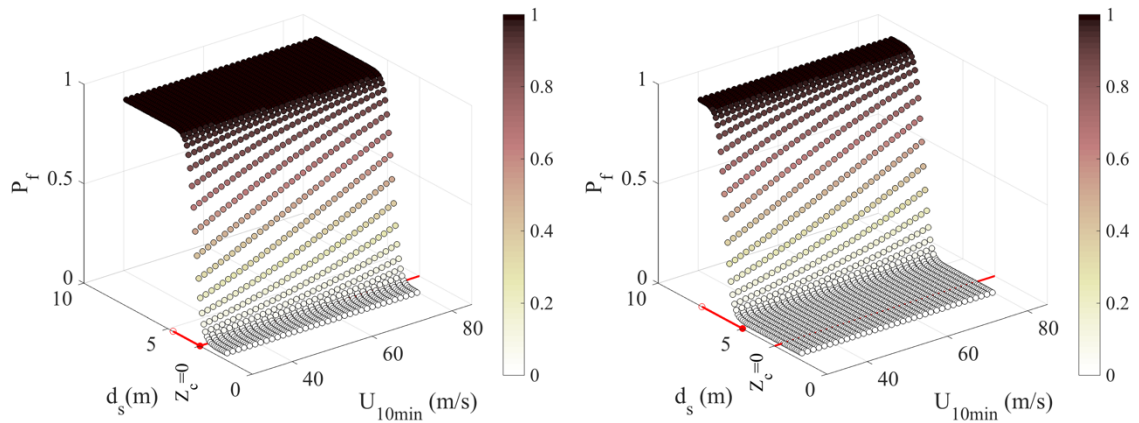


Fig. 3.7. Fragility surfaces for the studied bridge with (a) dowel connection – $\phi 2.54cm$ and (b) anchor bolts connection – $\phi 2.54cm$.

3.10. CONCLUSIONS

The goal of this paper was to implement an efficient, yet practical, approach for determining vulnerability of coastal bridges under hurricane events. A parameterized fragility assessment procedure has been presented and applied to a case study (coastal bridges in Georgia), including various bridge material and geometric parameters, two hazard intensity measures, and seven metamodells. The two hurricane hazard intensity parameters (U_{10min} and d_s) are proposed, and their feasibility has been assessed. The results

indicate that the proposed approach using the Random Forest model has been successfully implemented for simply supported concrete bridges. Furthermore, the results of six other metamodels have been comparatively assessed. It is concluded that the proposed parameterized fragility approach is effective for determining vulnerability of coastal bridges in terms of hurricane categories. Finally, it is also concluded that the proposed approach provides a highly efficient and practical solution for policy makers by developing fragility surfaces in terms of meaningful environmental hazard intensity parameters.

CHAPTER 4

PROBABILISTIC HURRICANE RISK ANALYSIS OF COASTAL BRIDGES INCORPORATING EXTREME WAVE STATISTICS¹

ABSTRACT

Coastal bridges sustained severe damage during hurricanes Ike, Katrina, and Ivan. Reducing the impact of future hurricane events to coastal bridges requires conducting a comprehensive risk analysis. A comprehensive hurricane risk analysis of bridges enables owners to assign resources to the most critical bridges in the inventory through a risk-informed decision making process. A simple risk analysis methodology for prioritizing coastal bridges in a regional inventory is proposed herein. This study presents an efficient methodology for fragility analysis and risk assessment of simply supported coastal bridges vulnerable to hurricane hazard. Various sources of uncertainty associated with hurricane hazard and bridge response are identified, and thereby establishing probability distributions. The novelty of the proposed method includes the consideration of uncertainties in extreme wave heights and wave period by means of a wave spectral density distribution in the calculation of wave forces. The proposed hurricane risk analysis method was successfully applied to coastal bridges located in the state of Georgia (U.S.A.). It is concluded that the hurricane hazard intensity is effectively quantified in terms of a single intensity measure (IM).

¹ A. Saeidpour, M. G. Chorzepa, S.A. Durham and J. K. Christian To be submitted.

4.1. INTRODUCTION

4.1.1. BACKGROUND

Hurricanes Ivan , Rita, and Katrina inflicted significant damage to bridges along the Gulf Coast of the United States in 2004 and 2005 (Cauffman 2006; Stearns and Padgett 2011), raising national concern about the vulnerability of coastal bridges. Consequently, the Federal Highway Administration (FHWA) and ten U.S. states conducted a research project with results published in the 2008 AASHTO “Guide specification for bridges vulnerable to coastal storms”, hereafter referred to as the ‘AASHTO guide’ (Kulicki and Mertz 2008). The AASHTO guide defines three levels of analysis with varying levels of complexity to derive wave and surge parameters and calculate wave forces. The Level 1 analysis is the most conservative of the three methods. When conducting Level-I analysis, the AASHTO guide prescribes equations to determine surge and wave parameters. The Level III analysis is computationally the most demanding method, because it requires simulating hypothetical hurricane scenarios and accounts for joint probabilities of various design parameters. The Level-II (mid-level) method is based on a simulation of the sea state to obtain Metocean (Kulicki and Mertz 2008) parameters. In this study, a Level-III analysis method is proposed as it produces more accurate results than Level-I and Level-II analyses and accounts for a joint probability of various design parameters.

There are a few studies on the risk assessment of bridges exposed to hurricane hazard. Ataei and Padgett proposed a fragility analysis method in which fragility of each bridge was separately assessed (Ataei and Padgett 2012). The two hurricane Intensity Measures (IM) selected in the study are: the maximum wave height, H_{max} , and distance between storm water elevation and deck low chord elevation, Z_c . Kameshwar and Padgett

(Kameshwar and Padgett 2014) proposed a surrogate modeling approach for multi-hazard fragility analysis and risk assessment of bridges vulnerable to seismic and hurricane hazards. Mondoro et al. (Mondoro et al. 2016) proposed a risk management strategy in which both deteriorating conditions of bridges under repeated traffic loads and repair/retrofit actions performed to mitigate hurricane hazard are considered through a multi-objective optimization algorithm.

4.1.2. SCOPE

This paper focuses on developing a framework for risk assessment of bridges exposed to hurricane hazard by incorporating uncertainties inherent in demand and capacity. The proposed framework is developed based on the following assumption: (1) past hurricanes identified the unseating and misalignment of simply supported spans as the predominant and most severe mode of failure among damaged bridges (Gutierrez et al. 2006; Okeil and Cai 2008; Padgett et al. 2008; Robertson et al. 2007; Stearns and Padgett 2011). Therefore, the damage state in this paper only represents the condition where unseating/shifting of bridge superstructure occurs. Other damage states such as scour and debris-impact related damage are not considered herein; (2) In evaluating the capacity, uncertainties associated with structural conditions and as-built conditions of anchor bolts/dowels are not considered in this study. Two bearing connections with anchor bolts or dowels are considered; (3) Swell generally refers to the waves generated by distant storms. In assessing the demand, it is assumed that bridges are located within the hurricane radius of maximum wind and that wind-generated waves govern; (4) Further, it is assumed that the surge heights obtained from the SLOSH Maximum of Maximum (MOM) data are associated with the upper-bound wind speed defined for each category in the Saffir-Simpson hurricane wind scale;

(5) Lastly, the risk measure considered in this study is the mean annual rate of exceeding the damage state described above.

4.1.3 SIGNIFICANCE

Hurricane risk analysis of bridges enables the stakeholders to assign their resources to the most critical bridges in the inventory through a risk-informed decision making process. In the proposed risk assessment framework, the intensity of hurricane hazard is effectively quantified in terms of a single intensity measure (IM). The maximum sustained wind speed is selected as the single intensity measure because of its efficiency and sufficiency (Luco and Cornell 2007) in quantifying the uncertainties in two major demand variables, surge height and wave characteristics. The maximum sustained wind speed is the peak 1-minute wind at the standard meteorological observation height of 10 m over unobstructed exposure (Schott et al. 2012). Furthermore, the quantification of hurricane hazard in terms of the maximum sustained wind speed facilitates the communication of risk with the owners because the hurricane categories are defined by the Saffir-Simpson hurricane wind scale based on maximum sustained wind speed (Schott et al. 2012). An efficient fragility analysis and risk assessment procedure, conditioned on the maximum sustained wind speed, is successfully applied to coastal bridges located in the state of Georgia (USA).

4.1.4. SUMMARY

This paper is organized in three sections. Section 4.2 presents the proposed methodology for fragility analysis of coastal bridges exposed to hurricane wave forces. In this section, a novel procedure is introduced to determine fragility functions by incorporating the uncertainties in extreme wave heights and wave periods in calculation of forces by deriving

their probabilistic distributions from wave spectra. In Section 4.3, the hurricane hazard curve, which describes the mean annual frequency of exceedance in terms of wind speed, is obtained from published return period of the 3-second peak gust wind speed. Finally, the hazard curve is convolved with the fragility functions obtained from Section 4.2 to evaluate the hurricane risk. The flowchart in Fig. 4.1 illustrates this the proposed framework. In the last section of this study, the proposed hurricane risk analysis method is applied to coastal bridges located in the state of Georgia.

4.2. FRAGILITY ANALYSIS METHODOLOGY

Fragility is a concept in the context of structural reliability which determines the probability of reaching or exceeding a specific damage state conditioned on a hazard intensity measure (IM) (Porter 2003).

4.2.1 INTENSITY MEASURE

An intensity measure (IM) suitable for fragility analysis is an environmental parameter(s) that effectively quantifies the intensity of a hazard so that, once it is established, the demand is not further affected by other hazard variables (Deierlein et al. 2003). In this study, the maximum sustained wind speed, U_{1-min} , was selected as the only intensity measure for the following reason.

AASHTO guide quantifies the maximum wave forces exerted on a bridge superstructure as a function of wave parameters (e.g. height and period) and surge height. As it will be shown in section 4.2.4-5, parameters of wind-generated waves can be obtained from wave spectra, which in turn is a function of wind speed.

Surge height is also correlated to wind speed. In the context of this paper, hurricane surge heights (d_s) are obtained from the SLOSH MOM data (Jelesnianski et al. 1992),

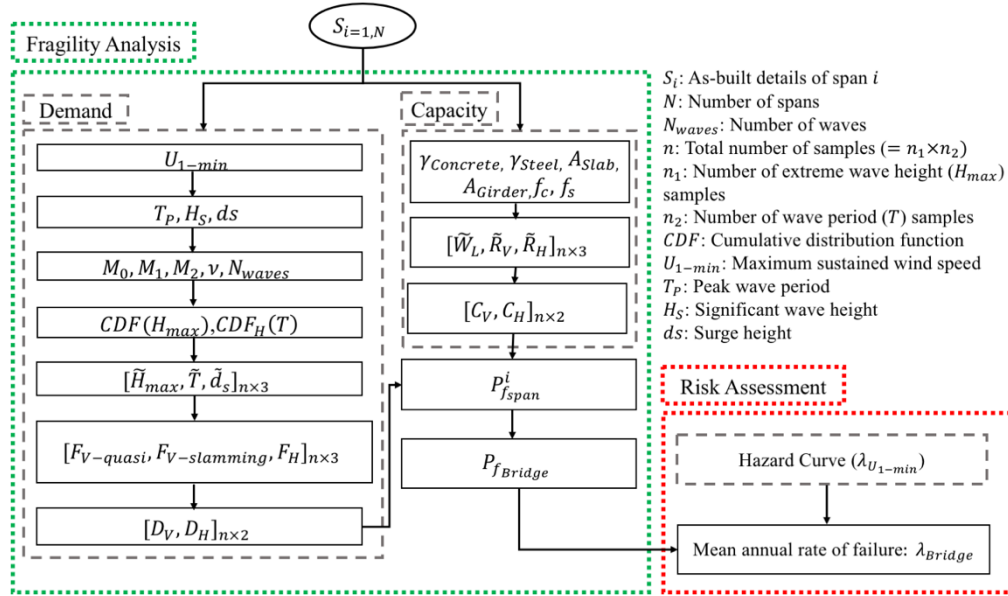


Fig. 4.1. Flowchart of the proposed risk assessment framework

which provides the worst case scenario surge heights under the perfect storm conditions at each location for each hurricane category. The SLOSH MOM data are categorized based on the Saffir-Simpson hurricane wind scale. Saffir-Simpson is a macro hurricane damage scale which describes possible hurricane impacts based on the maximum sustained wind speed (Schott et al. 2012). Each hurricane category is defined by an interval between two threshold wind speeds, and the MOM surge heights for each hurricane category are associated with the upper-bound maximum sustained wind speed of each category in the Saffir-Simpson scale (Mondoro et al. 2016; Phan et al. 2007).

4.2.2 DAMAGE STATE

The first step in determining fragility functions is to define the damage state(s). Past hurricanes identified the unseating and misalignment of simply supported spans as the

predominant severe mode of failure among damaged bridges (Gutierrez et al. 2006; Okeil and Cai 2008; Padgett et al. 2008; Robertson et al. 2007; Stearns and Padgett 2011). Therefore, the damage state in this paper represents the condition where unseating/shifting of bridge superstructure occurs.

4.2.3 DEMAND AND CAPACITY

Fragility can equivalently be interpreted as the probability of a demand exceeding a capacity, conditioned on a IM (Ching et al. 2009) defined in Section 4.2. Wave-induced vertical, slamming and horizontal forces are determined in accordance with the AASHTO guide. The vertical demand, D_V , is determined by Eq. (4.1), and the capacity is determined by Eq. (4.2). The summation of the deck weight and connection strength is the total uplift capacity of a bridge span.

$$D_V = (F_{V-quasi} + F_{V-slamming}) \times L_{span} \quad (4.1)$$

$$C_V = W_L \times L_{span} + 2 \times N_{Girder} \times R_V \quad (4.2)$$

The horizontal demand, D_H , and the capacity, C_H , are determined using Eq. (4.3) and Eq. (4.4), respectively.

$$D_H = F_H \times L_{span} \quad (4.3)$$

$$C_H = 2 \times N_{Girder} \times R_H \quad (4.4)$$

in which $F_{V-quasi}$, $F_{V-slamming}$ and F_H are the maximum vertical quasi-static, slamming and maximum horizontal quasi-static wave forces per unit length of the span (Kulicki and Mertz 2008); L_{span} , W_L are length and width of the span, respectively; N_{Girder} is the number of girders, and R_V , R_H are the strength of individual connections between the girders and substructure in the vertical and horizontal directions, respectively.

Probabilistic description of various sources of uncertainty, inherent in demand and capacity, must be defined before fragility analysis is performed. In the following subsections, various demand and capacity variables are introduced and their probability distributions are derived.

4.2.4. PROBABILISTIC DESCRIPTION OF DEMAND VARIABLE

As mentioned in section 4.2.3, structural demand is defined in terms of wave force components in the context of this study. Quantification of wave force components and their parameters is the next step in developing a probabilistic description for the demand.

Marine and Sheppard conducted an extensive experimental study to characterize wave forces acting on a bridge superstructure and proposed semi-empirical equations for maximum vertical, horizontal and slamming components of these forces, in terms of surge, wave, and bridge parameters (Sheppard and Marin 2009). The AASHTO guide recommends using these equations to calculate wave-induced forces on a bridge superstructure. These equations predict the wave forces in terms of wave and surge parameters.

AASHTO guide suggests using “Shore Protection Manual” (USACE 1984) equations to obtain deterministic estimates of wave and surge parameters values, which yield to conservative estimations of wave force magnitudes. On the other hand, the proposed risk assessment framework in this study considers uncertainties in wave forces parameters. The following subsections in this section defines the probabilistic descriptions of extreme wave heights, wave period and surge height.

4.2.4.1 PROBABILISTIC DESCRIPTION OF WAVE HEIGHTS

Short-term statistics of wave heights is considered, i.e. sea state is assumed to be a stationary process during the Passage of hurricane. Longuet-Higgins (Longuet-Higgins 1975) proposed the Rayleigh distribution for the relative wave amplitude, ξ , as shown in Eq. (4.5). This method assumes a Gaussian process for sea surface elevation and a narrow-banded wave spectrum.

$$f(\xi) = \xi \exp\left(-\frac{\xi^2}{2}\right) \quad (4.5)$$

where $\xi = A/\sqrt{M_0}$, A is the wave amplitude defined as half the vertical distance between crest and trough; and M_0 is the 0th moment of a wave spectrum. By virtue of the narrow-banded wave spectrum assumption, the wave height is considered twice the wave amplitude, $H \approx 2A$. By replacing A with $H/2$ and rewriting Eq. (4.5), the Rayleigh distribution of wave heights, H , is determined as follows:

$$f(H) = \frac{H}{4M_0} \exp\left(-\frac{H^2}{8M_0}\right) \quad (4.6)$$

Forristall (Forristall 1978) used 116 hours of hurricane generated waves in the Gulf of Mexico to investigate the validity of Eq. (4.6) and concluded that the Rayleigh distribution “overpredicts the heights of the higher waves” and proposed a two-parameter Weibull distribution for relative wave heights, \tilde{H} , as shown in Eq. (4.7) and concluded that the Weibull distribution provides a better fit for the wave data:

$$f(\tilde{H}) = \frac{a}{b} \tilde{H}^{a-1} \exp\left(-\frac{\tilde{H}^a}{b}\right) \quad (4.7)$$

in which $a = 2.126$ and $b = 8.42$ are the distribution parameters empirically determined using the wave data; and $\tilde{H} = H/\sqrt{M_0}$. In a later study, Longuet-Higgins (Longuet-Higgins 1980) proposed a rescaled shape of the Rayleigh distribution in Eq. (4.6), which

accounts for the width of the wave spectrum, and concluded that a modified Rayleigh distribution, Eq. (4.8), predicts the recorded wave heights just as well as the Weibull distribution. The modification factor, α , is given by Eq. (4.9) where ν is the spectrum bandwidth parameter determined by Eq. (4.10):

$$f(H) = \frac{H}{4\alpha M_0} \exp\left(-\frac{H^2}{8\alpha^2 M_0}\right) \quad (4.8)$$

$$\alpha = \sqrt{1 - \left(\frac{1}{8\pi^2} - \frac{1}{2}\right)\nu^2} \quad (4.9)$$

$$\nu = \sqrt{M_0 M_2 / M_1^2 - 1} \quad (4.10)$$

Several other studies examined the validity of these distributions, and some proceeded with proposed new formulations, which mostly are modifications of Rayleigh distribution in Eq. (4.6) (Casas-Prat and Holthuijsen 2010; Nayak and Panchang 2015; Tayfun 1983). Casas-Prat and Holthuijsen (Casas-Prat and Holthuijsen 2010) examined 10 million wave records measured by wave buoys in the Mediterranean Sea and compared them with various wave heights distributions. They concluded that the Weibull distribution in Eq. (4.7) and modified Rayleigh distribution in Eq. (4.8) provide a better fit whereas the original Rayleigh distribution in Eq. (4.6) overpredicts the recorded wave heights. In another study, Feng et al. (Feng et al. 2014) investigated 10 years of wave measurements from Norwegian sea and reconfirmed that the Weibull distribution yielded better results than the original Rayleigh distribution in predicting H_{\max}/H_s and H_{\max} (H_s : Significant wave height, H_{\max} : Maximum wave height). A recent study by Nayak and Panchang (Nayak and Panchang 2015) concluded that the original Rayleigh distribution (Eq. 6) overestimates various quantities associate with wave heights, and that the Weibull distribution provides a better fit to the recorded data.

Theoretical formulations, developed for determining wave heights and wave amplitudes distributions in deep water, such as those presented by Longuet-Higgins (Eq. (4.5), (6) and (8)), assume a Gaussian distribution of the sea surface displacement. Therefore, they are only applicable for analysis of bridges located in deep waters.

Many of the vulnerable coastal bridges are not built over a waterway and predicted hurricane surge elevation at their location does not exceed a few meters. Shallow water waves are the major concern for this group of bridges. Shallow water waves have different properties due to the nonlinear effects such as wave breaking; and general accepted theoretical assumptions, which leads to Rayleigh distribution for deep water waves, is not available for them (Holthuijsen 2010).

Despite the lack of theoretical basis, it has shown that the Rayleigh distribution reasonably works well for the shallow water waves (Thornton and Guza 1983). One of the first distributions for shallow water waves was the modified Rayleigh distribution proposed by Glukhovskiy (Glukhovskiy 1961), which accounts for the effect of depth-limited wave breaking. In this study, a modified formulation of Glukhovskiy equation, as proposed by Klopman (Klopman 1996), is considered:

$$f(H) = \frac{-A\kappa}{H} \exp \left(-A \left(\frac{H}{H_{rms}} \right)^\kappa \right) \quad (4.11)$$

where H_{rms} is the rms wave height given by $H_{rms} = H_s/\sqrt{2}$; $A = \left[\Gamma \left(\frac{2}{\kappa} + 1 \right) \right]^{\kappa/2}$; Γ is Gamma function; and κ is defined by Eq. (4.11-a) and is a function of $H^* = H_{rms}/d_s$.

$$\kappa = \frac{2}{1-\beta H^*} \quad (4.11-a)$$

$\beta = 0.7$ is an empirical parameter obtained from laboratory test results.

This study is primarily concerned with coastal bridges located in shallow waters although a number of other studies also addressed the deep water wave height and amplitude distributions (Naess 1985; Tayfun and Fedele 2007). Probability distributions of wave heights discussed in this section are summarized in Table 4.1.

4.2.4.2 CONDITIONAL PROBABILITY DISTRIBUTION OF WAVE PERIODS

Contrary to the wave heights distributions described in Section 4.2.4.1, limited information on distributions of wave periods is found in the literature. Longuet-Higgins (Longuet-Higgins 1983) proposed a joint distribution of relative wave amplitudes and relative wave periods and derived the conditional distribution of relative wave period as follows:

$$f(\eta|\xi) = \frac{\xi}{\sqrt{2\pi}} \exp\left(-\frac{\xi^2\eta^2}{2}\right) \quad (4.12)$$

in which ξ is relative wave amplitude given in Eq. (4.5); and η is the relative wave period defined by Eq. (4.13):

$$\eta = \frac{T - \bar{T}}{v\bar{T}} \quad (4.13)$$

where T is the wave period, defined as the time interval between successive zero up-crossings; \bar{T} is the mean spectral wave period; and v is the spectral bandwidth parameter determined by Eqs. (4.14) and (4.15), in which M_i is the i th moment of a wave spectrum.

$$\bar{T} = 2\pi \left(\frac{M_0}{M_1} \right), \quad (4.14)$$

$$v = \sqrt{\frac{M_2}{M_0} \frac{\bar{T}}{2\pi}} \quad (4.15)$$

As discussed in the last section, the assumptions made by Longuet-Higgins to derive statistical distributions of wave heights and wave periods are only true for deep water conditions and may not be applicable to shallow or transit water. In an attempt to

address this issue, Le Mehaute (Le Méhauté et al. 1986) proposed statistical properties of shallow water by linear transformation of deep water properties and concluded that wave periods distribution in shallow water is not Gaussian. He proposed a modified form of Longuet-Higgins equation (Eq. 4.16) for conditional distribution of relative wave periods, which includes a shoaling coefficient term (K_s), given by:

$$f(\eta|\xi) = \frac{\xi}{\sqrt{2\pi}} \exp\left(-\frac{\xi^2 \eta^2}{2K_s^2}\right) \quad (4.16)$$

in which ξ and η are defined in the previous section and K_s is:

$$K_s = 1/\left(\sqrt{1 + \frac{2kd_s}{\sinh 2kd_s}} \sqrt{\tanh kd_s}\right) \quad (4.17)$$

where k is the wave number ($= 2\pi/\lambda$) and d_s is the water depth.

As it can be seen Eq. (4.16) is no longer Gaussian since K_s is a function of wave period. The AASHTO Guide suggests using Eq. (4.18) obtained from the “Shore Protection Manual” (USACE 1984), to determine the wave length (λ) in shallow waters:

$$\lambda = \frac{gT^2}{2\pi} \sqrt{\tanh\left(\frac{4\pi^2 d_s}{T^2 g}\right)} \quad (4.18)$$

By rewriting Eq. (4.16) in terms of H , Eq. (4.19) is obtained which determines the conditional distribution of wave periods (T) for a given a wave height (H). The probability distributions of wave periods discussed in this section are summarized in Table 4.1.

$$f(T|H) = \frac{H}{2\nu\sqrt{2\pi M_0 \bar{T}}} \exp\left(-\frac{H^2(T-\bar{T})^2}{8\nu^2 M_0 K_s^2 \bar{T}^2}\right) \quad (4.19)$$

4.2.4.3. PROBABILISTIC DISTRIBUTION OF EXTREME WAVES

The joint probability distribution of individual wave heights and periods in a given stationary sea state, $f(H, T)$, is determined as follows:

$$f(H, T) = f(H) \cdot f(T|H) \quad (4.20)$$

Table 4.1. Probabilistic distributions of demand variables and their parameters used for fragility analysis

	Distribution type	Parameters	Application
Wave height: $f(H)$			
Forristall [1978]	Weibull	a, b, \tilde{H}	Deep water
Longuet-Higgins [1980]	Rayleigh	M_0	Deep water
Klopman [1999]	Rayleigh	H_{rms}, A, κ	Shallow water
Wave period: $f(T H)$			
Longuet-Higgins [1980]	Normal	\bar{T}, ν	Deep water
Le Mehaute [1981]	-	\bar{T}, ν, K_s	Shallow water
Water elevation: $f(d_s)$			
SLOSH	Uniform	d_s	-

in which $f(H)$ and $f(T|H)$ are the probability distribution functions of wave heights and conditional probability distribution of wave periods, respectively.

The proposed joint distribution density of individual heights (H) and wave periods (T) are shown in Fig. 4.2. The maximum wave heights is limited by the height of breaking waves (bottom end of contours in Fig. 4.2b) in accordance with the AASHTO Guide ($\min(0.65d_s, \lambda/7)$). In this figure, it is found that the most probable pair of wave height and period is $H \approx 2.2$ meters and $T \approx 5.0$ s.

The probability that height of a randomly selected wave is less than a certain value (i.e., an extreme value), $P(H < H_{max})$, denoted as CDF_1 herein, is obtained by Eq. (4.21), in which F denotes the cumulative distribution function of wave heights:

$$CDF_1 = P(H < H_{max}) = F(H) \quad (4.21)$$

The probability that no wave height exceeds H_{max} is equal to $(CDF_1)^N$, provided that the ‘ N ’ number of statistically independent random waves strike a coastal bridge during a hurricane. H_{max} denotes the extreme wave height during the hurricane and its cumulative distribution function, $(CDF_1)^N$, which is denoted by $F(H_{max})$. $F(H_{max})$ for

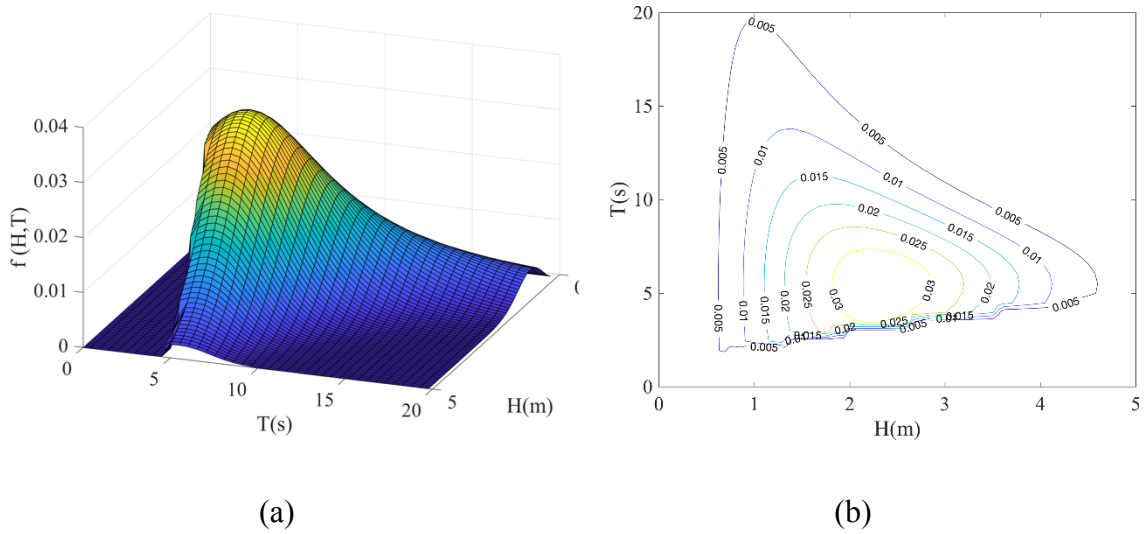


Fig. 4.2. (a) Surface (b) contour of the joint probability density of wave height and wave period ($H_s = 3.25m, \bar{T} = 6.7s, \nu = 1.07$)

selected number of waves ($N=100, 500, 1000,$ and 5000) using the same sea state is shown in Fig. 4.3. $F(H)$, cumulative distribution of individual wave heights, is also shown in the figure. It is clear that the probability distributions of extreme wave heights are dramatically different from the probability distribution of individual wave heights. While the maximum probable individual wave height does not exceed $5m$, extreme waves heights for $N = 3000$

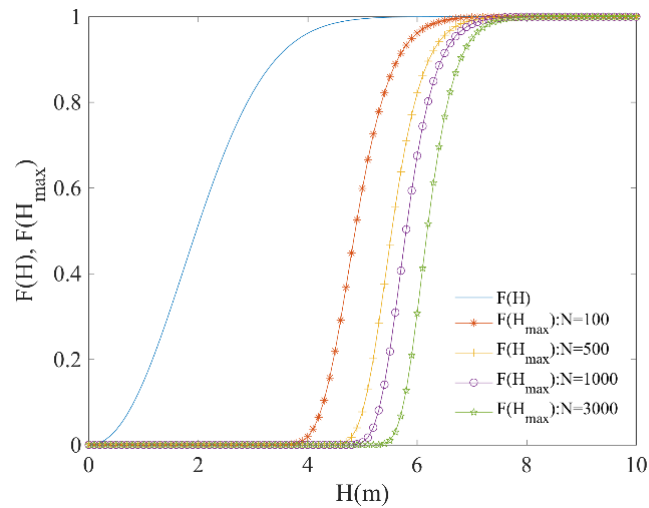


Fig. 4.3. $F(H_{max})$ for different values of N

(which approximately represents the number of waves during a 3hrs hurricane with a mean wave period \bar{T} of 10 seconds) range between 5.5m and 7.5m.

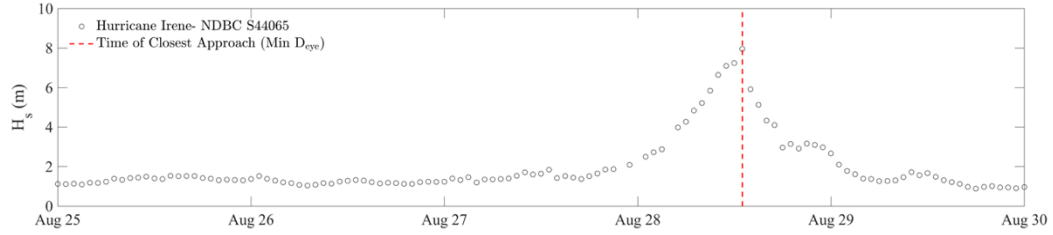
In this study, the number of waves (N) striking a bridge during a hurricane is considered as a random variable. N could be estimated as a function of hurricane duration (D_H) and hurricane mean wave period (\bar{T}) as shown in Eq. (4.22):

$$N = \frac{D_H}{\bar{T}} \quad (4.22)$$

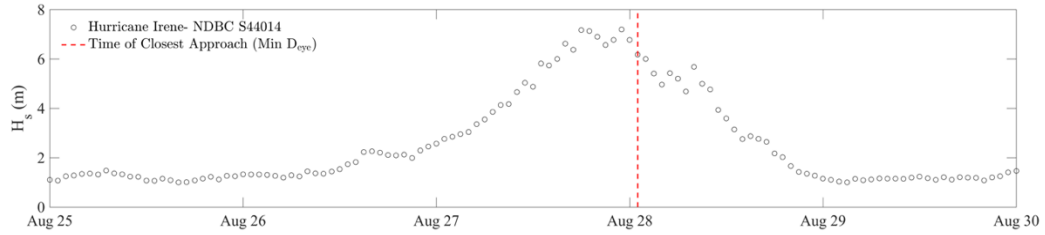
\bar{T} is defined in Eq. (4.14). D_H is estimated from past hurricane records. Fig. 4.4 shows variation of significant wave height, H_S , during passage of various hurricanes. The wave heights were estimated from the spectral density records of National Data Buoy Center (NDBC) stations. Each unfilled dot in Fig. 4.4 represents an estimated significant wave height, H_S , obtained from a 1-hour long record. The dashed line indicates the time when hurricane eye was at its closest distant from the station. It is observed that the time span during which extreme significant wave heights (and thus extreme wave height) occurred (D_H) ranges from 1 hour (see Fig.4.4a) to several hours as shown in Fig.4.4 (b), (c), and (d). Therefore, D_H is assumed to have a uniform distribution ranging between 1 and 6 hours.

4.2.4.4 PROBABILISTIC DISTRIBUTION OF SURGE HEIGHT

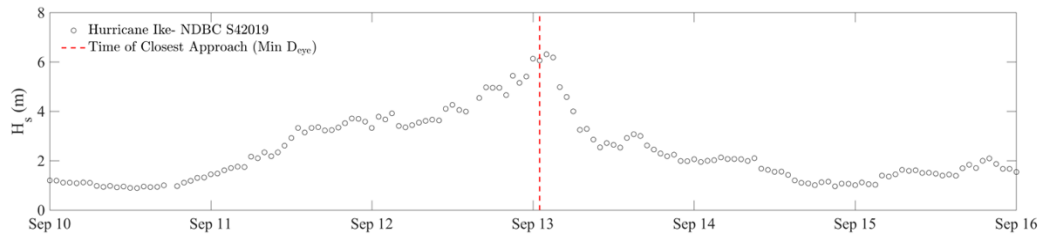
As mentioned in section 4.2.1, storm surge height elevation at the bridge location (d_s) in this study are obtained from publicly available NOAA SLOSH model “Maximum of the Maximum Envelope of High Water” (MOM) maps, which provide the worst case high water elevation at a particular location under perfect storm conditions (Jelesnianski et al. 1992). SLOSH accuracy is estimated to be within $\pm 20\%$, based on post hurricane high water marks and gauge observation.



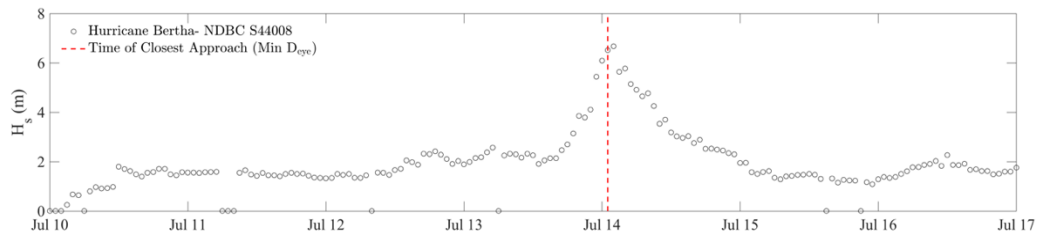
(a)



(b)



(c)



(d)

Fig 4.4. Variation of significant wave height H_s during passage of hurricane estimated from spectral density records of NDBC buoys stations (a) Hurricane Irene (2011)- Station 44065 (b) Hurricane Irene (2011)- Station 44014 (c) Hurricane Ike (2008)- Station 42019 (d) Hurricane Bertha (1996)- Station 44008

SLOSH MOMs maps provide storm water elevations for each Saffir-Simpson hurricane category. For sustained wind speeds in-between Saffir-Simpson hurricane categories,

linear interpolations has been used to estimate the storm water elevation and a uniform distribution ranging $\pm 20\%$ the estimated value is considered in this study.

4.2.5. WAVE SPECTRUM

In section 4.2.4, frequent references have been made to wave spectrum parameters while discussing various probabilistic descriptions of wave heights and wave periods. In fact, statistical properties of sea surface is correlated to its underlying energy spectrum (Forristall 1978). A brief description of wave spectrum concept, various formulations of wave spectrum available in the literature, and spectral parameters is provided in this section.

Characterization of sea waves as a stochastic process with spectral analysis was initially introduced in the 1970s and 1980s. It was estimated that, at any given time, the ocean surface is determined as the result of superimposed waves of different heights and periods. The total wave energy is unevenly spread among these waves, and ocean wave spectrum represents a distribution of wave energy among waves with different periods. Several idealized formulations for wave spectrum have been developed in the literature. Most wave spectra are expressed by a standard exponential equation in terms of the wave angular frequency as shown in Eq. (4.23):

$$S(\omega) = \frac{C_1}{\omega^5} \exp\left(-\frac{C_2}{\omega^4}\right) \quad (4.23)$$

where S is wave spectral density, ω is wave angular frequency and C_1, C_2 are constants.

One of the first wave spectra studied in the literature is the Pierson-Moskowitz (P-M) spectrum which was based on extensive measurements in the North Atlantic Ocean and is a function of $U_{19.5}$ defined as the wind speed measure at a height of 19.5 meters (Pierson and Moskowitz 1964). This spectrum was originally created under the fully developed sea

assumption (i.e., the wave crest phase speed equals the wind speed). However, Hasselmann et al. (Hasselmann et al. 1976) derived the same spectrum without fully developed sea assumption. A modified form of P-M spectrum with two parameters, namely Bretschneider Spectrum (B-S), was later developed and is widely used today since it does not require fully developed sea condition (Bretschneider 1959). The B-S spectrum expressed in terms of the angular frequency, ω , is as follows:

$$S_{B-S}(\omega) = \frac{5}{16} H_s^2 \omega_p^4 \omega^{-5} \exp\left(-\frac{5}{4} \left(\frac{\omega}{\omega_p}\right)^{-4}\right) \quad (4.24)$$

in which ω_p is the peak angular spectral frequency defined by the T_p is the peak spectral period, $\omega_p = 2\pi/T_p$.

Another significant international study, “The Joint North Sea Wave Observation Project (JONSWAP)” was carried out by collecting wave data from 13 stations in the North Sea, in order to investigate the fetch-limited waves. Hasselman et al. proposed a new spectrum after analyzing the recorded data obtained from the JONSWAP, which was referred to as “the JONSWAP spectrum” (Hasselmann et al. 1973). While JONSWAP is widely used by the offshore industry, further adjustments were proposed by other researchers to enhance the high frequency tail of the spectrum. Most wave spectra in the literature are formulated by an inversely proportional function of ω^{-5} (see Eq. 4.23), whereas, Battjes et al. (Battjes et al. 1987) demonstrated that estimating the wave spectrum in terms of ω^{-4} yields much better predictions in the high frequency band. This was later incorporated in the JONSWAP spectrum by Donelan et al. (Donelan et al. 1985), and Young made further amendments to represent the spectral parameters in terms of H_s and T_p (Young 1992). The modified form of the JONSWAP spectrum by Young, Eq. (4.25), is used for this study, and Equations (4.26) through (4.30) define the associated parameters.

$$S_{JONSWAP}(\omega) = \beta g^2 \omega_p^{-1} \omega^{-4} \exp\left(-\left(\frac{\omega}{\omega_p}\right)^{-4}\right) \gamma^\delta \quad (4.25)$$

$$\delta = \exp\left(-(\omega - \omega_p)^2 / 2\sigma_0^2 \omega_p^2\right) \quad (4.26)$$

$$\beta = 200 g^{-1.571} M_0^{0.786} T_p^{-3.143} \quad (4.27)$$

$$\gamma = 6.489 + 6 \log(2.649 \cdot 10^7 g^{-2.857} M_0^{1.429} T_p^{-5.714}) \quad (4.28)$$

$$\sigma_0 = 0.08 + 6.940 \cdot 10^{-26} g^{8.571} M_0^{-4.287} T_p^{17.412} \quad (4.29)$$

$$M_0 = H_s^2 / 16. \quad (4.30)$$

The JONSWAP spectrum was formulated using the similarity-law for deep water, which states that the shape of growing wind-generated wave spectra in deep water is reasonably consistent and thus can be described by a self-similar equation (Kitaigorodskii 1962). Therefore, the deep water spectra may not be directly applicable for fragility assessment of coastal bridges in shallow waters. Bouws et al. (Bouws et al. 1985) recognized that the wave number expression of the similarity-law can be developed for shallow water and proposed a frequency-depth dependency factor, $\phi(\omega, d_s)$, which transforms the JONSWAP spectrum developed for deep water into a spectrum for shallow water. They named the spectrum ‘TMA’ and successfully tested the spectrum with three available data sets (Battjes et al. 1987). The ‘TMA’ spectrum is described by Eq. (4.31), in which d_s is the water depth and the transformation formula for $\phi(\omega, d_s)$ is given by Eq. (4.32).

$$S_{TMA}(\omega, d_s) = S_{JONSWAP}(\omega) \phi(\omega, d_s) \quad (4.31)$$

$$\phi(\omega, d_s) = \frac{k^{-3}(\omega, d_s) \frac{\partial k(\omega, d_s)}{\partial \omega}}{k^{-3}(\omega, \infty) \frac{\partial k(\omega, \infty)}{\partial \omega}} \quad (4.32)$$

in Eq. (4.31), the wave number, κ , is defined by $2\pi/\lambda$, where λ is the wave length. A

simplified expression for Eq. (4.32) was proposed by Thomson and Vincent (Thompson and Vincent 1985) to determine ϕ in terms of ω_h :

$$\phi(\omega, d_s) = \begin{cases} 1/2 \omega_h^2 & \omega_h \leq 1 \\ 1 - 1/2 (2 - \omega_h)^2 & \omega_h > 1 \end{cases} \quad (4.33)$$

where $\omega_h = \omega \sqrt{d_s/g}$ and g is the gravitational constant.

Ochi and Hubble proposed a new wave spectrum which accounts for both wind and swell (Ochi and Hubble 1977). Wind is not the only mechanism by which ocean waves are created. In fact, waves generated at a specific point might be the results of a superposition of waves generated by different mechanisms. Hurricane-generated swell is a good example. Swell refers to the waves generated by distant storms which generally have longer periods than wind generated waves which generally have longer periods than wind generated waves (Lewandowski 2004). After statistical analysis of 800 wave spectra obtained from North Atlantic Ocean, Ochi and Hubble developed a family of spectra, each of which is the result of a superposition of a high frequency wind generated spectrum and a low frequency swell spectrum. This family of 11 spectra includes the most probable spectrum expected to occur for a particular sea state and upper and lower bound spectral shapes, which are probable to occur with a confidence coefficient of 0.95. Each of 11 Ochi-Hubble (O-H) spectra is formulated by Eq. (4.35), and $\omega_{01}, \omega_{02}, \lambda_1, \lambda_2$ for each spectra is obtained from Eq. (4.36):

$$S_{O-H}(\omega) = \frac{1}{4} \sum_{j=1}^2 \left(\frac{4\lambda_j+1}{4} \omega_{0j}^4 \right)^{\lambda_j} \frac{1}{\Gamma(\lambda_j)} \frac{H_{sj}^2}{\omega^{4\lambda_j+1}} \exp \left(-\frac{4\lambda_j+1}{4} \left(\frac{\omega_{0j}}{\omega} \right)^4 \right) \quad (4.35)$$

$$\omega_{01}, \omega_{02}, \lambda_1, \lambda_2 = a \exp(-bH_s) \quad (4.36)$$

see (Ochi and Hubble 1977) for a, b values for each spectra.

The four wave spectral density formulations discussed in this section are summarized in Table 4.2. To investigate the accuracy of these four spectra models in

Table 4.2. Summary of implemented wave spectra and their parameters

Spectrum	Parameters
Bretschneider (B-S) [1978]	H_s, ω_p
Modified JONSWAP [1992]	$\omega_p, \beta, \gamma, \delta$
TMA [1985]	$\omega_p, \beta, \gamma, \delta, d_s$
Ochi-Hubble (O-H) [1976]	$\omega_{01}, \omega_{02}, \lambda_1, \lambda_2$

predicting sea state parameters, spectral density records during hurricane Ike are compared with the predicted spectra obtained from using the four models. Hurricane Ike (2008) was an Atlantic hurricane which caused tremendous damage to infrastructure including bridges in Texas. The National Data Buoy Center (NDBC) owns and operates a network of several buoys and meteorological stations in various locations in the U.S. Hurricane Ike passed by multiple NDBC stations during its duration on record. Among them, station number 42019 was selected for this study because it is one of the two stations in the vicinity of Ike's track and is located in shallow coastal waters of the Atlantic Ocean. The other station (42035) was not considered because it traveled 35 miles southwest of its original location due to the hurricane.

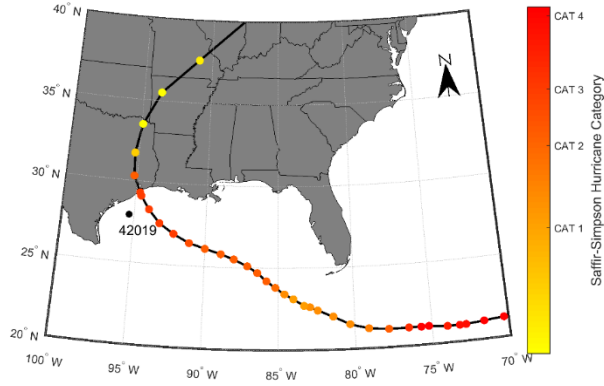
The hurricane Ike's track and the location of the NDBC station No. 42019 are shown in Fig. 4.6 (a). Fig. 4.6 (b) depicts significant wind radii for tropical storm force winds (34 knots), storm force winds (50 knots), and hurricane force winds (64 knots) recorded at 7:00 UTC on Sep 13th, 2008, when Ike made landfall on Galveston Island. Fig. 4.6 (c) compares recorded spectral density measured at station No. 42019 with predicted spectra in the hour leading to the landfall time.

The spectra predicted by the Ochi-Hubble model, noting that the most probable spectra is selectively shown in the figure, under-predicts the angular frequency of the peak

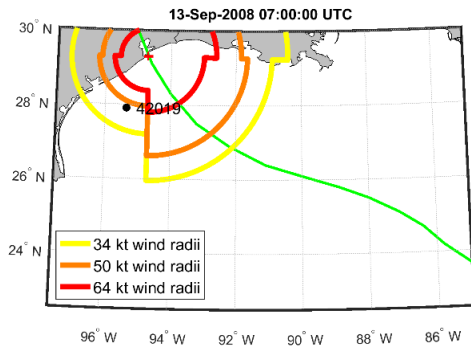
wave spectrum density, which results in overestimation of the peak wave period. The discrepancy between recorded and predicted spectra is explained by the fact that Ochi-Hubble spectra model includes the effect of low frequency swell waves, whereas recorded spectra is most likely governed by wind waves as stations is located inside the 34kt radii hurricane wind field. When comparing the TMA and JONSWAP models, it is observed that the total energy (area under the spectra) in the TMA model agree well with the total energy of the recorded spectra. This is reasonable because TMA is more accurate in shallow waters whereas JONSWAP model should work well for deep waters. Based on this fact and a comparison of the four models in Fig 4.6(c), it is concluded that the TMA spectra should be used in this study to estimate wave spectral parameters needed for calculation of wave height and period probabilities.

4.2.6. PROBABILISTIC MODELING OF DEMAND

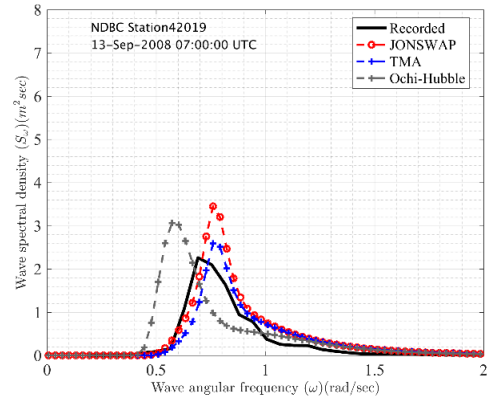
The probabilistic description of demand variables defined in the previous section are used to generate multiple realizations of demand, which in turn are used to obtain fragility functions by using the eleven steps shown in Fig. 4.1: (1) Find the estimated hurricane surge heights under each hurricane category for the high tide (d_s) from the SLOSH (MOM) maps for each span; (2) By linearly interpolating surge heights elevation obtained in step 1, scale surge heights for the sustained wind speed; (3) For each sustained wind speed, find spectral peak period, T_p , by Eq. (4.37) and significant wave height, H_s , by Eq. (4.38) in accordance with the AASHTO guide, where g : standard gravity (32.174 ft/sec^2), d : Average water depth over the fetch length (ft), U_t^* : Wind stress factor (ft/sec), F : Fetch length (ft):



(a)



(b)



(c)

Fig. 4.5 (a) Hurricane Ike's (2008) track and intensity and the buoy location at NDBC station No. 42019; (b) Hurricane Ike's significant wind radii when making a landfall in Galveston, Texas; and (c) Comparison of recorded and predicted spectra in the hour leading to the landfall.

$$T_p = 7.54 \tanh \left(0.833 \left(\frac{gd}{U_t^{*2}} \right)^{3/8} \right) \tanh \left(\frac{0.0379 \left(\frac{gF}{U_t^{*2}} \right)^{1/3}}{\tanh \left(0.833 \left(\frac{gd}{U_t^{*2}} \right)^{3/8} \right)} \right) \left(\frac{U_t^*}{g} \right) \quad (4.37)$$

$$H_s = 0.283 \tanh \left(0.53 \left(\frac{gd}{U_t^{*2}} \right)^{3/4} \right) \tanh \left(\frac{0.00565 \left(\frac{gF}{U_t^{*2}} \right)^{1/2}}{\tanh \left(0.53 \left(\frac{gd}{U_t^{*2}} \right)^{3/4} \right)} \right) \left(\frac{U_t^{*2}}{g} \right) \quad (4.38)$$

(4) Generate n_1 samples (\tilde{d}_s) from water elevation distribution using the Latin Hypercube Sampling (LHS) method; (5) Use H_s and T_p (when using Ochi-Hubble, JONSWAP or TMA spectrum) values from step 3 and \tilde{d}_s values (When using TMA spectrum) from step 4 to obtain wave spectrum; (6) Calculate the zeroth, first, and second moments of the spectrum (M_0, M_1, M_2) and spectrum bandwidth parameter ν ; (7) Find extreme wave height distribution, $F(H_{max})$. The Latin hypercube sampling (LHS) is used to obtain n_1 wave height samples (\tilde{H}_{max}) from the distribution. This is accomplished by dividing the distribution into n segments of the same probability and randomly picking a value from each segment. A uniform distribution ranging between 1 and 6 hours is used for storm duration; (8) For each of the extreme wave height samples in step 7, find the conditional probability of wave periods $F(T|H)$; (9) The LHS method is then used to generate n_2 samples wave period samples, \tilde{T} , out of each distribution function obtained in step 8, which yields to total number of $n_1 \times n_2$ samples ($\tilde{H}_{max}, \tilde{T}, \tilde{d}_s$); (10) $n_{total} = n_1 \times n_2$ samples generated in step 10 are used to obtain n_{total} realization of $F_{V-quasi}, F_{V-slamming}$ and F_H using the AASHTO guide. Finally, these values are used to obtain n_{total} realizations of demand in vertical and horizontal directions (D_V, D_H).

4.2.7 PROBABILISTIC MODELING OF CAPACITY

A majority of hurricane damaged bridges have either anchor bolt or dowel connections between bridge superstructure and substructure. Tensile strength of dowel connections was assumed negligent because grout was primarily used in dowel connections. However, shear strength of the dowels is considered in this study. Tensile and shear strength calculation of anchor bolts connection type are determined according to chapter 17 of the ACI 318 code

(ACI 2014). Connection tensile strength is considered as the minimum of the steel tensile strength, concrete breakout strength, pullout strength and concrete side-face blowout. For shear strength, the minimum of steel shear strength, concrete breakout strength, and concrete pryout strength was used.

4.2.8. FRAGILITY ANALYSIS OF A SINGLE-SPAN BRIDGE

For each bridge, fragility of each span is assessed. The probability of failure of i th bridge span, $P_{f_{span}}^i$, is expressed as:

$$P_{f_{span}}^i = P_{f_{span}}^i (D - C > 0 | U_{1-min}) \quad (4.39)$$

where D, C are demand and capacity.

To generate a fragility curve, Eq. (4.39) must be evaluated at incremental levels of U_{1-min} . This is accomplished by generating numerous estimates of demand and capacity at each level of U_{1-min} as previously explained and comparing the demand and capacity estimates to obtain observed probability of failure for a given span at a specific level of U_{1-min} :

$$P_{f_{span}}^i (D - C > 0 | U_{1min})_{Observed} = \frac{n_{failed}}{n_{total}} = \frac{\sum_1^{n_{total}} \mathbf{1}(D-C)}{n_{total}} \quad (4.40)$$

in which n_{total} is the number of generated demand and capacity estimates (sample size), number of failed bridges n_{failed} , and $\mathbf{1}()$ is the Indicator function defined as

$$\mathbf{1}(x) := \begin{cases} 0 & x \geq 0, \\ 1 & x < 0. \end{cases} \quad (4.41)$$

This is repeated to obtain total number of N_{obs} observed probability of failures. Traditionally, a log-normal cumulative distribution function is fitted to N_{obs} observed probability of failures to obtain a continuous estimate of probability of failure as a function of intensity measure as shown below:

$$P_{f_{span}}^i = P_{f_{span}}^i (D - C > 0 | U_{1-min}) = \Phi \left(\frac{\ln(U_{1-min}) - \hat{\mu}}{\hat{\beta}} \right) \quad (4.42)$$

where Φ is the standard normal cumulative distribution function; and $\hat{\mu}$ and $\hat{\beta}$ are mean and standard deviation estimates of U_{1-min} . This study uses the maximum likelihood method to find $\hat{\mu}$ and $\hat{\beta}$ from the observed probability of failure (Baker 2015).

Assuming a binomial distribution for number of failed bridges n_{failed} out of total n_{total} samples at each level of U_{1min} , the likelihood function, \mathcal{L} , is given by:

$$\mathcal{L} = \prod_{j=1}^{N_{obs}} \binom{(n_{total})_j}{(n_{failed})_j} (P_{obs})_j^{(n_{failed})_j} (1 - (P_{obs})_j)^{(n_{total})_j - (n_{failed})_j} \quad (4.43)$$

$P_{f_{span}}^i (D - C > 0 | U_{1-min})_{observed}$ is replaced with P_{obs} for ease of notation. Replacing fragility function defined in Eq. (4.42) in Eq. (4.43) yields:

$$\mathcal{L} = \prod_{j=1}^{N_{obs}} \binom{(n_{total})_j}{(n_{failed})_j} \Phi \left(\frac{\ln((U_{1-min})_j) - \tilde{\mu}}{\tilde{\beta}} \right) \left(1 - \Phi \left(\frac{\ln((U_{1-min})_j) - \tilde{\mu}}{\tilde{\beta}} \right) \right) \quad (4.44)$$

MLE is accomplished by finding estimated lognormal distribution parameters $\hat{\mu}$ and $\hat{\beta}$ such that \mathcal{L} is maximized. Equivalently, this could be done by maximizing the logarithm of the likelihood function, which is numerically easier to obtain:

$$\begin{aligned} \{\hat{\mu}, \hat{\beta}\} = \underset{\tilde{\mu}, \tilde{\beta}}{\operatorname{argmax}} \{ & \sum_{j=1}^{N_{obs}} \ln \left(\binom{(n_{total})_j}{(n_{failed})_j} \right) + (n_{failed})_j \ln \left(\Phi \left(\frac{\ln((U_{1-min})_j) - \tilde{\mu}}{\tilde{\beta}} \right) \right) + \\ & ((n_{total})_j - (n_{failed})_j) \ln \left(1 - \Phi \left(\frac{\ln((U_{1-min})_j) - \tilde{\mu}}{\tilde{\beta}} \right) \right) \} \end{aligned} \quad (4.45)$$

The accuracy in the probability estimation depends on the sample size, n_{total} , particularly for smaller probabilities of failure. In this study, n_{total} was selected to achieve a $C_v = 0.05$ (Echard et al. 2011) at each level of U_{1-min} , as shown in Eq. (4.46):

$$C_v = \sqrt{\frac{1 - P_{f_{span}}^i}{P_{f_{span}}^i n_{total}}} \quad (4.46)$$

where C_v is coefficient of variation.

2.9. AN OVERALL BRIDGE FRAGILITY AS A SERIES SYSTEM

The fragility of an overall bridge (or multiple spans) is determined by considering each bridge structure as a series system. That is, a failure of a single span will lead to loss of functionality of the entire bridge. The lower and upper bounds of bridge probability of failure, $P_{f_{Bridge}}$, are obtained by Eq. (4.47).

$$\max(P_{f_{span}}^i) < P_{f_{Bridge}} < 1 - \prod_{i=1}^N (1 - P_{f_{span}}^i) \quad (4.47)$$

in which $P_{f_{span}}^i$ is the probability of failure of 'i'th span; and N is the number of spans.

4.3 RISK ASSESSMENT METHODOLOGY

Once the fragility functions of bridges are obtained, they are used to quantify the risk of failure, which in turn can help decision makers prioritize their resources for the most critical assets. For the proposed risk assessment procedure, it is necessary to define a probabilistic model for hurricane hazard, which describes the frequency of the hazard occurrence as a function of an intensity measure (i.e., maximum sustained wind speed).

Vickery et al. (Vickery et al. 2009) proposed a hurricane simulation model by using historical data of past hurricanes. In this model, numerous hypothetical hurricane tracks were generated and simulated using the statistical distributions derived from the inventory of past hurricanes to derive a probabilistic model for hurricane wind speeds along the coastal regions of the United States. The ASCE 7 hurricane wind speeds (ASCE 1994) and HAZUS hurricane model (Vickery et al. 2006) are based on the model developed by Vickery et al.

In this study, the hurricane wind speed return periods proposed by Vickery et al. is used to derive the hurricane hazard curve. Wind speeds provided by Vickery et al. are 3-sec peak gust wind speeds and thus are converted to the 1-min averaged maximum sustained wind speed (U_{1-min}), to be consistent with the Saffir-Simpson scale, which also has been used as the Intensity Measure for fragility estimation. Finally, the risk is quantified in terms of the mean annual rate of bridge failure (λ_{Bridge}):

$$\lambda_{Bridge} = \int \left(\frac{dP_{f_{Bridge}}}{dU_{1-min}} \right) \lambda_{U_{1-min}} dU_{1-min} \quad (4.48)$$

in which $P_{f_{Bridge}}$ is the fragility function, and $\lambda_{U_{1-min}}$ is the mean annual rate of exceedance for the sustained wind speed.

4.4 IMPLEMENTATION OF THE PROPOSED RISK ASSESSMENT

4.4.1 BACKGROUND

The proposed risk assessment methodology presented in the previous sections was implemented in this section for risk analysis of coastal bridges in the state of Georgia. More than 490 bridges in Georgia along the Atlantic coast of the United States were identified as potentially vulnerable based on the SLOSH MOM Category 5 surge height . Fig. 4.6. shows median and quartiles of extracted surge heights under different hurricane categories and two tidal conditions (low tide and high tide). As it can be seen, median surge height has constantly increased from CAT1M to CAT5H, however, it does not exceed 5m. Maximum predicted surge elevation also does not exceed 9m. Therefore, shallow water equations are used to obtain probabilistic distribution of wave parameters.

The National Bridge Inventory (NBI) database provides bridge types, and 77% of the vulnerable bridges were found to be simply supported. Nonetheless, there is no sufficient

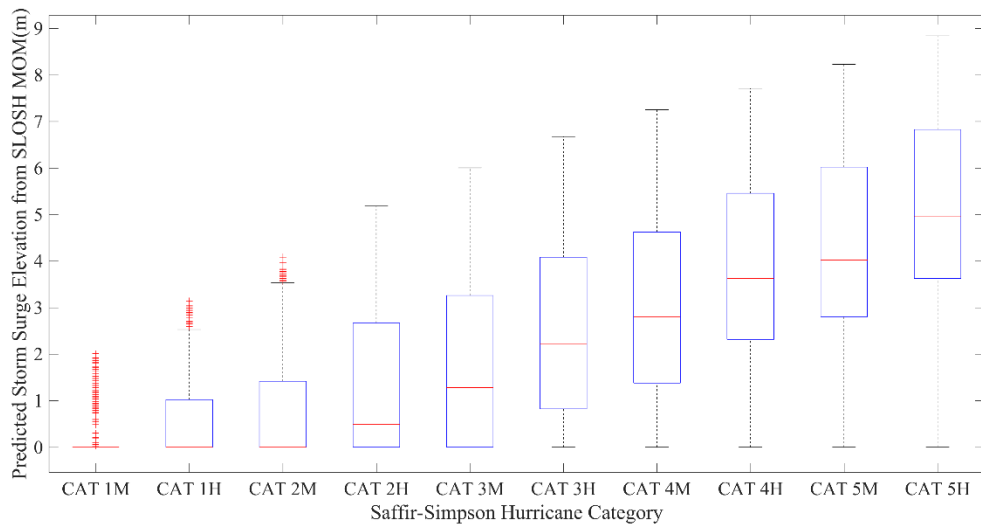


Fig.4.6. Median and quartiles of predicted storm surge elevation from SLOSH MOM for Georgia coastal bridges (CAT: category, M: mean tide, H: high tide)

information for bearing connection details to evaluate the prevailing failure mode (e.g., anchor failure) described in Section 4.2. Therefore, construction and as-built plans of bridges were obtained from the Georgia Department of Transportation (GDOT) to document the structural details. Each bridge was analyzed, and a fragility function for each bridge span, as well as upper-bound and lower-bound fragilities for bridges, were generated.

4.4.2 PROBABILITY DISTRIBUTIONS OF CAPACITY VARIABLES USED FOR FRAGILITY ANALYSIS

The deck weight is the primary resisting force against uplift wave forces. Once the weight is overcome, the superstructure/substructure connections are engaged. The cross sectional area of girders and deck slab were obtained from construction plans for deck weight calculations. For a bridge span with similar concrete girders, the weight of superstructure per unit length of deck , W_L , was determined as follows:

$$W_L = A_{Slab} \gamma_{Concrete} + N_{Girder} A_{Girder} \gamma_{Concrete} \quad (4.49)$$

where $\gamma_{Concrete}, \gamma_{Steel}$ are concrete and steel densities, and A_{Slab}, A_{Girder} are cross sectional areas of slab and girders. In this study, both steel and concrete densities ($\gamma_{Concrete}, \gamma_{Steel}$) have a Gaussian distribution (JCSS 2001), the parameters are provided in Table 4.3. To account for uncertainty in the deck weight resulting from workmanship and inconsistencies between construction and as-built plans, a uniform distribution ranging $\pm 5\%$ of calculated cross sectional area of slab (A_{Slab}) and girders (A_{Girder}) was considered. For spans with steel girders, $\gamma_{Concrete}$ was replaced with γ_{Steel} in Eq. (4.49).

To account for the uncertainty associated with material strength when estimating the connection strength, a normal and a lognormal distribution is used for concrete and steel strength (Ellingwood and Hwang 1985), respectively, with parameters shown in Table 4.3. Anchors bolts and dowels diameter, embedment length into concrete, and other structural dimensions are treated deterministically as they are obtained from as-built plans although uncertainties may exist in such variables (e.g., conditions of anchor bolts and errors in installation of dowels).

4.4.3 FRAGILITY ANALYSIS RESULTS

Figure 4.7 includes the hurricane fragility curve for a bridge, which is built over the Bull River on US 80 in Chatham county. This bridge consists of 62 simply-supported standard precast beam spans. The total bridge span length is 1070.11m, and each span length ranges between 14.60m and 19.5m. The bridge width is 12.40m, and girders are attached on a bent cap-beam using 2.54cm diameter anchor bolts.

The significant difference observed among fragility curves of the spans in Fig. 4.7 is due to the elevation variation and the arch-shape longitudinal profile of the bridge

Table 4.3. Probabilistic distributions of capacity variables and their parameters used for fragility analysis

	Distribution	Parameters	Unit
Concrete density ($\gamma_{Concrete}$)	$\mathcal{N}(\mu, \sigma)^a$	$\mu = 2400, \sigma = 96$	kg/m ³
Steel density (γ_{Steel})	$\mathcal{N}(\mu, \sigma)^a$	$\mu = 7850, \sigma = 78.5$	kg/m ³
Slab area(A_{Slab}), girders area(A_{Girder})	$U(a, b)^b$	$a = 0.95 A_{Plan}, b=1.05A_{Plan}^c$	m ²
Concrete strength(f_c)	$\mathcal{N}(\mu, \sigma)^a$	$\mu = (f_c)_{Plan}^d, \sigma = 4.3$	MPa
Steel strength(f_s)	lognormal(α, β) ^e	$\alpha = \log((f_s)_{Plan}^f), \beta = 4.3$	MPa

^aNormal distribution with mean μ and standard deviation σ

^bUniform distribution with minimum a and maximum b

^cCross sectional area from as-built plans

^dConcrete strength from as-built plans

^eLog-normal distribution with logarithmic mean α and logarithmic standard deviation β

^fSteel strength from as-built plans

towards the mid-span location, which results in greater freeboard for middle spans. The significant difference between bridge upper bound and lower bound fragilities is also interesting. The real fragility of the system is between these two bounds. For bridges with fewer spans, this difference will be smaller. However, as the number of spans becomes bigger the effect of dependency between spans reliability becomes more evident.

4.4.4 RISK ASSESSMENT OUTCOMES

Fig. 4.8 shows the maximum hurricane 3-sec peak gust wind speed return period along the coast of Georgia and South Carolina. To obtain the hazard curve shown in Fig. 4.10 which is needed to take the integral in Eq. (4.48), the 3-sec peak gust wind speed was converted to 1-min averaged sustained wind speed using equations provided in the AASHTO guide. In addition, the return period is converted to the mean annual rate of occurrence, $\lambda_{U_{1-min}}$. Fragility functions of bridges obtained in the previous section and hazard curve shown in Fig.4.9 are used in Eq. (4.45) to obtain the mean annual rate of failure (λ_{Bridge}) for each bridge.

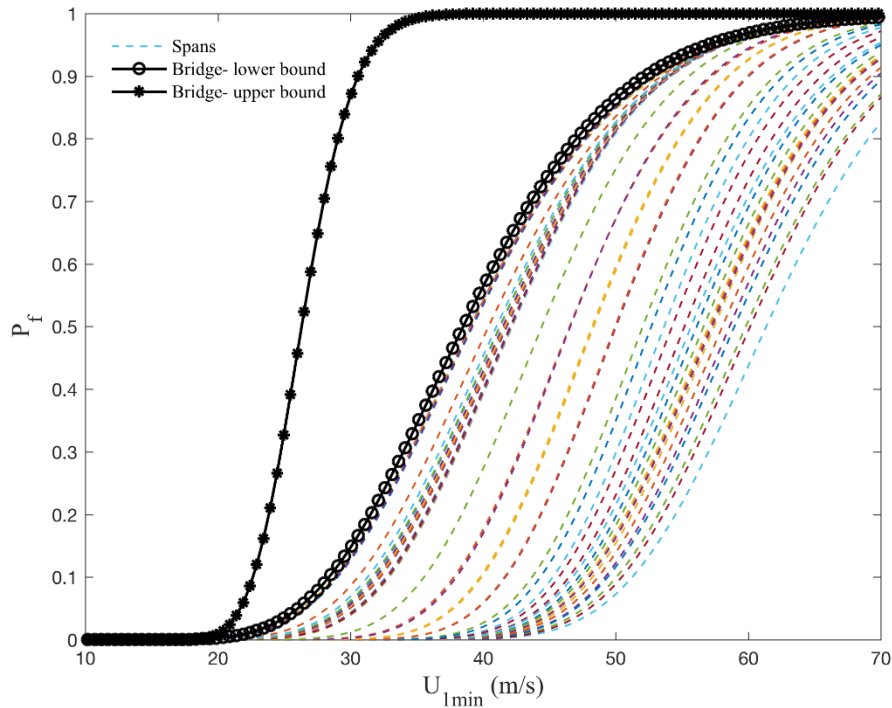


Fig. 4.7- Spans, lower bound and upper bound fragility curves

Fig. 4.10 shows λ_{Bridge} for Georgia's coastal bridges. In Fig. 4.11, λ_{Bridge} of bridges versus their distance from the shoreline provided by the NOAA National Shoreline (Vickery et al. 2009) is shown. It is concluded that seventeen bridges, all within 5km from the shoreline, have the mean annual rate of occurrence, λ_{Bridge} , greater than 0.1. Therefore, it could be concluded that distance from the shoreline could serve as an initial criterion to identify the most critical coastal bridges. Various other factors including average daily traffic, importance of the bridge, detour length and repair/retrofit costs must be considered to choose between these bridges.

4.5 CONCLUSIONS

There is an increasing need for quantifying vulnerability and risk of transportation assets such as bridges. This study addresses two critical issues: (1) determining hurricane risk of

bridges in terms of a significant environmental parameter, which is the maximum sustained wind speed; (2) quantifying risks for coastal bridges subjected to hurricane-induced waves. The proposed fragility analysis methodology is promising for predicting a probability of bridge failure in terms of the maximum sustained wind speed. The single hazard intensity parameter (wind speed) used for the hurricane categories, enables a more meaningful fragility assessment than any available methods. Furthermore, the proposed risk assessment scheme enhances both accuracy and efficiency because it considers uncertainties inherent in various demand and capacity variables and it is easy to implement. The proposed fragility analysis and risk assessment methodologies were successfully applied to Georgia's coastal bridges potentially vulnerable to hurricane hazard, and they were found that the results are valuable for risk-based asset management planning.

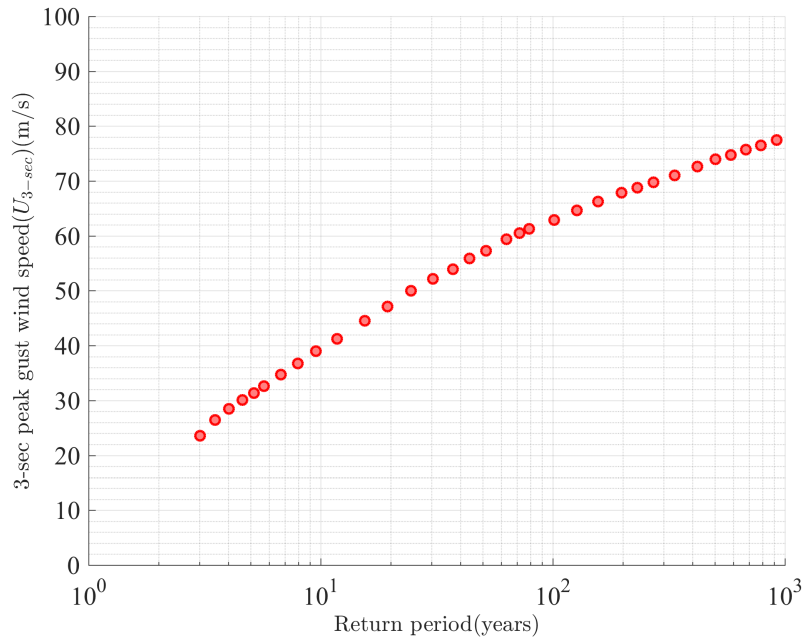


Fig. 4.8- Maximum hurricane induced wind speeds on land along GA/SC coastline versus return period (Rebuilt from (Vickery et al. 2009))

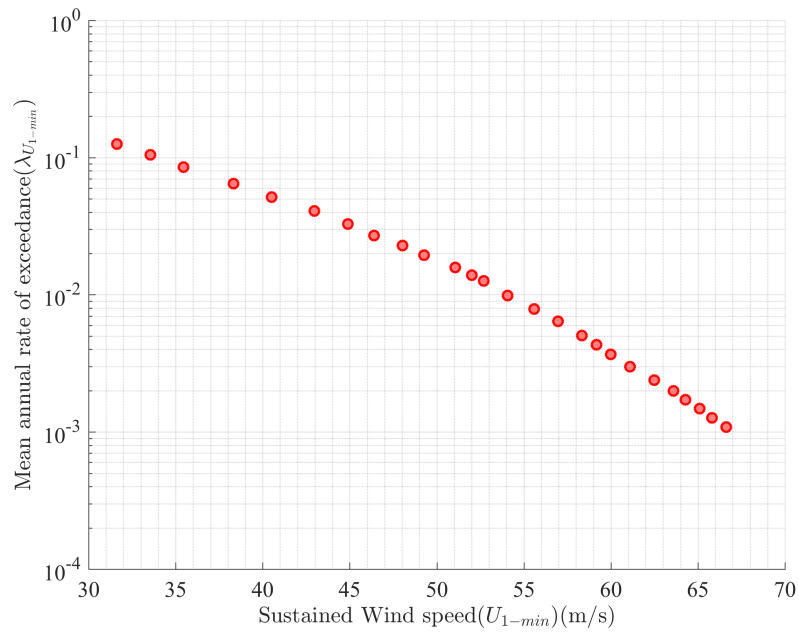


Fig. 4.9- Maximum hurricane induced wind speeds on land along GA/SC coastline versus mean annual rate of occurrence ($\lambda_{U_{1-min}}$)

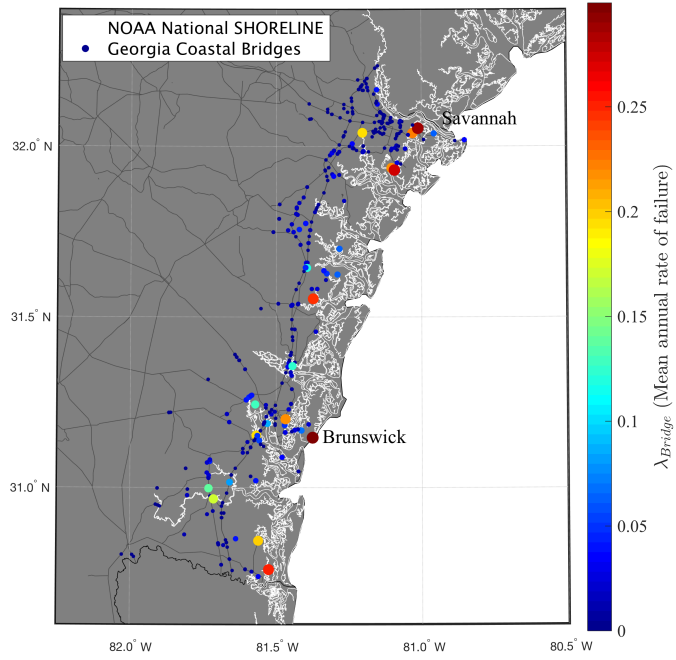


Fig. 4.10- Mean annual rate of failure (λ_{Bridge}) of coastal bridges in the state of Georgia, U.S.A.

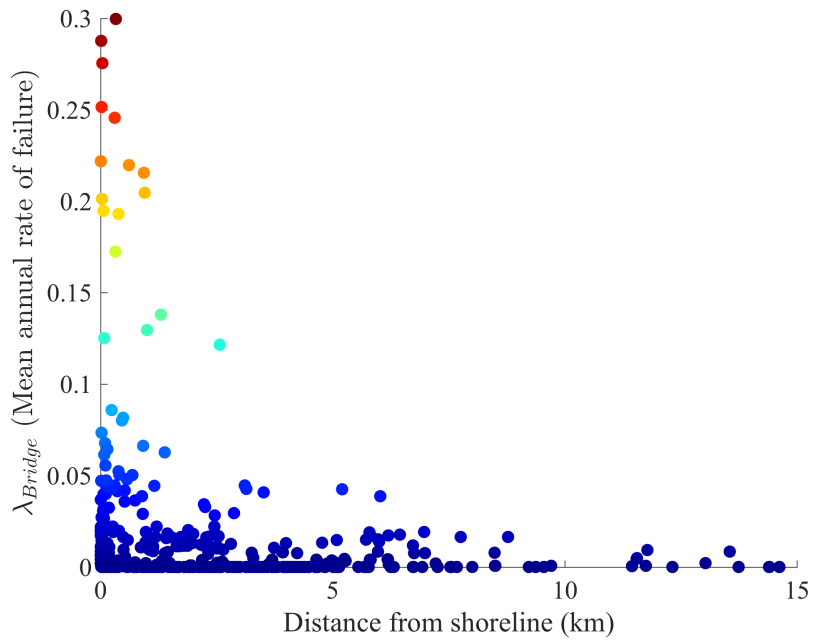


Fig. 4.11- Mean annual rate of failure (λ_{Bridge}) of Georgia's coastal bridges vs. their distance from the shoreline

CHAPTER 5

SUMMARY AND CONCLUSIONS

With the population growth in coastal counties and urbanization rate on a sharp rise, reliability of coastal transportation infrastructure against natural hazards becomes critically important. It is thus extremely important to understand how these natural disasters are likely to impact coastal transportation network to quantify the magnitude and extent of expected damage across the transportation system, predicting structural resilience for specific at-risk or mission critical bridges, estimating loss of system capacity through the network grid, and planning to mitigate infrastructure or operational vulnerabilities.

Past hurricane events such as Ike, Katrina, and Ivan have clearly demonstrated how they could disrupt the coastal transportation network by inflicting severe damage to critical nodes of the network, which are bridge structures. However, a comprehensive risk assessment method for bridges exposed to hurricane hazard is not available in the literature.

This study provides a structured risk assessment framework for coastal bridges exposed to hurricane hazard. Such framework is essential for minimizing the potential loss caused by hurricane events in coastal communities and planning for post-disaster response and recovery operations. This study is expected to assist decision makers in coastal communities in identifying the most critical nodes of transportation network and allocate their resources to most needed bridges.

Existing literature on the subject was reviewed to identify the possible types of damage to bridge structures by hurricane hazard. Various parameters controlling the bridge response and hurricane intensity were identified, and their uncertainty was incorporated in the proposed framework. The main contributions of this dissertation are listed as follows:

1. A parametric finite element model for analysis of bridges subjected to hurricane-induced wave was built. The proposed model was specifically configured to capture the bridge deck unseating/shifting mode of failure by implementing of contact elements.
2. Vulnerable bridges along the coastline of the state of Georgia (U.S.A) were identified by GIS analysis. Information and coordinates of bridges located within Georgia coastal counties were extracted from the National Bridge Inventory (NBI). The maximum predicted surge height for each hurricane category was extracted from the NOAA SLOSH model to identify surge prone areas of Georgia coast. These data were collected in a Geodatabase and were analyzed in ArcGIS to identify vulnerable bridges along the coast of Georgia.
3. A parameterized fragility analysis method was proposed. Advantages of metamodels, in comparison to traditional fragility methods, was highlighted. It was found that the proposed metamodel can efficiently reduces the computational cost. The storm water elevation and wind speed are used as new intensity measures in order to quantify the hurricane hazard intensity and generating fragility surfaces.

4. Performance of various classification methods were compared in terms of classification accuracy, and the Random Forest method was shown to be the most accurate method for fragility analysis of bridges subject to hurricane hazard.
5. Various sources of uncertainty in demand, capacity, and hurricane were identified, and their uncertainties were incorporated in the proposed risk assessment. A novel method was proposed to incorporate the extreme wave heights and wave period uncertainty in a fragility estimation.
6. An efficient fragility analysis method for simply supported bridges was proposed. The proposed fragility analysis methodology is promising for predicting probabilities of bridge failure in terms of the maximum sustained wind speed. The single hazard intensity parameter (wind speed) used for the hurricane categories enables a more meaningful fragility assessment than any available methods.
7. A simple method for scoring of bridges in an inventory based on their mean annual rate of failure was introduced. The proposed risk-based scoring method can be used for ranking and prioritizing bridges for maintenance and retrofit.
8. The proposed risk assessment scheme enhances both accuracy and efficiency because it considers uncertainties inherent in various demand and capacity variables. Furthermore, it is easy and straightforward to implement.
9. The proposed fragility analysis and risk assessment methodologies were successfully applied to Georgia's coastal bridges potentially vulnerable to hurricane hazard, and the results are found beneficial and valuable for risk-based asset management planning.

CHAPTER 6

FUTURE RESEARCH

This research proposed an efficient framework for risk assessment of coastal bridges subjected to hurricane wave forces. There is abundant room for improvement in various aspects of this study:

1. In addition to hurricane wave forces, there are other hazards that threaten coastal bridges, such as scour and debris impact. Future research should address the vulnerability of coastal bridges to these hazards to obtain a multihazard risk assessment framework.
2. Future research should also consider the effect of aging. Particularly, deterioration of anchor bolts and dowels due to aggressive environments such as increased humidity and its effect on the overall bridge vulnerability should be investigated.
3. A compressive loss assessment framework which accounts for direct and indirect costs of bridge failure should be developed. Various factors including average daily traffic, detour length and repair/retrofit cost should be considered in such framework.
4. It is recommended that resilience and sustainability of bridges be also investigated in future studies. Vulnerability analysis method proposed in this study is the first step towards resilience and sustainability analysis of bridges.

5. More research is needed to study the mechanism and magnitude of hurricane wave forces acting on a bridge superstructure. AASHTO guide provide conservative estimation of wave forces and does not address their variation in time.

6. Some agencies are now using real-time bridge monitoring systems. Future work can apply hurricane hindcasting models to establish a real-time hurricane monitoring and risk assessment of bridges. This can help authorities to make informed decision to protect coastal communities in real-time and efficiently coordinate their emergency operations.

References

- ACI (2014). "Building code requirements for structural concrete (ACI 318-14) and commentary." American Concrete Institute.
- ASCE (1994). "Minimum design loads for buildings and other structures." Amer Society of Civil Engineers.
- Ataei, N. (2013). "Vulnerability Assessment of Coastal Bridges Subjected to Hurricane Events." RICE UNIVERSITY.
- Ataei, N., and Padgett, J. E. (2012). "Probabilistic modeling of bridge deck unseating during hurricane events." *Journal of Bridge Engineering*, 18(4), 275-286.
- Baesch, J., Batac, T., Bottomley, G., Dorney, C., Erchul, M., Gupton, E., Keller, J., Kinghorn, R., Lennon, J., and Louie, B. (2014). "Impacts of Climate Change and Variability on Transportation Systems and Infrastructure: The Gulf Coast Study, Phase 2, Task 3.2: Engineering Analysis and Assessment."
- Baker, J. W. (2015). "Efficient analytical fragility function fitting using dynamic structural analysis." *Earthquake Spectra*, 31(1), 579-599.
- Battjes, J., Zitman, T., and Holthuisen, L. (1987). "A reanalysis of the spectra observed in JONSWAP." *Journal of physical oceanography*, 17(8), 1288-1295.
- Bea, R., Iversen, R., and Xu, T. (2001). "Wave-in-deck forces on offshore platforms." *Journal of Offshore Mechanics and Arctic Engineering*, 123(1), 10-21.
- Berry, M., Parrish, M., and Eberhard, M. (2004). "PEER structural performance database user's manual (version 1.0)." *University of California, Berkeley*.
- Bouws, E., Günther, H., Rosenthal, W., and Vincent, C. (1985). "Similarity of the wind wave spectrum in finite depth water: 1. Spectral form." *Journal of Geophysical Research: Oceans*, 90(C1), 975-986.
- Bozorgnia, M., and Lee, J.-J. "Wave structure interaction during hurricane ivan simulated by a two-phase flow model." *Proc., Coastal Hazards*, ASCE, 33-44.
- Bradner, C., Schumacher, T., Cox, D., and Higgins, C. (2010). "Experimental setup for a large-scale bridge superstructure model subjected to waves." *Journal of waterway, port, coastal, and ocean engineering*, 137(1), 3-11.
- Bretschneider, C. L. (1959). "Wave variability and wave spectra for wind-generated gravity waves." CORPS OF ENGINEERS WASHINGTON DC BEACH EROSION BOARD.
- Caltrans, L. (2008). "Bridge Design Aid." *California Department of Transportation, Sacramento, CA*.
- Casas-Prat, M., and Holthuijsen, L. H. (2010). "Short-term statistics of waves observed in deep water." *Journal of Geophysical Research: Oceans*, 115(C9).
- Cauffman, S. A. (2006). *Performance of Physical Structures in Hurricane Katrina & Hurricane Rita: A Reconnaissance Report*, DIANE Publishing.
- Chen, Q., Wang, L., Zhao, H., and Douglass, S. L. (2007). "Prediction of storm surges and wind waves on coastal highways in hurricane-prone areas." *Journal of Coastal Research*, 1304-1317.
- Choi, E. (2002). "Seismic analysis and retrofit of mid-America bridges."
- Cuomo, G., Shimosako, K.-i., and Takahashi, S. (2009). "Wave-in-deck loads on coastal bridges and the role of air." *Coastal Engineering*, 56(8), 793-809.

- Dietrich, J., Zijlema, M., Westerink, J., Holthuijsen, L., Dawson, C., Luetlich, R. A., Jensen, R., Smith, J., Stelling, G., and Stone, G. (2011). "Modeling hurricane waves and storm surge using integrally-coupled, scalable computations." *Coastal Engineering*, 58(1), 45-65.
- Donelan, M. A., Hamilton, J., and Hui, W. H. (1985). "Directional spectra of wind-generated waves." *Philosophical Transactions of the Royal Society of London A: Mathematical, Physical and Engineering Sciences*, 315(1534), 509-562.
- Douglass, S. L., Chen, Q., Olsen, J., Edge, B., and Brown, D. (2006). "Wave forces on bridge decks." *Coastal Transportation Engineering Research and Education Center, Univ. of South Alabama, Mobile, Ala.*
- Douglass, S. L., Hughes, S., Rogers, S., and Chen, Q. (2004). "The impact of Hurricane Ivan on the coastal roads of Florida and Alabama: a preliminary report." *Rep. to Coastal Transportation Engineering Research and Education Center, Univ. of South Alabama, Mobile, Ala.*
- Douglass, S. L., and Krolak, J. (2008). *Highways in the coastal environment.*
- Echard, B., Gayton, N., and Lemaire, M. (2011). "AK-MCS: an active learning reliability method combining Kriging and Monte Carlo simulation." *Structural Safety*, 33(2), 145-154.
- Ellingwood, B., and Hwang, H. (1985). "Probabilistic descriptions of resistance of safety-related structures in nuclear plants." *Nuclear Engineering and Design*, 88(2), 169-178.
- Forristall, G. Z. (1978). "On the statistical distribution of wave heights in a storm." *Journal of Geophysical Research: Oceans*, 83(C5), 2353-2358.
- Gernay, T., Elhami Khorasani, N., and Garlock, M. (2016). "Fire Fragility Curves for Steel Buildings in a Community Context: A Methodology." *Engineering Structures*.
- Guikema, S., and Gardoni, P. (2009). "Reliability estimation for networks of reinforced concrete bridges." *Journal of Infrastructure Systems*, 15(2), 61-69.
- Gutierrez, C., Cresanti, R., and Jeffrey, W. (2006). "Performance of physical structures in Hurricane Katrina and Hurricane Rita: A reconnaissance report." *NIST Technical Note*, 1476.
- Hasselmann, K., Barnett, T., Bouws, E., Carlson, H., Cartwright, D., Enke, K., Ewing, J., Gienapp, H., Hasselmann, D., and Kruseman, P. (1973). "Measurements of wind-wave growth and swell decay during the Joint North Sea Wave Project (JONSWAP)." Deutsches Hydrographisches Institut.
- Hasselmann, K., Sell, W., Ross, D., and Müller, P. (1976). "A parametric wave prediction model." *Journal of Physical Oceanography*, 6(2), 200-228.
- Holthuijsen, L. H. (2010). *Waves in oceanic and coastal waters*, Cambridge University Press.
- Huang, W., and Xiao, H. (2009). "Numerical modeling of dynamic wave force acting on Escambia bay bridge deck during Hurricane Ivan." *Journal of waterway, port, coastal, and ocean engineering*, 135(4), 164-175.
- Itoh, Y., and Gu, H. (2009). "Prediction of aging characteristics in natural rubber bearings used in bridges." *Journal of Bridge Engineering*, 14(2), 122-128.
- JCSS (2001). "The Probabilistic model code." URL: www.jcss.ethz.ch, Joint committee on structural safety.

- Jelesnianski, C. P., Chen, J., and Shaffer, W. A. (1992). "SLOSH: Sea, lake, and overland surges from hurricanes." US Department of Commerce, National Oceanic and Atmospheric Administration, National Weather Service.
- Jin, J., and Meng, B. (2011). "Computation of wave loads on the superstructures of coastal highway bridges." *Ocean Engineering*, 38(17), 2185-2200.
- Kaplan, P. "Wave impact forces on offshore structures: re-examination and new interpretations." *Proc., Offshore Technology Conference*, Offshore Technology Conference.
- Kaplan, P., Murray, J., and Yu, W. (1995). "Theoretical analysis of wave impact forces on platform deck structures." American Society of Mechanical Engineers, New York, NY (United States).
- Karamlou, A., and Bocchini, P. (2015). "Computation of bridge seismic fragility by large-scale simulation for probabilistic resilience analysis." *Earthquake Engineering & Structural Dynamics*, 44(12), 1959-1978.
- Kitaigorodskii, S. (1962). "Applications of the theory of similarity to the analysis of wind-generated wave motion as a stochastic process." *Izv. Geophys. Ser. Acad. Sci., USSR*, 1, 105-117.
- Kulicki, J. M., and Mertz, D. R. (2008). *Guide Specifications for Bridges Vulnerable to Coastal Storms*, AASHTO.
- Le Méhauté, B., Lu, C., and Ulmer, E. "Transformation of statistical properties of shallow water waves." *Proc., Proceedings the 1981 Conference on Wave Dynamics and Radio Probing of the Ocean Surface OM Phillips, K. Hasselmann*, 181-191.
- Lewandowski, E. M. (2004). *The dynamics of marine craft: maneuvering and seakeeping*, World scientific.
- Longuet-Higgins, M. S. "On the joint distribution of wave periods and amplitudes in a random wave field." *Proc., Proceedings of the Royal Society of London A: Mathematical, Physical and Engineering Sciences*, The Royal Society, 241-258.
- Longuet-Higgins, M. (1975). "On the joint distribution of the periods and amplitudes of sea waves." *Journal of Geophysical Research*, 80(18), 2688-2694.
- Longuet-Higgins, M. S. (1980). "On the distribution of the heights of sea waves: some effects of nonlinearity and finite band width." *Journal of Geophysical Research: Oceans*, 85(C3), 1519-1523.
- Mander, J. B., Priestley, M. J., and Park, R. (1988). "Theoretical stress-strain model for confined concrete." *Journal of structural engineering*, 114(8), 1804-1826.
- Marin, J., and Sheppard, D. M. "Storm surge and wave loading on bridge superstructures." *Proc., Structures Congress 2009*, ASCE Austin, TX, 557-566.
- Maroney, B. H. (1995). *Large scale bridge abutment tests to determine stiffness and ultimate strength under seismic loading*.
- Mazzoni, S., McKenna, F., Scott, M. H., and Fenves, G. L. (2006). "OpenSees command language manual." *Pacific Earthquake Engineering Research (PEER) Center*.
- McConnell, K., Allsop, W., and Cruickshank, I. (2004). *Piers, jetties and related structures exposed to waves: guidelines for hydraulic loadings*, Thomas Telford.
- Mondoro, A., Frangopol, D. M., and Soliman, M. (2016). "Optimal Risk-Based Management of Coastal Bridges Vulnerable to Hurricanes." *Journal of Infrastructure Systems*, 23(3), 04016046.

- Morison, J., Johnson, J. W., and O'Brien, M. P. (1953). "Experimental studies of forces on piles." *Coastal Engineering Proceedings*, 1(4), 25.
- Nayak, S., and Panchang, V. (2015). "Coastal Wave-Height Statistics during Hurricane Ike." *Journal of Waterway, Port, Coastal, and Ocean Engineering*, 142(3), 04015026.
- Nielson, B. G. (2005). "Analytical fragility curves for highway bridges in moderate seismic zones." PhD, GeorgiaTech.
- Ochi, M. K., and Hubble, E. N. (1977). "Six-parameter wave spectra." *Coastal Engineering 1976*, 301-328.
- Okeil, A. M., and Cai, C. (2008). "Survey of short-and medium-span bridge damage induced by Hurricane Katrina." *Journal of Bridge Engineering*, 13(4), 377-387.
- Padgett, J., DesRoches, R., Nielson, B., Yashinsky, M., Kwon, O.-S., Burdette, N., and Tavera, E. (2008). "Bridge damage and repair costs from Hurricane Katrina." *Journal of Bridge Engineering*, 13(1), 6-14.
- Phan, L. T., Simiu, E., McInerney, M., Taylor, A., Glahn, B., and Powell, M. (2007). "Methodology for development of design criteria for joint hurricane wind speed and storm surge events: Proof of concept." *NIST Technical Note*, 1482.
- Pierson, W. J., and Moskowitz, L. (1964). "A proposed spectral form for fully developed wind seas based on the similarity theory of SA Kitaigorodskii." *Journal of geophysical research*, 69(24), 5181-5190.
- Porter, K. A. "An overview of PEER's performance-based earthquake engineering methodology." *Proc., Proceedings of ninth international conference on applications of statistics and probability in civil engineering*.
- Robertson, I., Yim, S., Riggs, H., and Young, Y. "Coastal bridge performance during Hurricane Katrina." *Proc., 3rd International Conference on Structural Engineering, Mechanics and Computation, Cape Town, South Africa*.
- Schott, T., Landsea, C., Hafele, G., Lorens, J., Taylor, A., Thurm, H., Ward, B., Willis, M., and Zaleski, W. (2012). "The Saffir-Simpson hurricane wind scale." *NOAA/National Weather Service [Internet]*, 1-4.
- Sebastian, A., Proft, J., Dietrich, J. C., Du, W., Bedient, P. B., and Dawson, C. N. (2014). "Characterizing hurricane storm surge behavior in Galveston Bay using the SWAN+ ADCIRC model." *Coastal Engineering*, 88, 171-181.
- Serinaldi, F., and Cuomo, G. (2011). "Characterizing impulsive wave-in-deck loads on coastal bridges by probabilistic models of impact maxima and rise times." *Coastal Engineering*, 58(9), 908-926.
- Sheppard, D. M., and Marin, J. (2009). "Wave loading on bridge decks."
- Spacone, E., Filippou, F. C., and Taucer, F. F. (1996). "Fibre beam-column model for non-linear analysis of R/C frames: Part I. Formulation." *Earthquake engineering and structural dynamics*, 25(7), 711-726.
- Stearns, M., and Padgett, J. E. (2011). "Impact of 2008 Hurricane Ike on bridge infrastructure in the Houston/Galveston region." *Journal of Performance of Constructed Facilities*, 26(4), 441-452.
- Tayfun, M. A. (1983). "Nonlinear effects on the distribution of crest-to-trough wave heights." *Ocean Engineering*, 10(2), 97-106.

- Thompson, E. F., and Vincent, C. (1985). "Significant wave height for shallow water design." *Journal of Waterway, Port, Coastal, and Ocean Engineering*, 111(5), 828-842.
- USACE (1984). "Shore protection manual." *Army Engineer Waterways Experiment Station, Vicksburg, MS. 2v*, US Army Corps of Engineers.
- Vickery, P. J., Lin, J., Skerlj, P. F., Twisdale Jr, L. A., and Huang, K. (2006). "HAZUS-MH hurricane model methodology. I: Hurricane hazard, terrain, and wind load modeling." *Natural Hazards Review*, 7(2), 82-93.
- Vickery, P. J., Wadhera, D., Twisdale Jr, L. A., and Lavelle, F. M. (2009). "US hurricane wind speed risk and uncertainty." *Journal of structural engineering*, 135(3), 301-320.
- Young, I. (1992). "The determination of spectral parameters from significant wave height and peak period." *Ocean engineering*, 19(5), 497-508.

Appendix A

- IMPLEMENTATION OUTCOMES

A.1 Initial Screening – Submerged Bridges

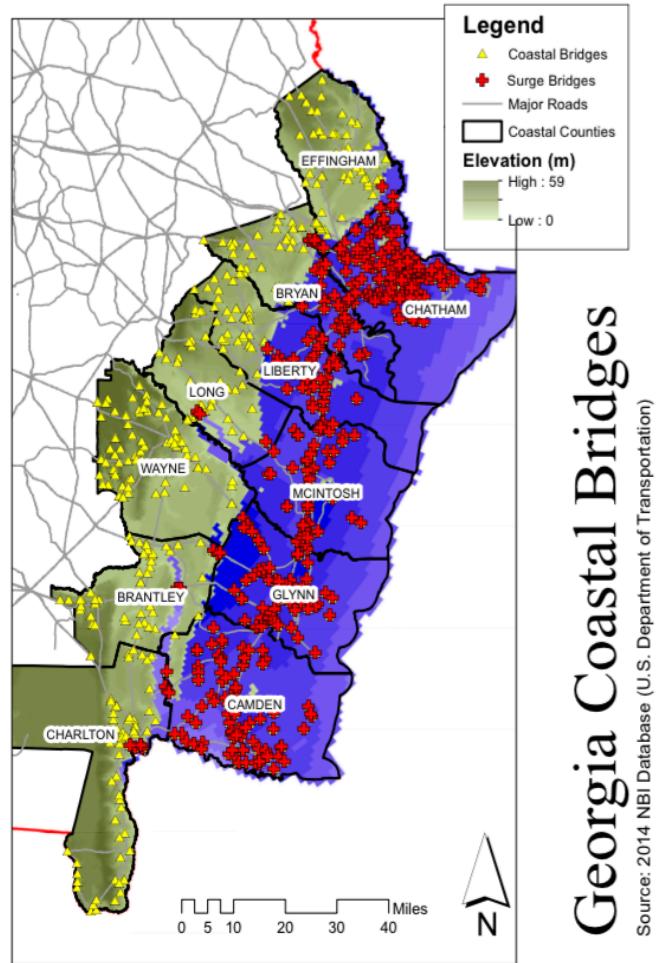
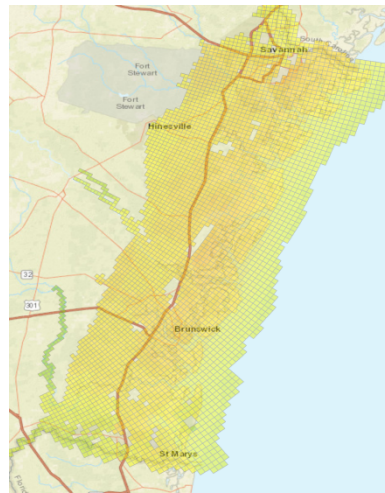


Fig. A.1. 586 Potentially Surge-prone Bridges in the Coastal Georgia Region.



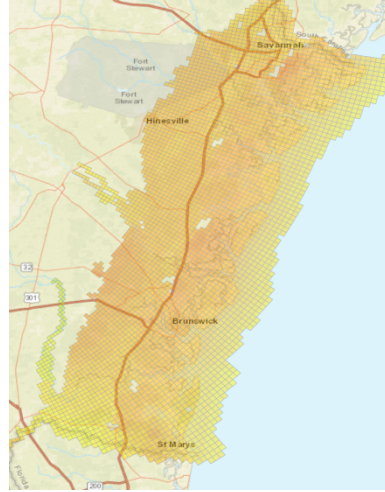
(a) Category 1



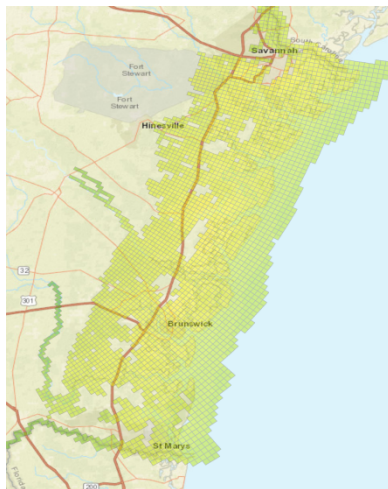
(d) Category 4



(b) Category 2



(e) Category 5



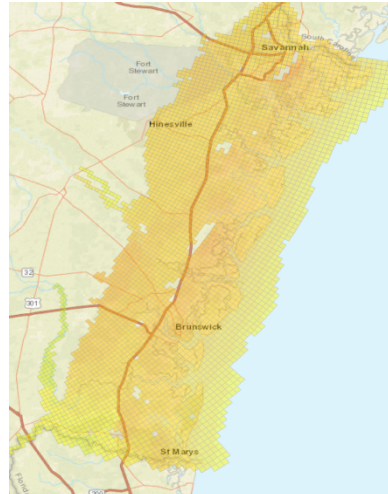
(c) Category 3



Fig. A.2. SLOSH Storm Water Elevations (Mean tide).



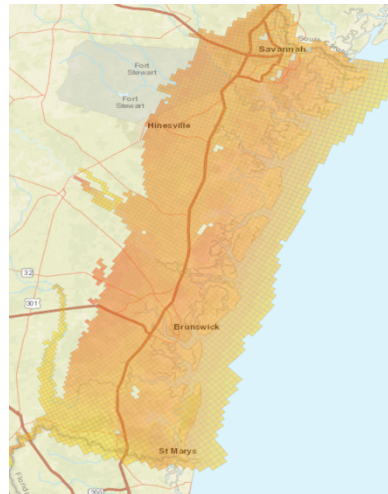
(a) Category 1



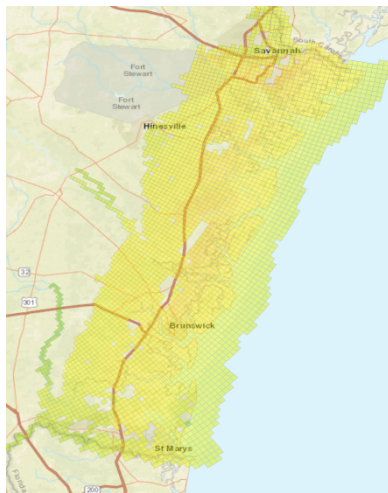
(d) Category 4



(b) Category 2



(e) Category 5



(c) Category 3



Fig. A.3. SLOSH Storm Water Elevations (High tide).

Table A.1. The Number of Bridges Considered Submerged for Each Category.

Hurricane Category	CAT 1	CAT 2	CAT 3	CAT 4	CAT 5
Count (Mean-tide)	0	66	216	302	338
Count (High-tide)	18	156	273	325	353

Table A.2. The Number of Bridges (Including Culverts) Submerged - by Owners.

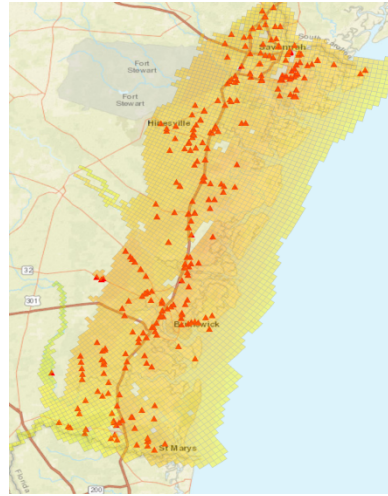
Method of Evaluation	Owner	Number of submerged bridges				
		CAT 1	CAT 2	CAT 3	CAT 4	CAT 5
Initial Screening (High Tide)	State Highway Agency	7	88	164	204	228
	County Highway Agency	10	61	94	104	108
	City/Municipal Highway Agency	1	6	14	16	16
	State Park/Forest/Reservation	0	1	1	1	1
	Total	18	156	273	325	353

Table A.1. The Number of Bridges (Not Including Culverts) Submerged - by Owners.

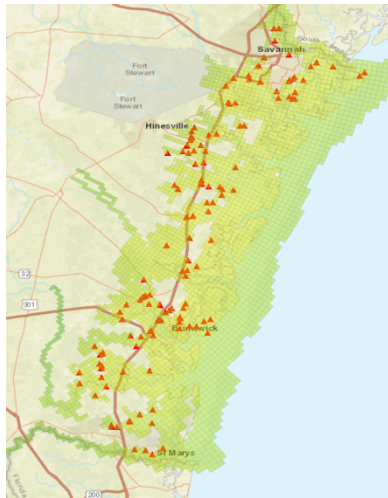
Method of Evaluation	Owner	Number of submerged bridges				
		CAT 1	CAT 2	CAT 3	CAT 4	CAT 5
Initial Screening (High Tide)	State Highway Agency	7	75	124	152	172
	County Highway Agency	9	49	71	74	77
	City/Municipal Highway Agency	1	5	11	12	12
	State Park/Forest/Reservation	0	1	1	1	1
	Total	17	130	207	239	262



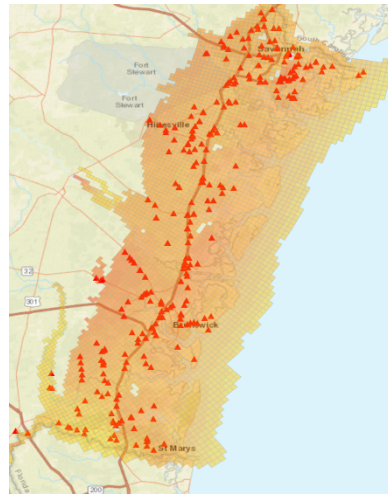
(a) Category 1



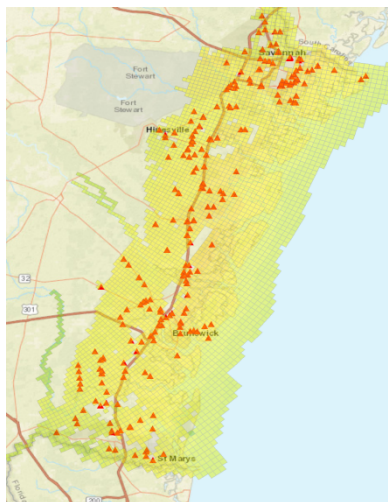
(d) Category 4



(b) Category 2



(e) Category 5

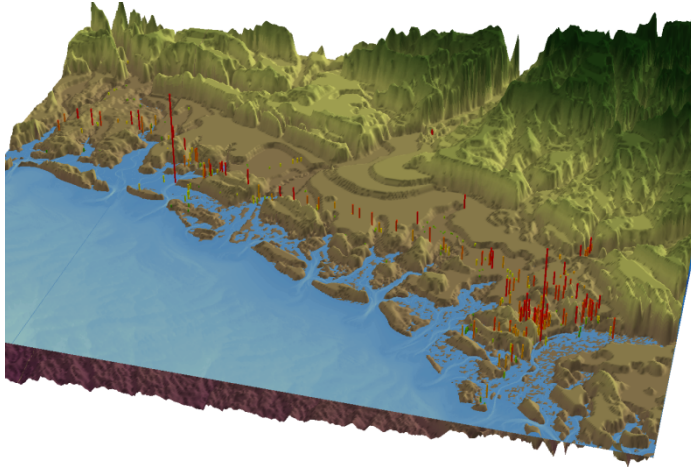


(c) Category 3

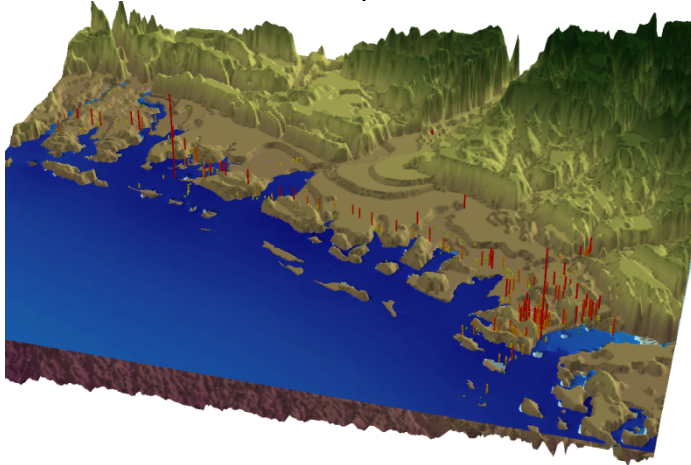


Scale (NAVD88): elevation, ft

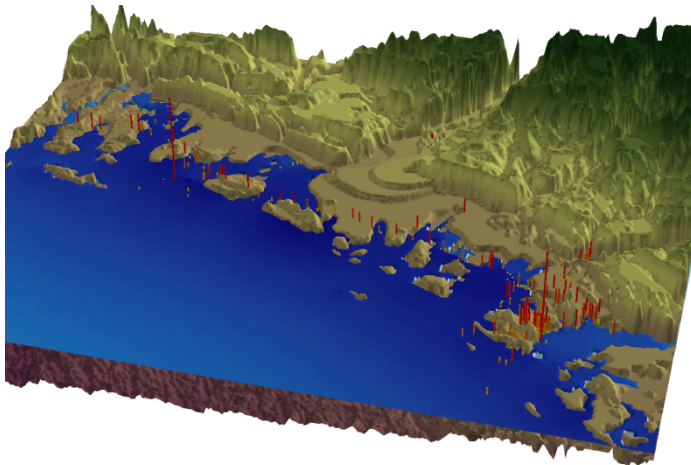
Fig. A.4. Submerged Bridges for High Storm Water Level (High-tide).



(a) Mean Low Water: The average of all the low water heights observed over the National Tidal Datum Epoch.

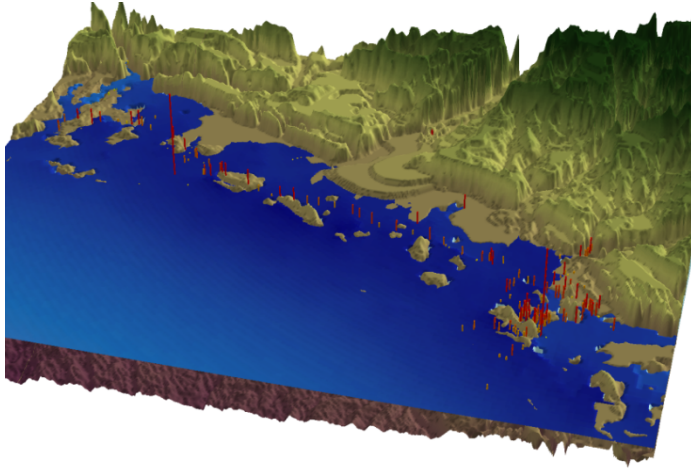


(b) Category 1

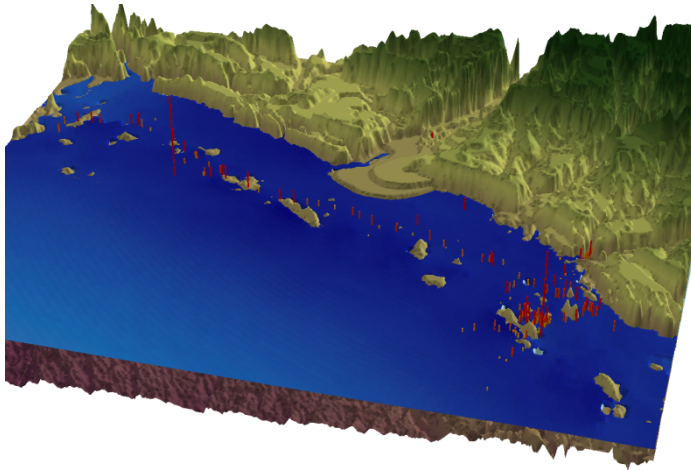


(c) Category 2

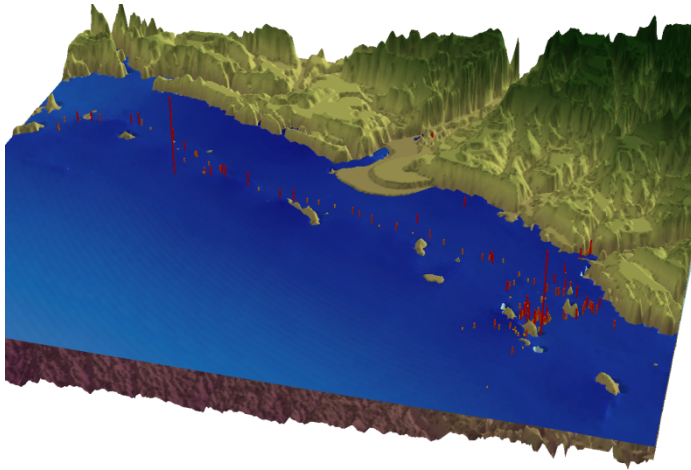
Fig. A.5. Bridge Elevations vs. SLOSH Storm water elevations using the ArcScene program.



(d) Category 3



(e) Category 4



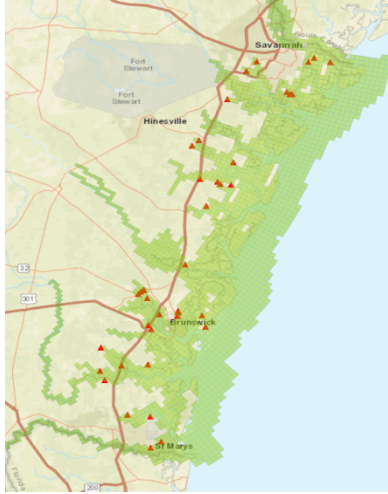
(f) Category 5

Fig. A.6. Continued– Bridge Elevations vs. SLOSH Storm water elevations using the ArcScene program.

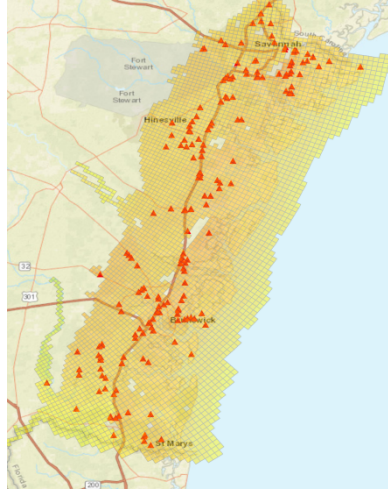
A.2 Level I Analysis Outcomes

Table A.2. The Number of Bridges by Owners Considered Failed Using the Level I Method.

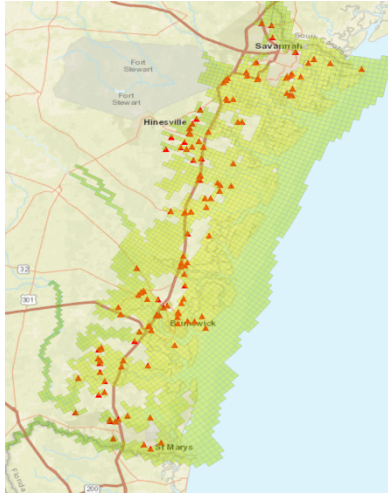
Method of Evaluation	Owner	Number of bridges considered failed				
		CAT 1	CAT 2	CAT 3	CAT 4	CAT 5
AASHTO Level 1 (High Tide)	State Highway Agency	21	105	155	180	211
	County Highway Agency	22	45	63	65	66
	City/Municipal Highway Agency	1	5	8	11	17
	State Park/Forest/ Reservation	0	1	1	1	1
	Total	44	156	227	257	295



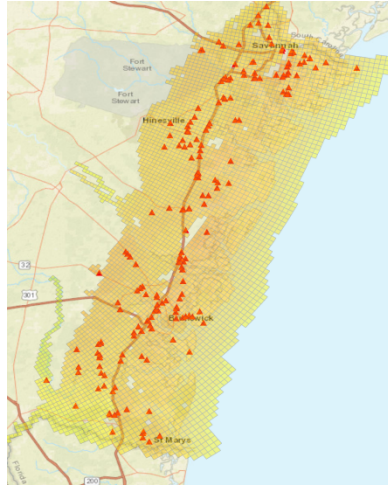
(a) Category 1



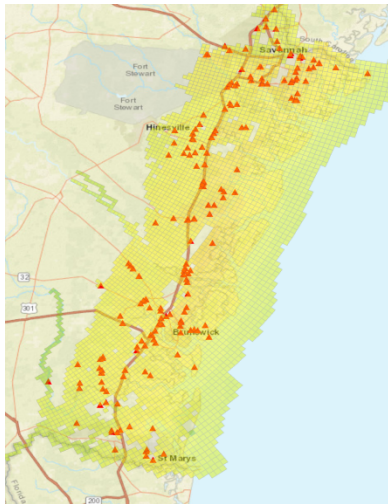
(d) Category 4



(b) Category 2



(e) Category 5



(c) Category 3

Fig. A.7. Bridges Considered Failed by Level I Analysis.

Table A.5. The Number of Bridges by Connection Types Considered Failed Using Level I.

Method of Evaluation	Super-Substructure Connection Type	Number of bridges considered failed				
		CAT 1	CAT 2	CAT 3	CAT 4	CAT 5
AASHTO Level 1 (High Tide)	Dowels	38	131	185	199	219
	Anchor Bolts	6	19	32	47	65
	Others (e.g., dowels & anchors)	0	6	10	11	11
	Total	44	156	227	257	295

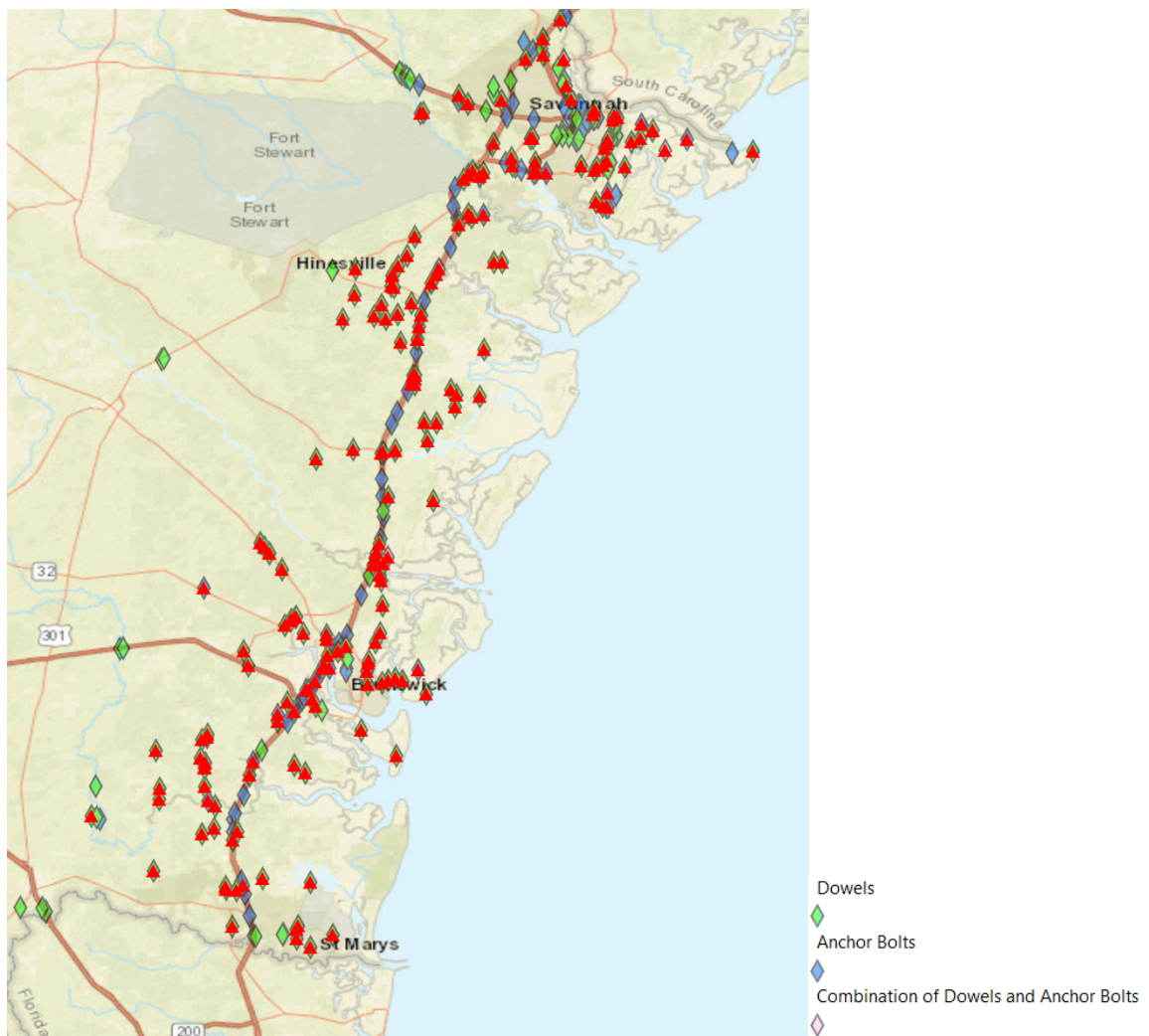
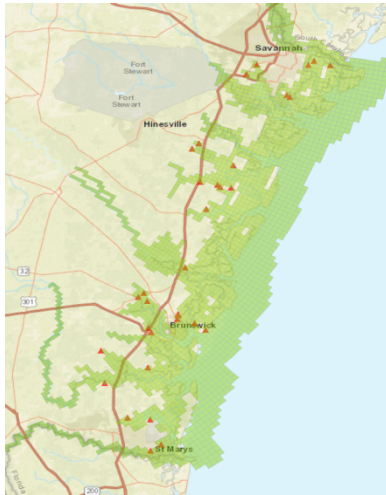


Fig. A.8. Level-I Failed Bridges by Bearing Connection Types.
 (Note: Failed bridges are indicated by the red ‘triangle’ symbol).

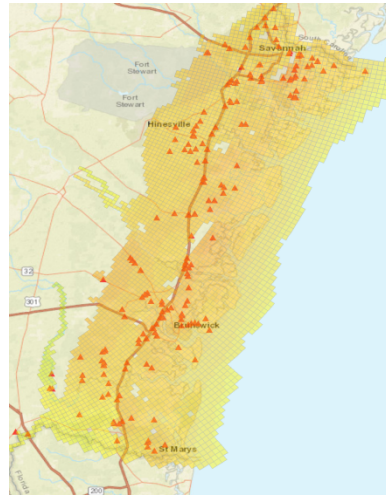
A.3 Level II Analysis Outcomes

Table A.6. The Number of Bridges by Probability of Failure Thresholds.

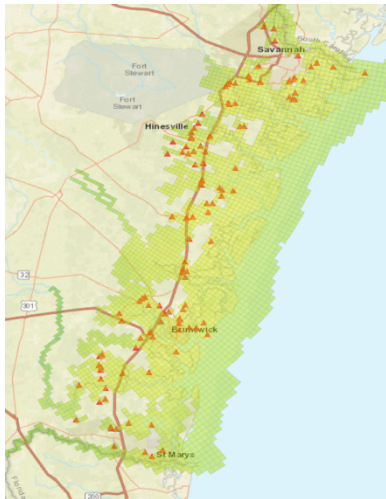
Method of Evaluation	Probability of Failure Threshold	Number of bridges considered failed				
		CAT 1	CAT 2	CAT 3	CAT 4	CAT 5
AASHTO Level 2 (High Tide)	> 80 %	43	151	210	235	265
	> 90%	41	150	206	233	258
	> 95%	35	144	204	231	254



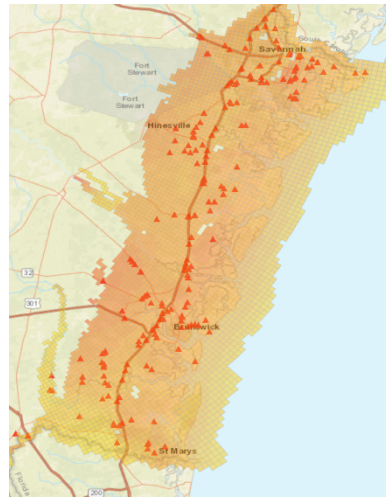
(a) Category 1



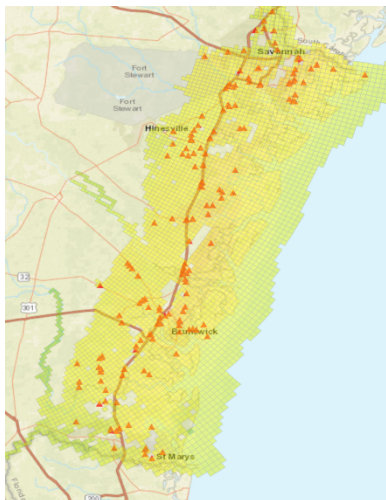
(d) Category 4



(b) Category 2



(e) Category 5

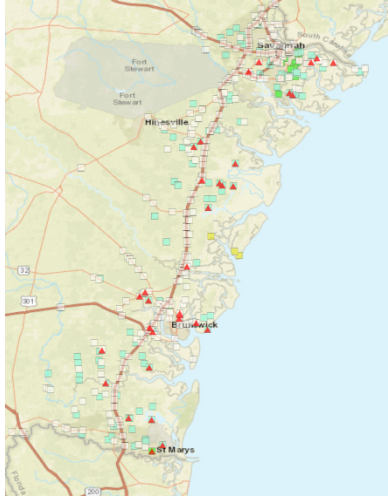


(c) Category 3

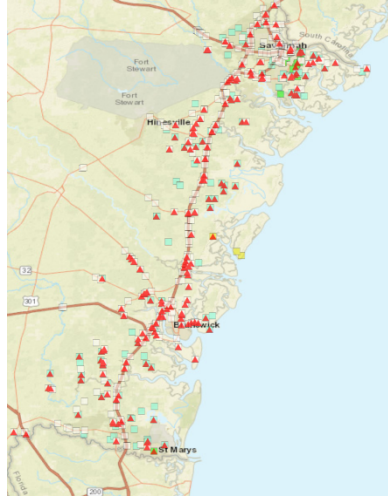
Fig. A.9. Vulnerable Bridges (>95% probability of failure) by Level II Assessment.

Table A.7. The Number of Bridges Vulnerable by Owners.

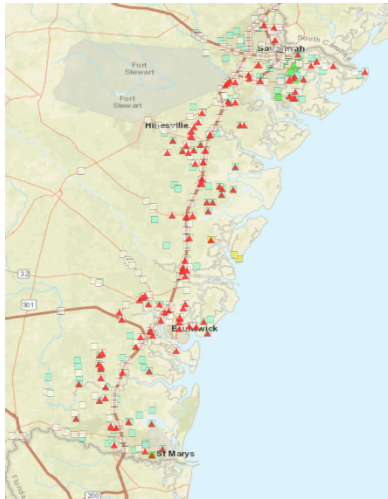
Method of Evaluation	Owner	Number of bridges considered failed				
		CAT 1	CAT 2	CAT 3	CAT 4	CAT 5
AASHTO Level 2 (High Tide)	State Highway Agency	16	94	137	159	179
	County Highway Agency	18	45	58	63	65
	City/Municipal Highway Agency	1	4	8	8	9
	State Park/Forest/ Reservation	0	1	1	1	1
	Total	35	144	204	231	254



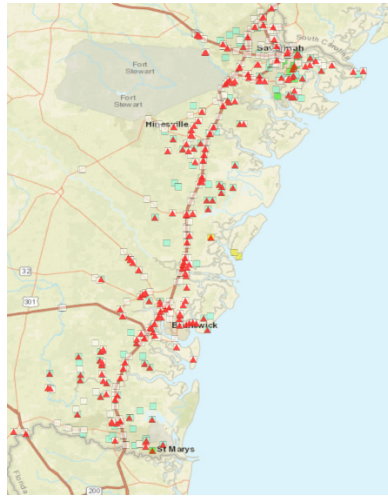
(a) Category 1



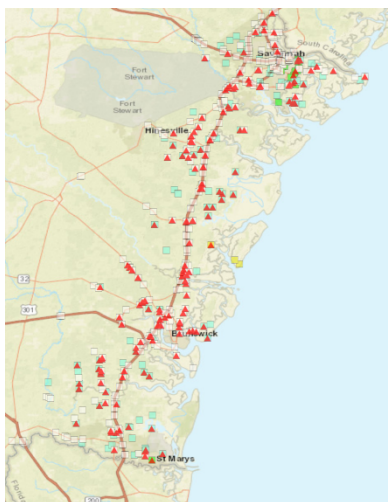
(d) Category 4



(b) Category 2



(e) Category 5



(c) Category 3

Legend:

Owner

State Highway Agency



County Highway Agency



City or Municipal Highway Agency



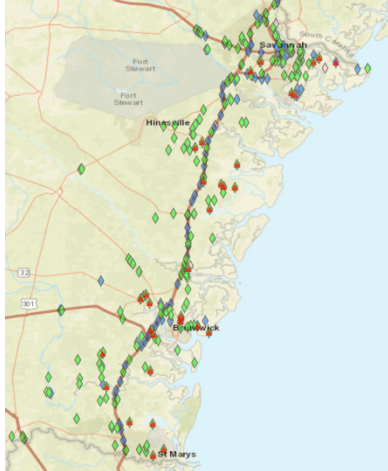
State Park, Forest, or Reservation Agency



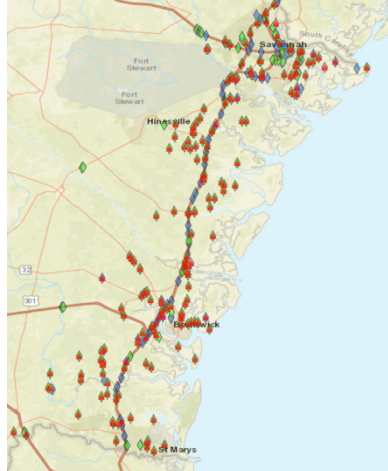
Fig. A.10. Potentially Vulnerable Bridges and Coastal Bridges by Owners.

Table A.8. Potentially Vulnerable Bridges by Connection Types.

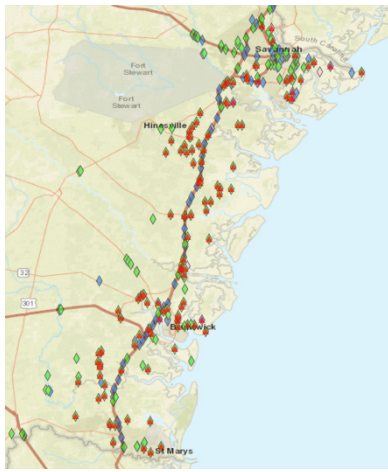
Method of Evaluation	Super-Substructure Connection Type	Number of bridges considered failed				
		CAT 1	CAT 2	CAT 3	CAT 4	CAT 5
AASHTO Level 1 (High Tide)	Dowels	38	131	185	199	219
	Anchor Bolts	6	19	32	47	65
	Others (e.g., dowels & anchors)	0	6	10	11	11
	Total	44	156	227	257	295
AASHTO Level 2 (High Tide)	Dowels	33	128	173	194	204
	Anchor Bolts	2	11	22	26	39
	Others (e.g., dowels & anchors)	0	5	9	11	11
	Total	35	144	204	231	254



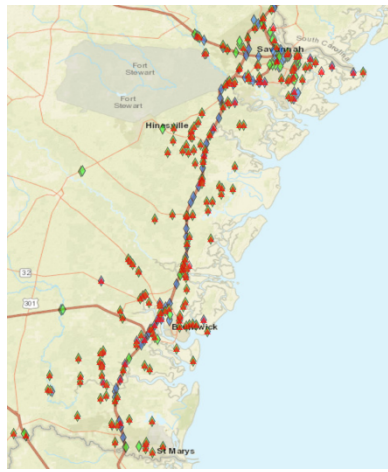
(a) Category 1



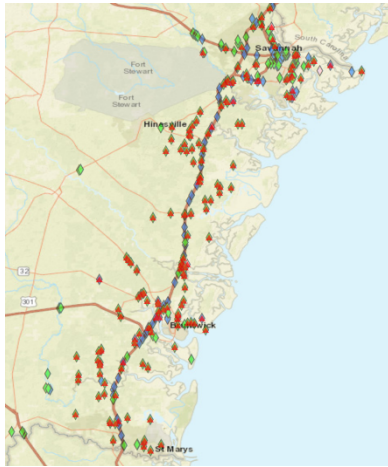
(d) Category 4



(b) Category 2



(e) Category 5



(c) Category 3

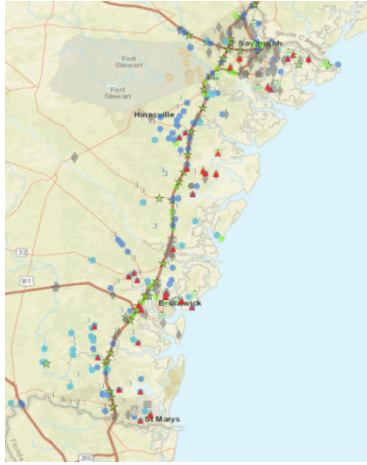
Legend:

- Super to Substructure Connection Type
- Dowels
- Anchor Bolts
- Combination of Dowels and Anchor Bolts

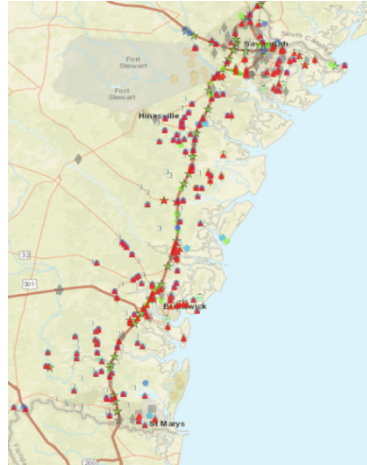
Figure A.11. Potentially Vulnerable Bridges and Coastal Bridges by Connection Types.

Table A.9. Potentially Vulnerable Bridges by Superstructure Types.

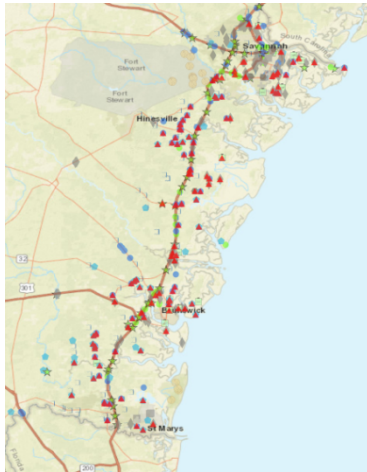
Method of Evaluation	Super-structure Type	Number of bridges considered failed				
		CAT 1	CAT 2	CAT 3	CAT 4	CAT 5
AASHTO Level 2 (High Tide)	Prestressed Conc Channel Beam	0	0	3	3	3
	Prestressed Slab	0	2	2	2	2
	Prestressed Concrete Girder/ Floor beam	11	32	51	59	65
	Concrete Slab	12	28	36	41	41
	Concrete Tee Beam	9	65	90	98	104
	Steel Continuous Girder	1	6	10	11	15
	Steel Girder/Floor beam	0	0	0	4	9
	Others	2	7	8	9	11
	Total	35	144	204	231	254



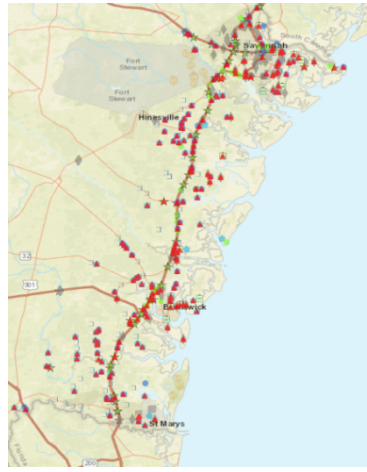
(a) Category 1



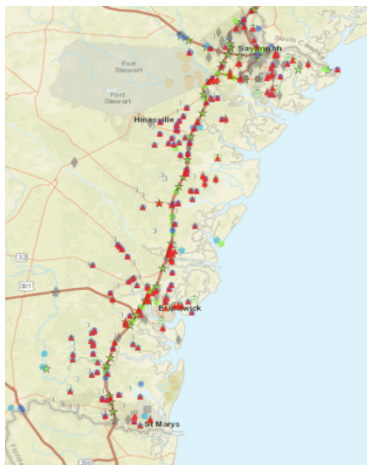
(d) Category 4



(b) Category 2



(e) Category 5



(c) Category 3

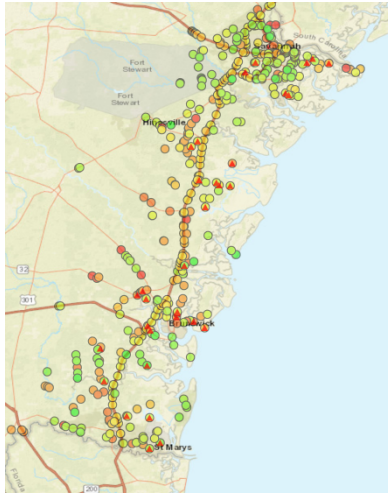
Legend:

- ☐ Superstructure Type
- ▣ Others
- Wood or Timber Stringer/Multi-beam or Girder
- ⊕ Prestressed Concrete Channel Beam
- Prestressed Slab
- ◆ Prestressed Concrete Girder and Floorbeam System
- ⬢ Prestressed concrete Box Beam or Girders - Multiple
- ★ Steel Continuous Girder and Floorbeam System
- Steel Girder and Floorbeam System
- Culvert
- Concrete Slab
- Concrete Tee Beam

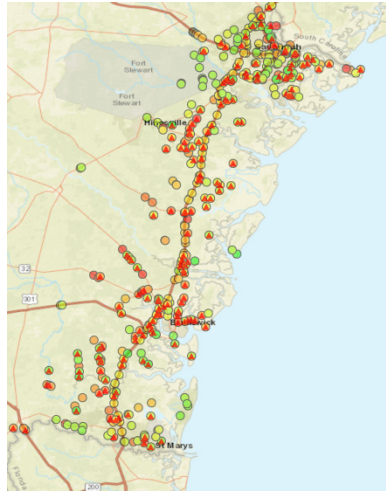
Fig. A.12. Potentially Vulnerable Bridges and Coastal Bridges by Superstructure Types.

Table A.10. Potentially Vulnerable Bridges by Year Constructed.

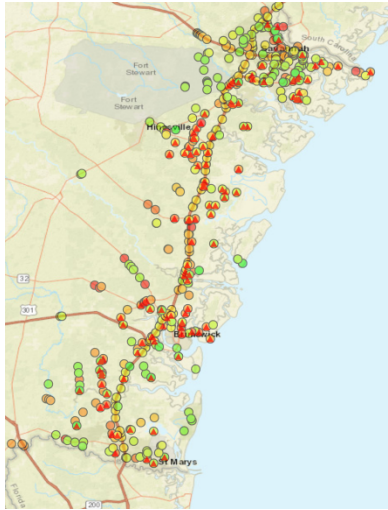
Method of Evaluation	Year Constructed	Number of bridges considered failed				
		CAT 1	CAT 2	CAT 3	CAT 4	CAT 5
AASHTO Level 2 (High Tide)	1922-1940	0	1	1	1	1
	1941-1950	1	10	11	11	11
	1951-1960	8	35	41	46	48
	1961-1970	5	28	34	36	47
	1971-1980	3	30	49	59	66
	1981-1990	13	19	24	26	27
	1991-2000	3	9	24	32	34
	2001-2010	2	12	20	20	20
	2011-2014	0	0	0	0	0
	Total	35	144	204	231	254



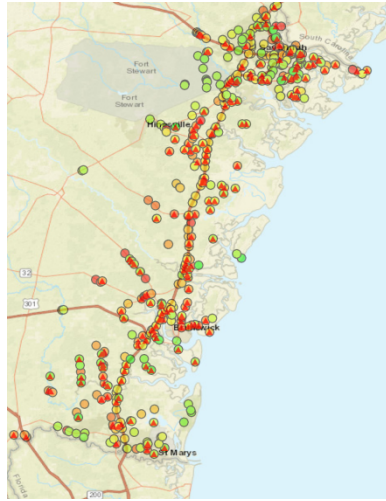
(a) Category 1



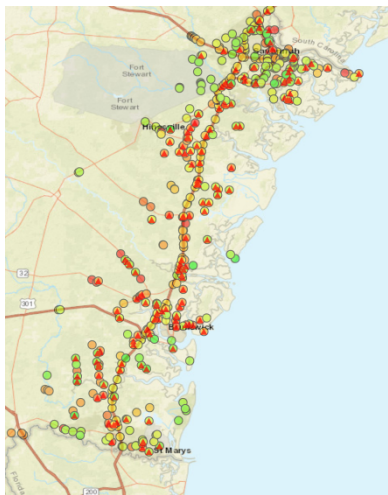
(d) Category 4



(b) Category 2



(e) Category 5



(c) Category 3

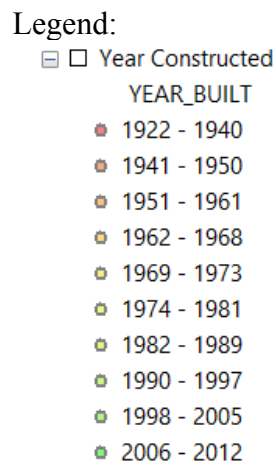


Fig. A.133. Potentially Vulnerable Bridges and Coastal Bridges by Year Constructed.

Table A.11. Potentially Vulnerable Bridges on the Hurricane Evacuation Route.

Method of Evaluation	Bridge ID	Probability of Failure (%), rounded to the nearest ones place					
		CAT 1	CAT 2	CAT 3	CAT 4	CAT 5	
AASHTO Level 2 (High Tide)	2900240	0	0	95	100	100	
	2900310	0	0	0	0	96	
	2900330	0	0	0	0	100	
	2900340	0	0	0	0	100	
	2900510	0	100	100	100	100	
	2900520	0	100	100	100	100	
	4900020	0	0	0	100	100	
	5100320	0	100	100	100	100	
	5100330	0	99	100	100	100	
	5100630	100	100	100	100	100	
	5100650	97	100	100	100	100	
	5100710	0	0	47	100	100	
	5100730	0	99	100	100	100	
	5100760	0	0	1	78	100	
	5100820	0	0	96	100	100	
	5100830	0	0	96	100	100	
	5101630	0	10	85	100	100	
	10300230	0	0	0	7	100	
	10300240	0	0	0	10	100	
	12700220	0	0	100	100	100	
	12700230	0	100	100	100	100	
	12700270	100	100	100	100	100	
	12700280	92	100	100	100	100	
	12700290	93	100	100	100	100	
	12700310	88	100	100	100	100	
	12700320	95	100	100	100	100	
	12700340	0	100	100	100	100	
	12700720	0	100	100	100	100	
	12700780	0	2	93	100	100	
	12750100	0	21	100	100	100	
	12750110	0	30	100	100	100	
	12750120	0	20	100	100	100	
	12750130	0	7	100	100	100	
	12750140	0	21	100	100	100	
	12750150	0	7	100	100	100	
	12750160	0	92	100	100	100	
	12750170	0	91	100	100	100	
	12750180	0	3	93	100	100	
	17900200	0	100	100	100	100	
	Total count-bridges w $P_f > 95\%$		4	16	28	33	39



(a) Category 1



(d) Category 4



(b) Category 2



(e) Category 5



(c) Category 3

Fig. A.14. Potentially Vulnerable Bridges on the Hurricane Evacuation Route.

A.4 Risk Assessment

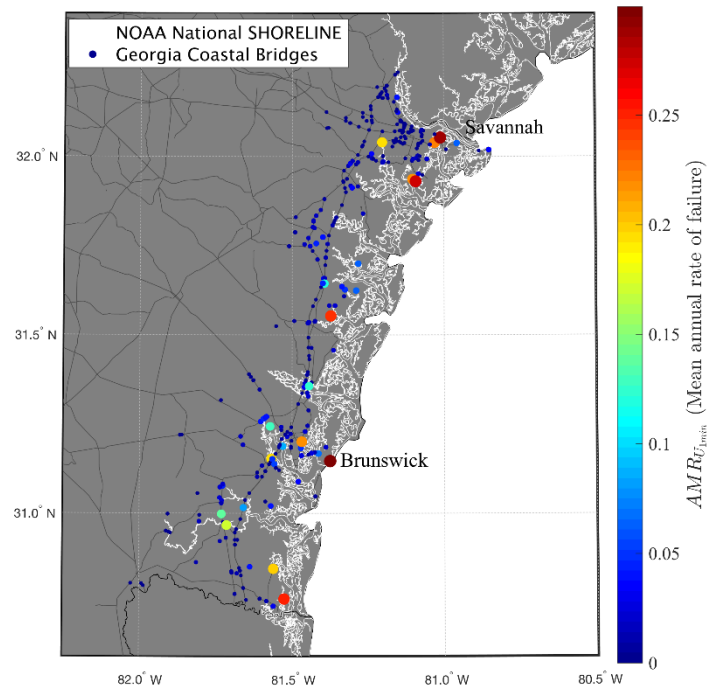


Fig. A.15. Mean Annual Rate of Failure.

Table A.12. Ten bridges with the mean annual rate of failure greater than 0.1.

Method of Evaluation	Bridge ID	Mean Annual Rate of Bridge Failure
Risk Assessment	19100130	0.122
	19150100	0.125
	12750040	0.130
	3900070	0.138
	3950470	0.172
	5100450	0.193
	12700410	0.195
	3950290	0.201
	12700070	0.205
	12700740	0.216
	5101450	0.220
	5100630	0.222
	19150040	0.246
	3950510	0.251
	5150080	0.276
	5150130	0.288
	12750030	0.300
	Total count-bridges	17